NASA TECHNICAL MEMORANDUM

NASA TM X-2787

NASA TM X-2787

AN INVESTIGATION OF HYDRAULIC-LINE RESONANCE AND ITS ATTENUATION

by John L. Sewall, David A. Wineman, and Robert W. Herr

Langley Research Center
Hampton, Va. 23665

NATIONAL AERONAUTICS AND SPACE ADMINISTRATION • WASHINGTON, D. C. • DECEMBER 1973

1. Report No.	2. Government Accession No.	3. Recipient's Catalog No.
NASA TM X-2787		

4. Title and Subtitle	5. Report Date
AN INVESTIGATION OF HYDRAULIC-LINE RESONANCE AND ITS ATTENUATION	December 1973
	6. Performing Organization Code

7. Author(s)	8. Performing Organization Report No.
John L. Sewall, David A. Wineman, and Robert W. Herr	L-8738
	10. Work Unit No.
9. Performing Organization Name and Address	501-22-05-01
NASA Langley Research Center Hampton, Va. 23665	11. Contract or Grant No.
	13. Type of Report and Period Covered
12. Sponsoring Agency Name and Address	Technical Memorandum
National Aeronautics and Space Administration Washington, D.C. 20546	14. Sponsoring Agency Code

15. Supplementary Notes

16. Abstract

An investigation of fluid resonance in high-pressure hydraulic lines has been made with two types of fluid dampers (or filters) installed in the line. One type involved the use of one or more closed-end tubes branching at right angles from a main line, and the other type was a fluid muffler installed in-line. These devices were evaluated in forced vibration tests with oscillatory disturbances over a 1000-Hz range applied to one end of the line and with oscillatory pressures measured at various stations along the main pipe. Limited applications of acoustic-wave theory to the branched systems are also included. Results show varying attenuations of pressure perturbations, depending on the number and location of branches and the type of muffler. Up to three branches were used in the branch-resonator study, and the largest frequency range with maximum attenuation was obtained for a three-branch configuration. The widest frequency ranges with significant attenuations were obtained with two types of fluid mufflers.

17. Key Words (Suggested by Author(s))	18. Distribution Statement
Vibration Hydraulic-line resonance Acoustic-wave theory Hydraulic muffler Branch-pipe damper	Unclassified – Unlimited

19. Security Classif. (of this report)	20. Security Classif. (of this page)	21. No. of Pages	22. Price*
Unclassified	Unclassified	77	Domestic, $3.75 Foreign, $6.25

*For sale by the National Technical Information Service, Springfield, Virginia 22151

AN INVESTIGATION OF HYDRAULIC-LINE RESONANCE AND ITS ATTENUATION

By John L. Sewall, David A. Wineman, and Robert W. Herr
Langley Research Center

SUMMARY

An investigation of fluid resonance in high-pressure hydraulic lines has been made with two types of fluid dampers (or filters) installed in the line. One type involved the use of one or more closed-end tubes branching at right angles from a main pipe, and the other type was a fluid muffler installed in-line. Evaluations of these devices were made in forced vibration tests in which oscillatory disturbances over a 1000-Hz range were applied to one end of the line and oscillatory pressure responses were measured at various stations along the main pipe line. Limited applications of acoustic-wave theory to the branched systems are also included.

Results show varying attenuations of pressure perturbations with frequency, depending on the number and location of branches and the type of muffler. Up to three branches were considered in the branch-resonator study, and the largest frequency range containing maximum attenuation was obtained for a three-branch configuration. The widest frequency ranges with acceptable and significant pressure attenuations were obtained with either of two types of mufflers of equivalent volumes. One of these was a commercial damper with an intricate internal flow arrangement which gave pressure attenuations over a slightly wider frequency range than the other type, which was a simple expansion chamber.

The study also included exploratory tests of structural-fluid interactions in a closed-end U-tube configuration, and results of these tests illustrated the possible pressure reductions obtainable near structural and fluid resonances as a consequence of adequately anchoring the piping system.

INTRODUCTION

Pumps transmitting fluid through hydraulic lines under high pressure impart periodic pulses to the fluid which can induce undesirable vibrations. The crash of an advanced fighter-aircraft prototype was traced to a break in the hydraulic line of the control system because of severe localized responses to periodic pressure pulsations produced by a pump operating at high frequencies. These responses were associated with strong structural-fluid resonances which were not sufficiently damped by fluid leakage internal to the aircraft

hydraulic system. Moreover, there was no accumulator and, therefore, no pressure reservoir to absorb flow disturbances generated by the pump. A solution to this problem was sought by introducing damping (or attenuating) devices into the fluid line to reduce resonant oscillations to an acceptable level.

Fluid resonance in hydraulic lines and its attenuation have been widely studied and are based on the fundamentals of wave propagation through continuous media, as presented in references 1 and 2, for example. Reference 1 includes the development and application of these principles to the acoustics of fluid in pipes with straight branches and Helmholtz resonators. Reference 2 contains a review of water-hammer research, pressure and flow-scaling relations, and related useful design information. The work presented in reference 3 is also design-oriented and includes some basic data on fluid properties important to fluid vibration.

Basic studies of fluid dynamics in straight transmission lines are reported in references 4 to 12. Reference 4 presents the first of a series of studies conducted at the NASA Lewis Research Center on the dynamic behavior of hydraulic fluid in a long line subjected to sinusoidal pulses at one end and having variable impedance at the other end of the line. References 5 and 6 give solutions based on various forms of the Navier-Stokes equations for fluid flow in pipes. The natural longitudinal frequency of the pipeline itself is also shown in reference 5 to have a pronounced effect on oscillatory pressure responses. Reference 7 is a theoretical treatise on fluid dynamic response to periodic and nonperiodic inputs at one end of a hydraulic line terminated at the other end by nonlinear orifice conditions. Reference 8 demonstrates the application of finite-element technology applied to the flow of blood.

Viscosity effects are treated in varying depth in references 5 to 15, with references 5 and 9 offering somewhat more on the subject than the others. The effect of viscosity in Newtonian fluids is shown in reference 5 to depend on the parameter $a\left(\frac{\omega}{\nu}\right)^{1/2}$ where a is the inside radius of the fluid line, ω is the frequency of fluid oscillation, and ν is the kinematic (or effective) viscosity. An increase in the magnitude of this parameter is associated with a decrease in the viscosity effect, and a value approaching infinity corresponds to a low-viscosity fluid oscillating at very high frequencies in a large-diameter tube. For non-Newtonian fluids (such as Mil-O-5606 and other aircraft hydraulic oils), where the effective viscosity decreases with increasing shear rate (which varies from one fluid to another), $a/\sqrt{\nu}$ is shown to be the governing viscosity parameter. In reference 9 the application of acoustic-wave theory to viscous Newtonian fluids is demonstrated for sinusoidal disturbance propagation in long, straight, cylindrical, nonvibrating pipelines. This work is reinforced in reference 10, in which the method of characteristics was applied to the one-dimensional model of transient flow and showed good agreement with experiment, particularly in accurate prediction of distortion effects characteristic of water-hammer response.

In reference 11, a small viscosity effect is shown for such liquids as water, kerosene, alcohol, and others having a low value of ν. The relation between conduit flexibility and fluid viscosity is discussed in reference 12, which shows that elastic pipeline walls exert considerable influence on the spatial propagation of the modes of a viscous fluid.

References 13 to 16 are concerned with various attenuating devices used to reduce oscillations in fluid lines. These devices may be roughly classified in three groups: branch resonators, mufflers (or filters), and internal dampers. In the first group, the use of closed-end branches, or standpipes, perpendicular to a main hydraulic line is described in references 13 and 14. In reference 13, measured pressure-perturbation ratios agree closely with analytical predictions of these ratios which are based on acoustic-wave theory for nonviscous fluid in a hydraulic line with a branch located at the midpoint of the line and having a length equal to half that of the line. Results of this study show large attenuation of pressure perturbations at discrete frequencies for which the branch length is an odd multiple of quarter-wave length. This implies essentially complete reflection of waves at the branch junction and no wave motion downstream from this point. In reference 14, it is shown that a large number of short branch resonators, closely spaced relative to the wave length of the sinusoidal disturbance, can effectively attenuate sinusoidal perturbations to a very low level over a wide frequency range. Each of the branches (so-called shunt assemblies in ref. 14) has a small accumulator at the closed end and a flow constriction near the branch junction. Two different types of constriction (shunt element) are evaluated, and transmission theory is shown to predict accurately the attenuation constant and the ratio of downstream-to-upstream pressures.

The second group of fluid perturbation attenuators consists of mufflers of various types introduced into a hydraulic line and includes single or multiple expansion chambers and parallel branch configurations. Considerable knowledge about these devices is contained in the comprehensive investigation reported in reference 15, in which the attenuation properties of over 75 mufflers and muffler combinations are measured and compared with attenuation properties calculated by acoustic-wave theory. Although this work was done with air as the test medium, the results are also applicable to liquids as long as viscosity and compressibility differences between gases and liquids are taken into account. Equations relating pressures and flows at the ends of multiple parallel branch configurations are given in reference 6 without experimental confirmation.

In the third group of attenuators, pressure amplitudes of fluid oscillations are reduced by the introduction of flexible tubes or bars into the main fluid line. The possibilities of these inserts producing substantial reductions in fluid oscillatory pressures over a wide frequency range are discussed in reference 16, in which test results are reported for single- or multiple-walled tubes or for a sponge-rubber bar contained within the fluid lines.

In support of an investigation of the aircraft accident mentioned earlier, the Langley Research Center evaluated various fluid dampers and studied fluid pressure responses in hydraulic lines subjected to oscillatory disturbances. This work, reported herein, consisted of a test program and limited analytical studies. Vibration tests were conducted on straight liquid-filled pipes with and without standpipe branches located at various points along the pipe, and also with and without mufflers in the pipe. Reference 13 provided the initial stimulus for the branch-pipe tests with one, two, or three branches at various distances from one end of the main pipe and with two branches at a common junction. Hydraulic fluid at moderate-to-high static pressure levels was subjected to ripples, or oscillatory pressure pulses, introduced at one end of the line by two different shaker configurations. Most of the tests were conducted with the downstream end of the main line capped, but some results were obtained with an accumulator at this end.

Muffler tests were made for two distinct expansion chambers of the same volume but with differing internal flow arrangements, and results of these two tests are compared with each other and with results of the straight line without a muffler. In addition, vibration tests were made on a U-shaped closed-end pipe in order to study structural-fluid interactions.

The test program was complemented by calculations based on the acoustic-wave-theory presentations of references 4 and 13 for branch-pipe configurations and also on a finite-element model utilizing the NASTRAN computer program. In the first of these analytical studies, the procedures described in reference 13 for a single-branch configuration are applied herein to obtain interterminal pressure and flow ratios for systems with more than one branch. The finite-element approach allows for fluid-structural coupling due to both lateral and longitudinal motions of the pipes and can also approximate the effects of filters, as well as branch resonators, in the system. Reference 17 contains the essentials of this approach, along with interesting results. It should be noted that both of these analytical methods involve linear theory, and direct comparison of analytical results with test results is not possible because the amplitudes and pressures in the test program were sufficiently large to be considered nonlinear.

SYMBOLS

The measurements and calculations were made in the U.S. Customary Units, which are shown in parentheses following the International System of Units, SI.

c speed of sound in hydraulic fluid

d diameter of hydraulic fluid in main pipe

d_k, d_m	diameter of hydraulic fluid in kth and mth branch pipes (see figs. 32 and 36, respectively, also eqs. (14) and (31))
f	frequency, $\omega/2\pi$, Hz
h_k, h_m	length of kth and mth branches (see figs. 32 and 36, respectively, also eqs. (9) and (32))
$j = \sqrt{-1}$	
l	total length of main pipe
l_1, l_2, l_3, l_4	lengths along main pipe (see figs. 34 to 50)
P(x)	pressure perturbation amplitude at station x along main pipe
P_0	inlet pressure perturbation amplitude, P(0)
P_E	exit pressure perturbation amplitude, $P(l)$
P_i	pressure perturbation amplitude at ith station along main pipe (i = 1, 2, 3)
$P_{3,r}$	peak-to-peak pressure fluctuation of main pipe without branches; reference pressure for branched configurations
$P_{A,k}$, $P_{A,m}$	pressure perturbation amplitude at branch inlet (see figs. 32 and 36, respectively)
$P_{B,k}$, $P_{B,m}$	pressure perturbation amplitude at closed end of branch (see figs. 32 and 36, respectively)
$U_{A,k}$, $U_{A,m}$	velocity perturbation amplitude at branch inlet (see figs. 32 and 36, respectively)
$U_{B,k}$, $U_{B,m}$	velocity perturbation amplitude at closed end of branch (see figs. 32 and 36, respectively)
U(x)	velocity perturbation amplitude at station x along main pipe
U_0	inlet velocity perturbation amplitude, U(0)

U_E	exit velocity perturbation amplitude
x	longitudinal coordinate of main pipe (see fig. 32)
y	branch coordinate (see fig. 32)
Z_o	characteristic impedance of hydraulic fluid, ρc
Z_E	exit impedance
z(x)	dimensionless impedance at station x (see eq. (5))
ρ	mass density of hydraulic fluid
ω	frequency, $2\pi f$, rad/sec

EXPERIMENTAL INVESTIGATION

Hydraulic Line With Branch Resonators

As is shown in references 13 and 14, one method for reducing oscillations caused by a pump in a hydraulic system – also called pump ripple – involves the installation of branch resonators or dampers along and perpendicular to the main line of fluid flow. In the present test program, oscillatory pressures were measured to determine attenuation magnitudes and frequencies for various single- and multiple-branch systems. Lack of sufficient instrumentation for measuring flow rates, and particularly the inlet-flow profile, precluded quantitative determination of relationships between oscillatory fluid pressures and velocities, not only at the inlet but also elsewhere in the system.

Test setups.- Two separate test systems were used in this study and are shown schematically in figures 1 and 2. Longitudinal and lateral pipe motions were constrained as much as possible in both systems in an effort to isolate fluid resonances from structural pipe resonances. In each system, hydraulic fluid (low viscosity) was excited by pressure pulsations introduced at one end of a hydraulic line that was capped at the other end for most of the tests, and oscillatory pressure amplitudes were measured by means of resistance-wire strain-gage transducers statically calibrated to 6.895 MN/m^2 (1000 psi) and offset from the main line by means of T-joints at the locations indicated in figures 1 and 2. (Pressure transducer 2 failed early in the test program.) These pressures were measured at discrete frequencies ranging from less than 100 Hz to over 900 Hz, and resonant frequencies were located approximately within the discrete-frequency intervals.

The static pressure level ranged from 4.825 to 10.34 MN/m^2 (700 to 1500 psi) in the setup of figure 1 and was about 10.34 MN/m^2 (1500 psi) in the setup of figure 2.

In the test setup of figure 1, the fluid in the system was excited by a hydraulic shaker with its driving cylinder locked and the pressure pulses into the fluid controlled by a servovalve. The downstream end of the line was closed at the vacuum pump-down valve. In this apparatus, an attempt was made to hold peak-to-peak pressure fluctuations (double amplitude) constant at the inlet throughout the frequency range. However, due to the power limitation of the servovalve, the level of inlet pressure fluctuations dropped off as the frequency increased. This trend is shown in figure 3 by the circular symbols which represent pressure fluctuations in the station closest to the inlet in the line without branches. In tests with branches, the root-mean-square (rms) current value to the servovalve was adjusted to the values used in the test without branches. Since the back pressure on the servovalve does affect the flow into the system, it is evident that the forcing function did not remain constant.

In order to gain better control of the input forcing function, the test setup shown in figure 2 was devised. Here a diaphragm ripple generator was connected to a large electrodynamic shaker, and it was possible to hold the displacement of the diaphragm constant for frequencies up to 650 Hz. It was also possible to obtain constant, but reduced, displacements at higher frequencies up to the maximum g levels of the shaker; however, it should be noted that even with a constant displacement, the volume disturbance did not remain constant because of the resilience of the diaphragm.

As shown in figure 2, an accumulator was attached at the end of line. Tests were made with the accumulator included or excluded, depending on whether the shut-off valve at the end of line was open or closed.

Results.- Results of tests with branch resonators are presented in figures 4 to 7 for the apparatus of figure 1 (test system I) and in figures 8 to 20 for the apparatus of figure 2 (test system II). Pressure fluctuations at the station closest to the downstream end of each branch configuration (pressure transducer 3 in figs. 1 and 2) are divided by pressure fluctuations at the corresponding station on the pipe without branches (figs. 3, 8, and 14), and the ratio $P_3/P_{3,r}$ is shown as a function of frequency. (Because resonant frequencies were only approximately located, the points in figs. 3 to 20 are not connected.)

These results indicate that for a single-branch configuration with a quarter-wavelength resonator located closest to the inlet (fig. 5), 0.25 to 0.1 attenuation (75- to 90-percent reduction in pressure) is possible within the region of the branch resonant frequency (area indicated by arrows in figure). The use of two or more dampers of dif-

ferent wavelengths extends the attenuation of pressure fluctuations over wider frequency ranges (see figs. 6 and 7) and also reduces the boost in pressure fluctuations at frequencies above and below the branch resonant frequencies. The largest frequency range with maximum attenuations was obtained for the three-branch configuration of figure 7, in which branches of different lengths were located at well-separated positions along the length of the main pipe.

The effects of the accumulator in the system can be seen in a comparison of figures 8, 9, 10, 11, and 13 with figures 14, 15, 16, 17, and 20. In the system without branches (figs. 8 and 14), there appear to be fewer high-level pressure peaks with the accumulator included (open) than without it (accumulator closed). Moreover, the peak pressure levels are lower with the accumulator open than with it closed. The systems with branches show a somewhat reversed tendency, that is, more high-level discrete-frequency pressure peaks with the accumulator than without it (compare figs. 9, 10, 11, and 13 with figs. 15, 20, 16, and 17, respectively). Moreover, there appears to be no consistent significant effect of the accumulator on pressure attenuations for the systems with branches.

Other results show the effects of two branches at the same location and of branch entrance. For the first of these effects, comparison of figure 13 with figure 9 shows less variation in pressure peaks over the full frequency range for the two-branch configuration than for the single-branch configuration with larger branch diameter; however, the single-branch configuration resulted in higher attenuations. Concerning the branch-inlet effect, figures 11 and 12 indicate opposite results for a 90° bend and a rounded inlet; that is, with the 90° bend in the branch near its inlet, the attenuations were higher over upper and lower frequency ranges than in the middle (fig. 11), whereas with the rounded branch inlet, the attenuation was higher in the middle frequency range than over the upper and lower ranges (fig. 12).

Hydraulic Line With Mufflers

Another means of attenuating pump-ripple pressures is by use of mufflers, or filters, in the hydraulic line. Part of the experimental work undertaken in this study involved the evaluation of a commercial pulsation damper which was considered for installation in the prototype aircraft that crashed and was to be placed in the hydraulic line as close to the pump as practicable. According to the manufacturer of this filter, it consists of a series of resonating chambers interconnected by impedance flow tubes and combines the salient features of the Helmholtz resonator (e.g., ref. 1), the Quincke tube (e.g., ref. 3) and a low-pass acoustic filter.

Test apparatus.- A smaller model of the filter was made available for the present tests, in which pressure fluctuations were measured and compared for three systems: a

straight, closed-end hydraulic line with no damper, the same system with the commercial filter installed near the ripple generator, and the closed-end pipe with a single expansion chamber having the same volume as the commercial unit and also located near the ripple generator. Dimensions of the three test systems are given in figure 21. The hydraulic line was similar to that of figure 2 and was 342.9 cm (135.0 in.) long with a 0.953-cm (3/8-in.) outside diameter and a 0.1245-cm (0.049-in.) thick wall. This line was restrained from moving by means of rigid clamps at each end. Three pressure transducers were installed in the line, as indicated in figure 21. Two of these transducers were located near the inlet (P_1) and outlet (P_2) of the mufflers, and the third transducer (P_3) was located near the closed end of the line. For ease of fabrication, the inside diameter of the single expansion chamber muffler was made somewhat smaller than the diameter of the commercial muffler. This necessitated a longer cylindrical chamber in order to keep its volume equal to that of the commercial muffler.

The ripple generator consisted of a 1.91-cm (3/4-in.) diameter piston which was driven by a 133.4-kN (30 000-lb) force electrodynamic shaker. For these tests, the piston was driven through a constant oscillatory amplitude of ±0.0635 mm (±0.0025 in.) for frequencies up to 490 Hz. Above this frequency, the force limitation of the shaker combined with the mass of the driving coil restricted the maximum acceleration of the driving piston to 60g.

Results of muffler tests.- The ripple pressures (single amplitude) of the hydraulic line without a muffler are shown as functions of frequency in figure 22. The reduced response amplitudes apparent at the higher frequencies in figure 22(b) are attributable to the smaller amplitude of the ripple-generator piston at these frequencies.

The variation of measured pressure fluctuations with frequency for the system with the commercial damper installed is shown in figure 23. As may be seen, the ripple pressure at the muffler outlet (P_2) is less than that at the muffler inlet (P_1) throughout the frequency range. At frequencies above 500 Hz, the pressure pulsations at the muffler outlet and near the end of the closed line (P_3) are extremely low. Results obtained with a single expansion chamber are given in figure 24, and pressure fluctuations downstream from the muffler are also very low at frequencies above 600 Hz.

In figure 25, the ratio of outlet pressure to inlet pressure for both the commercial damper and the single expansion chamber are plotted as functions of frequency. Either damper is seen to provide appreciable attenuation of pressure pulsations over a wide frequency range. Moreover, the frequency range is wider than that of any of the branched systems considered. The commercial damper clearly provides greater attenuation over a wider frequency range than does the expansion chamber. The commercial damper is effective down to about 200 Hz and the expansion chamber to about 375 Hz. The sharp

pressure ratio peak at 735 Hz for the expansion chamber is attributed to the sharp drop in P_1 at this frequency, as may be seen in figure 24. A somewhat similar behavior accounts for the peak in P_2/P_1 near 400 Hz for the commercial damper.

U-Tube Configuration

The experiments reported thus far are concerned with fluid resonances and their attenuation. In an effort to determine the effect of tube motion on pressure fluctuations, the U-tube configuration shown in figure 26 was assembled with both fixed and removable pipe anchors as shown. Tests were intended to determine whether or not anchoring the hydraulic system of the prototype aircraft previously referred to would significantly reduce pressure fluctuations due to pump ripple.

The U-tube was excited by the electrodynamic shaker and ripple generator (test system II in fig. 2), with hydraulic fluid supplied through the shut-off valve indicated in the lower part of figure 26. Aluminum tubing of 0.635-cm (1/4-in.) outside diameter and 0.89-mm (0.035-in.) wall thickness was used. Oscillating pressures were measured at stations 1 and 2 along the horizontal legs, and oscillatory pipe deflections were measured at the center of the vertical leg by means of an optical wedge (deflection target). Tests were conducted with all anchor locations fixed (supported) and with some anchors removed at the locations indicated (unsupported). A structural resonance of this system occurred at about 167 Hz and a fluid resonance at 515 Hz.

Pressure fluctuations are shown in figures 27 and 28 as functions of frequency for the same input displacements to the ripple generator for supported and unsupported conditions. As can be seen, supporting the tube at the locations indicated in figure 26 resulted in decreased levels of pressure fluctuations in the vicinity of both structural and fluid resonant frequencies. This is particularly evident in the low frequency (structural) range of figures 27 and 28.

Figure 29 compares response amplitudes at the deflection target for two input ripple displacements for the configuration shown in figure 26 in the unsupported condition. The fact that doubling the input displacements caused only small differences in response amplitudes near the structural resonance suggests that the general level of amplitudes (and pressures) are high enough to be considered nonlinear.

ANALYTICAL INVESTIGATION

The acoustic-wave theory presented in reference 4 and applied in reference 13 to a hydraulic line with a single-branch resonator is utilized herein to calculate inlet-to-exit perturbation pressure and flow ratios for a pipe with more than one branch resonator.

Basic assumptions include fluid incompressibility, the existence of undamped acoustic waves within the system, neglect of longitudinal motion of the pipe itself, and negligible velocity of mean fluid flow relative to fluid sonic speed.

Straight Pipe Relations

In reference 4, differential equations of motion relating fluid pressure and flow perturbations in a straight pipe are solved to give

$$P(x) = U(0)Z_o \frac{(Z_E + Z_o)e^{\frac{j\omega(l-x)}{c}} + (Z_E - Z_o)e^{-\frac{j\omega(l-x)}{c}}}{(Z_E + Z_o)e^{\frac{j\omega l}{c}} - (Z_E - Z_o)e^{-\frac{j\omega l}{c}}} \tag{1}$$

$$U(x) = U(0) \frac{(Z_E + Z_o)e^{\frac{j\omega(l-x)}{c}} - (Z_E - Z_o)e^{-\frac{j\omega(l-x)}{c}}}{(Z_E + Z_o)e^{\frac{j\omega l}{c}} - (Z_E - Z_o)e^{-\frac{j\omega l}{c}}} \tag{2}$$

for pressure and velocity perturbations P(x) and U(x) at any station x along the line in response to a sinusoidal pressure input at one end of the pipe. The positive and negative exponentials represent transmitted and reflected waves in the pipe, respectively. The input forcing frequency is denoted by ω, c is the fluid sonic speed, l is the length of the line, Z_E is the impedance at the downstream end of the line, and Z_o is the characteristic impedance ρc where ρ is the mass density of the fluid.

Equations (1) and (2) may also be written as

$$P(x) = P_E \cosh \frac{j\omega}{c}(l - x) + Z_o U_E \sinh \frac{j\omega}{c}(l - x) \tag{3}$$

$$Z_o U(x) = P_E \sinh \frac{j\omega}{c}(l - x) + Z_o U_E \cosh \frac{j\omega}{c}(l - x) \tag{4}$$

Dividing equation (3) by equation (4) gives the dimensionless impedance $\frac{P(x)}{Z_o U(x)}$

$$z(x) = \frac{\cosh \frac{j\omega}{c}(l - x) + \frac{Z_o}{Z_E} \sinh \frac{j\omega}{c}(l - x)}{\sinh \frac{j\omega}{c}(l - x) + \frac{Z_o}{Z_E} \cosh \frac{j\omega}{c}(l - x)} \tag{5}$$

If the pipe is capped at $x = l$, the fluid velocity perturbation $U_E = 0$, whence the impedance $Z_E = \frac{P_E}{U_E}$ becomes infinite, and equation (5) reduces to

$$z(x) = \coth \frac{j\omega}{c}(l - x) = -j \cot \frac{\omega}{c}(l - x) \tag{6}$$

When $x = 0$, $z(0) = 0$ is satisfied by

$$\frac{\omega l}{c} = \frac{(2n - 1)\pi}{2} \qquad (n = 1, 2, \ldots) \tag{7}$$

from which the well-known fundamental organ-pipe frequency $f = \frac{c}{4l}$ is obtained when $n = 1$ for a pipe open at one end and closed at the other. The corresponding pressure-perturbation distribution along the pipe is readily obtained from equation (3) which, for the capped pipe, reduces to the simple relation

$$\frac{P(x)}{P_E} = \cos \frac{\omega}{c}(l - x) \tag{8}$$

Variations of this ratio and its inverse with frequency are shown in figures 30 and 31 for $x = 0$, and resonances are indicated by the uncapped peaks of P_E/P_0 at odd integral multiples of the organ-pipe frequency.

Branch-Pipe Equations

Equations for terminal perturbation pressure and flow ratios in hydraulic lines with straight branches at right angles to the main pipe may be developed by application of equations (1) to (4), together with conditions of continuity of pressure and flow at a junction between the main pipe and a branch. The continuity conditions require that the pressures in all parts of the junction be equal and that the mass flow of fluid into the junction from upstream be equal to the mass flow into the branch pipe and downstream portion of the main pipe.

Assuming the branch coordinate to be given by y as shown in figure 32, equations (3) and (4) may be applied to give

$$P_k(y) = P_{B,k} \cosh \frac{j\omega}{c}(h_k - y) + Z_0 U_{B,k} \sinh \frac{j\omega}{c}(h_k - y) \tag{9}$$

$$Z_0 U_k(y) = P_{B,k} \sinh \frac{j\omega}{c}(h_k - y) + Z_0 U_{B,k} \cosh \frac{j\omega}{c}(h_k - y) \tag{10}$$

for the kth (k = 1, 2, . . .) branch, where $P_{B,k}$ and $U_{B,k}$ are pressure and velocity perturbations at the free end of the branch (point B in fig. 32) and h_k is the branch length. With the branch assumed capped, $U_{B,k} = 0$ and equations (9) and (10) reduce to

$$P_k(y) = P_{B,k} \cosh \frac{j\omega}{c}(h_k - y) \tag{11}$$

$$Z_o U_k(y) = P_{B,k} \sinh \frac{j\omega}{c}(h_k - y) \tag{12}$$

At the junction of the branch and the main pipe, the continuity conditions of pressure and flow may be written as

$$P_{k,1} = P_{A,k} = P_{k,2} \tag{13}$$

$$\frac{\pi d^2}{4} U_{k,1} = \frac{\pi d_k^2}{4} U_{A,k} + \frac{\pi d^2}{4} U_{k,2} \tag{14}$$

where, as shown in figure 32, the subscripts k,1 identify conditions in the main pipe just upstream of the junction, the subscripts k,2 identify conditions just downstream of the junction, and the subscripts A,k identify conditions at the branch entrance (y = 0). The inside pipe diameters of the main and branch pipes are denoted by d and d_k, respectively; dividing through by the cross-sectional area of the main pipe gives equation (14) in somewhat more convenient form as follows:

$$U_{k,1} = \left(\frac{d_k}{d}\right)^2 U_{A,k} + U_{k,2} \tag{15}$$

Series of branches.- For the single-branch configuration illustrated in figure 33, k = 1; terminal pressure and flow ratios can be obtained in the manner described in reference 13 and may be written as shown in figure 33, where equations (11), (12), (13), and (15) have been used with k = 1.

Equations for the terminal pressure and flow ratios for the two-branch configuration (k = 1,2) shown in figure 34 can be developed from the single-branch equations written in the form

$$P_0 = P_{2,1}\left[\cosh\frac{j\omega}{c}(l_1 + l_2) + \left(\frac{d_1}{d}\right)^2 \tanh\frac{j\omega h_1}{c}\sinh\frac{j\omega l_1}{c}\cosh\frac{j\omega l_2}{c}\right]$$

$$+ Z_o U_{2,1}\left[\sinh\frac{j\omega}{c}(l_1 + l_2) + \left(\frac{d_1}{d}\right)^2 \tanh\frac{j\omega h_1}{c}\sinh\frac{j\omega l_1}{c}\sinh\frac{j\omega l_2}{c}\right] \quad (16)$$

$$Z_o U_0 = P_{2,1}\left[\sinh\frac{j\omega}{c}(l_1 + l_2) + \left(\frac{d_1}{d}\right)^2 \tanh\frac{j\omega h_1}{c}\cosh\frac{j\omega l_1}{c}\cosh\frac{j\omega l_2}{c}\right]$$

$$+ Z_o U_{2,1}\left[\cosh\frac{j\omega}{c}(l_1 + l_2) + \left(\frac{d_1}{d}\right)^2 \tanh\frac{j\omega h_1}{c}\cosh\frac{j\omega l_1}{c}\sinh\frac{j\omega l_2}{c}\right] \quad (17)$$

where P_E, U_E for the single-branch configuration are replaced by $P_{2,1}, U_{2,1}$ for the two-branch system at the main branch station 2,1 just upstream from the second junction. Between the second junction and the end of the main pipe in figure 34, equations (3) and (4) may be applied to give the perturbation ratios

$$\frac{P_{2,2}}{P_E} = \cosh\frac{j\omega l_3}{c} + \frac{Z_o}{Z_E}\sinh\frac{j\omega l_3}{c} \quad (18)$$

$$\frac{Z_o U_{2,2}}{P_E} = \sinh\frac{j\omega l_3}{c} + \frac{Z_o}{Z_E}\cosh\frac{j\omega l_3}{c} \quad (19)$$

where subscripts 2,2 identify conditions downstream from the second junction. At the branch entrance station A,2, y = 0 and from equations (11) and (12) for k = 2,

$$\frac{P_{A,2}}{P_{B,2}} = \cosh\frac{j\omega h_2}{c} \quad (20)$$

$$\frac{Z_o U_{A,2}}{P_{B,2}} = \sinh\frac{j\omega h_2}{c} \quad (21)$$

Combining equations (13) and (15) with equations (20) and (21) gives

$$\frac{P_{B,2}}{P_E} = \frac{P_{B,2}}{P_{A,2}} \frac{P_{A,2}}{P_E} = \frac{P_{B,2}}{P_{A,2}} \frac{P_{2,1}}{P_E} = \frac{P_{B,2}}{P_{A,2}} \frac{P_{2,2}}{P_E} = \frac{1}{\cosh \frac{j\omega h_2}{c}} \frac{P_{2,2}}{P_E} \tag{22}$$

$$\frac{Z_o U_{A,2}}{P_E} = \frac{Z_o U_{A,2}}{P_{B,2}} \frac{P_{B,2}}{P_E} = \tanh \frac{j\omega h_2}{c} \frac{P_{2,2}}{P_E} \tag{23}$$

$$\frac{Z_o U_{2,1}}{P_E} = \left(\frac{d_2}{d}\right)^2 \frac{Z_o U_{A,2}}{P_E} + \frac{Z_o U_{2,2}}{P_E} = \left(\frac{d_2}{d}\right)^2 \tanh \frac{j\omega h_2}{c} \frac{P_{2,2}}{P_E} + \frac{Z_o U_{2,2}}{P_E} \tag{24}$$

Dividing equations (16) and (17) each through by P_E for the two-branch configuration and substituting equations (18), (19), and (24) for the ratios $P_{2,1}/P_E$ and $Z_o U_{2,1}/P_E$ leads to the two-branch terminal-ratio equations given in figure 34.

Equations for terminal pressure and flow ratios for the three-branch configuration (k = 1,2,3) of figure 35 can be developed in a similar manner from the two-branch equations written in the form

$$P_0 = P_{3,1}\left\{\cosh \frac{j\omega}{c}(l_1 + l_2 + l_3) + \left(\frac{d_1}{d}\right)^2 \tanh \frac{j\omega h_1}{c} \sinh \frac{j\omega l_1}{c} \cosh \frac{j\omega}{c}(l_2 + l_3)\right.$$

$$\left. + \left(\frac{d_2}{d}\right)^2 \tanh \frac{j\omega h_2}{c} \cosh \frac{j\omega l_3}{c}\left[\left(\frac{d_1}{d}\right)^2 \tanh \frac{j\omega h_1}{c} \sinh \frac{j\omega l_1}{c} \sinh \frac{j\omega l_2}{c} + \sinh \frac{j\omega}{c}(l_1 + l_2)\right]\right\}$$

$$+ Z_o U_{3,1}\left\{\sinh \frac{j\omega}{c}(l_1 + l_2 + l_3) + \left(\frac{d_1}{d}\right)^2 \tanh \frac{j\omega h_1}{c} \sinh \frac{j\omega l_1}{c} \sinh \frac{j\omega}{c}(l_2 + l_3)\right.$$

$$\left. + \left(\frac{d_2}{d}\right)^2 \tanh \frac{j\omega h_2}{c} \sinh \frac{j\omega l_3}{c}\left[\left(\frac{d_1}{d}\right)^2 \tanh \frac{j\omega h_1}{c} \sinh \frac{j\omega l_1}{c} \sinh \frac{j\omega l_2}{c} + \sinh \frac{j\omega}{c}(l_1 + l_2)\right]\right\} \tag{25}$$

$$Z_oU_0 = P_{3,1}\left\{\sinh\frac{j\omega}{c}(l_1 + l_2 + l_3) + \left(\frac{d_1}{d}\right)^2 \tanh\frac{j\omega h_1}{c}\cosh\frac{j\omega l_1}{c}\cosh\frac{j\omega}{c}(l_2 + l_3)\right.$$

$$\left. + \left(\frac{d_2}{d}\right)^2 \tanh\frac{j\omega h_2}{c}\cosh\frac{j\omega l_3}{c}\left[\left(\frac{d_1}{d}\right)^2 \tanh\frac{j\omega h_1}{c}\cosh\frac{j\omega l_1}{c}\sinh\frac{j\omega l_2}{c} + \cosh\frac{j\omega}{c}(l_2 + l_3)\right]\right\}$$

$$+ Z_oU_{3,1}\left\{\cosh\frac{j\omega}{c}(l_1 + l_2 + l_3) + \left(\frac{d_1}{d}\right)^2 \tanh\frac{j\omega h_1}{c}\cosh\frac{j\omega l_1}{c}\sinh\frac{j\omega}{c}(l_2 + l_3)\right.$$

$$\left. + \left(\frac{d_2}{d}\right)^2 \tanh\frac{j\omega h_2}{c}\sinh\frac{j\omega l_3}{c}\left[\left(\frac{d_1}{d}\right)^2 \tanh\frac{j\omega h_1}{c}\cosh\frac{j\omega l_1}{c}\sinh\frac{j\omega l_2}{c} + \cosh\frac{j\omega}{c}(l_1 + l_2)\right]\right\} \tag{26}$$

where P_E, U_E for the double-branch system are replaced by $P_{3,1}, U_{3,1}$ at station 3,1 just upstream from the third branch junction. Between the third junction and the end of the main pipe in figure 35, equations (3) and (4) may again be applied to give the ratios

$$\frac{P_{3,2}}{P_E} = \cosh\frac{j\omega l_4}{c} + \frac{Z_o}{Z_E}\sinh\frac{j\omega l_4}{c} \tag{27}$$

$$\frac{Z_oU_{3,2}}{P_E} = \sinh\frac{j\omega l_4}{c} + \frac{Z_o}{Z_E}\cosh\frac{j\omega l_4}{c} \tag{28}$$

where the subscripts 3,2 identify conditions just downstream from the third junction. Proceeding in the manner used for the one- and two-branch pipes, the flow relation for the third junction (analogous to eq. (24)) is found to be

$$\frac{Z_oU_{3,1}}{P_E} = \left(\frac{d_3}{d}\right)^2 \tanh\frac{j\omega h_3}{c}\frac{P_{3,2}}{P_E} + \frac{Z_oU_{3,2}}{P_E} \tag{29}$$

Dividing equations (25) and (26) each by P_E for the three-branch configuration and substituting equations (27), (28), and (29) for the ratios $P_{3,1}/P_E$ and $Z_oU_{3,1}/P_E$ leads to the equations given in figure 35.

Branches at a common junction.- The same procedure described in the preceding section can be applied to the system with more than one branch at the same junction with the main pipe. In the notation of figure 36, the continuity relations of equations (13) and (15) may be written as

$$P_C = P_{A,1} = P_{A,2} = \cdots P_{A,m} = P_D \tag{30}$$

$$U_C = \sum_{m=1}^{M} \left(\frac{d_m}{d}\right)^2 U_{A,m} + U_D \tag{31}$$

For the mth branch

$$\frac{P_{A,m}}{P_{B,m}} = \cosh \frac{j\omega h_m}{c} \tag{32}$$

$$\frac{Z_o U_{A,m}}{P_{B,m}} = \sinh \frac{j\omega h_m}{c} \tag{33}$$

Applying equations (3) and (4) to main-pipe sections on either side of the junction results in the following:

$$\frac{P_0}{P_C} = \cosh \frac{j\omega l_1}{c} + \frac{Z_o}{Z_C} \sinh \frac{j\omega l_1}{c} \tag{34}$$

$$\frac{Z_o U_0}{P_C} = \sinh \frac{j\omega l_1}{c} + \frac{Z_o}{Z_C} \cosh \frac{j\omega l_1}{c} \tag{35}$$

$$\frac{P_D}{P_E} = \cosh \frac{j\omega l_2}{c} + \frac{Z_o}{Z_E} \sinh \frac{j\omega l_2}{c} \tag{36}$$

$$\frac{Z_o U_D}{P_E} = \sinh \frac{j\omega l_2}{c} + \frac{Z_o}{Z_E} \cosh \frac{j\omega l_2}{c} \tag{37}$$

From equations (30) to (32),

$$\frac{P_{B,m}}{P_E} = \frac{P_{B,m}}{P_{A,m}} \frac{P_{A,m}}{P_E} = \frac{P_{B,m}}{P_{A,m}} \frac{P_C}{P_E} = \frac{1}{\cosh \frac{j\omega h_m}{c}} \frac{P_D}{P_E} \tag{38}$$

$$\frac{Z_o U_{A,m}}{P_E} = \frac{Z_o U_{A,m}}{P_{B,m}} \frac{P_{B,m}}{P_E} = \tanh \frac{j\omega h_m}{c} \frac{P_D}{P_E} \tag{39}$$

$$\frac{Z_o U_C}{P_E} = \frac{P_D}{P_E} \sum_{m=1}^{M} \left(\frac{d_m}{d}\right)^2 \tanh \frac{j\omega h_m}{c} + \frac{Z_o U_D}{P_E} \tag{40}$$

Equations (34) and (35) may be written as

$$\frac{P_0}{P_E} = \frac{P_C}{P_E} \cosh \frac{j\omega l_1}{c} + \frac{Z_o U_C}{P_E} \sinh \frac{j\omega l_1}{c} \tag{41}$$

$$\frac{Z_o U_0}{P_E} = \frac{P_C}{P_E} \sinh \frac{j\omega l_1}{c} + \frac{Z_o U_C}{P_E} \cosh \frac{j\omega l_1}{c} \tag{42}$$

Substitution of equations (36), (37), and (40) into equations (41) and (42) gives the equations shown in figure 36.

Analytical Results

Perturbation terminal pressure ratios were calculated for each of the branch-resonator configurations tested in the experimental program and also for some conceptual configurations. In all calculations, the downstream end of the main pipe was assumed to be closed, whence the impedance Z_E is infinite at this point. Thus, the terminal pressure ratios are given only by the real parts of the equations in figures 33 to 36 for P_0/P_E, and uncapped pressure ratios occur at particular frequencies in the plots of figures 30, 31, and 37 to 50. The speed of sound in the hydraulic fluid was chosen as 1.237 km/sec (48 700 in./sec).

Direct comparison between analytical and experimental pressure ratios is not generally possible because of the large pressure amplitudes of the test program in contrast to the analytical pressure amplitudes, which are linear. However, approximate agreement is indicated in experimental and analytical frequencies for resonances $\left(\left|P_E/P_0\right| \to \infty\right)$ and maximum attenuations $\left(\left|P_E/P_0\right| = 0\right)$. In order to facilitate these comparisons, however tenuous, figure numbers of the analytical plots are matched with the corresponding figure numbers of the experimental plots in table 1.

Main pipe without branches.- As previously noted, the pressure ratios in figures 30 and 31 for test systems I and II were computed from the simple cosine relation of equation (8) with x = 0. Within a 100-Hz frequency range, analytical resonances occurred for system I at 203 Hz and 609 Hz and for system II at 88, 264, 440, 615, 791, and 968 Hz. Comparison of terminal pressure ratios in figure 30 with the nearly corresponding experimental ratios from figure 3 for test system I shows fair agreement between experimental and analytical trends for frequencies up through the first resonance and beyond but poor agreement near and above the second resonance. A somewhat similar observation may be made for test system II which had the same number of experimental and analytical resonant peaks up to 900 Hz and deteriorating agreement between experimental and analytical resonant frequencies above the first resonance, as is evident by comparing figures 8 and 31. These discrepancies may be partially due to the fact that more precise values of resonant frequencies were not actually determined either for these tests or for tests of the branched configurations. Despite these deficiencies, the overall fluid resonant response behavior of these pipes without branches seems well enough understood to permit some appraisal of attenuation capabilities of the branched systems.

Main pipe with branches.- Variations of analytical pressure ratios with frequency for the single-branch test systems are presented in figures 37 to 42. Because the same branch length was used in all these cases, maximum attenuation of the pressure perturbation occurred at 406 Hz, as indicated by the generally discontinuous rise in $\left|P_0/P_E\right|$ and corresponding zero value of $\left|P_E/P_0\right|$ at this frequency. For an equilateral system, such as shown in figure 38, the minimum value of $\left|P_E/P_0\right|$ is 1/2 rather than zero owing to the finite limit of the product $\tan \frac{\omega h_1}{c} \sin \frac{\omega h_1}{c} \cos \frac{\omega h_1}{c}$ for $h_1 = l_1 = l_2$ in the equation for P_0/P_E given in figure 33. Moreover, the attenuation of this system clearly remains nearly at a relative maximum $\left(\left|P_E/P_0\right| \approx 1/2\right)$ over a wide range of frequencies (about 200 Hz) in contrast to the other single-branch configurations for which pressure perturbations are attenuated over narrower frequency bands with one resonant frequency very close to the discrete frequency of maximum attenuation $\left(\left|P_E/P_0\right| = 0\right)$. The effect of branch location on this resonant frequency appears to be opposite for the two test systems, that is, for test system II with the branch near an end of the main pipe (figs. 39, 40, and 42), this closest resonance tends to be farther removed from the frequency of maximum attenuation

than with the branch near the middle (fig. 41), whereas a reverse tendency is indicated for test system I (figs. 37 and 38).

The effects on analytical pressure perturbations of additional branches in series are shown in figures 43 and 44 (corresponding to figs. 6 and 7 for experimental results). Results for test system I with two branches appear in figure 43 and show frequencies of maximum attenuation at 406 Hz and 609 Hz corresponding to the longer and shorter of the two branches, respectively. Attenuated pressure perturbations are indicated over a frequency range of about 300 Hz interrupted by a resonance at 485 Hz. The presence of a third branch extended the range even farther, as figure 44 shows. Here, with the third frequency of maximum attenuation equal to 725 Hz, reduced values $|P_E/P_0|$ occurred near 406 Hz and from about 850 to 950 Hz, and $|P_E/P_0| = 0$ from about 600 to 750 Hz. This last uninterrupted 150-Hz frequency range of maximum attenuation resembles a similar experimental behavior shown in figure 7. These results suggest that pressure attenuations can be extended over a wider frequency range by adding more branches of different lengths. A possible extrapolation of this idea is a large number of closely spaced branches distributed along the main pipe as suggested by Robert J. Blade of NASA Lewis Research Center in official correspondence. Indeed, he and Carl M. Holland (ref. 14) show the effectiveness of a special distributed-branch system in reducing pressure perturbations to a very low continuous level over a maximum frequency range.

Results for two equal branches at a common junction are shown in figure 45. Here the effect of a smaller branch diameter than main diameter is included, and the analytical pressure perturbations are very similar to those shown in figure 41 for the single-branch configuration with equal branch and main-pipe diameters. These results, in addition to another to be discussed, suggest that multiple branches at a common junction with the main pipe may not be as effective pressure attenuators as branches in series.

Results of other branched systems.- Pressure-perturbation ratios were also calculated for a number of other branched systems featuring arbitrary variations in branch length, location, and cross-sectional diameter. Sample results of these calculations are presented in figures 46 to 50 and give some indication of the sensitivity of system attenuation to these properties.

Figures 46 to 48 show theoretical pressure ratios for particular two- and three-branch combinations in series. Comparison of figure 46 with figure 44 indicates that holding the branch length the same in a three-branch configuration had the effect of shifting the maximum pressure-ratio attenuations to another frequency band. That is, with each branch length equal to the longest branch length in figure 44 (76.2 cm (30.0 in.)), minimum $|P_E/P_0|$ values moved from the 600- to 750-Hz range in figure 44 to the 400- to 600-Hz range in figure 46. Variations of pressure ratios with frequency for systems with branches

closer to the exit (or capped) end of the main line (denoted by point E) than to the inlet end (denoted by point 0) are shown in figures 47 and 48. In figure 47, the two-branch configuration of figure 43 has simply been shifted toward the capped end so that l_3 is 15.2 cm (6.0 in.) from point E, and comparison of the two figures shows generally better attenuation characteristics because of this change. The resonance of 591 Hz in figure 47 appears to be sharply defined and may therefore not have as adverse an effect on pressure attenuation as resonances extending over wider frequencies. Somewhat similar effects are evident for the three-branch system of figure 48, in which a combination of three closely spaced branches of equal length are located close to point E and there are two sharply defined resonances at 355 and 465 Hz within the frequency band of highest attenuation. Other results (not shown) indicate smaller frequency bands of attenuated pressure ratios with this branch combination close to the inlet and near the middle of the main pipe.

Figures 49 and 50 show the effects of increasing the number and the diameters of branch resonators located at a common junction on the main pipe. The pressure response characteristics in both figures are clearly similar to those in figure 45. Comparison of figures 49 and 45 shows that reduced pressure ratios $|P_E/P_0|$ were obtained over slightly wider frequency ranges near the maximum attenuation frequency as the number of branches was increased. Figure 50 reveals a similar effect of increasing branch diameters, with even lower values of $|P_E/P_0|$ over wider frequency bands interrupted by more sharply defined resonances.

CONCLUDING REMARKS

An investigation of fluid resonance and its attenuation in high-pressure hydraulic lines is reported. The study was aimed at understanding fluid vibrations in simplified hydraulic systems and evaluating two different types of fluid pulsation dampers, or attenuators. One of these types featured one or more closed-end tubes, or standpipes, branching from a main pipe, and the other type was a fluid muffler installed in the main pipe line. In addition, certain structural-fluid interactions were explored in a closed-end U-tube. Most of the study involved forced vibration testing, with conventional hydraulic fluid excited by a 1000-Hz range of oscillatory disturbances at one end of a system that was closed at the other end. Limited applications of acoustic-wave theory to the branched systems are also included.

Results for the branched systems show varying attenuations of pressure perturbations, depending on the number and location of branches along the main hydraulic line. Maximum reductions in pressure perturbations for the single-branch configuration were obtained with the branch near the main inlet or near the exit. These reductions were somewhat less but still significant when the branch was located near the middle of the

main pipe, and they occurred over limited frequency ranges. Increasing the number of branches along the main pipe from one to three resulted in large pressure attenuations over wider frequency ranges, and the largest frequency range containing maximum attenuation was obtained for three branches of different lengths at relatively separated positions along the main pipe. The use of more than one branch at the same location did not produce as much attenuation as did branches in series (i.e., at different locations along main pipe). Mounting an accumulator at the exit end of the main pipe without branches resulted in fewer high-level resonant peaks than with the exit closed, but no significant effects of the accumulator on pressure attenuations could be observed for the branched systems.

The muffler vibration tests showed that either a commercial damper with an intricate internal flow arrangement or a single expansion chamber of equivalent volume produced attenuated pressure perturbations over wider frequency ranges than those of the branched systems. The frequency range of the commercial damper was a little larger than that of the expansion chamber.

Vibration tests of the U-tube configuration demonstrated the need for adequately anchoring the tube structure to reduce the levels of pressure perturbations near structural and fluid resonant frequencies.

Langley Research Center,
National Aeronautics and Space Administration,
Hampton, Va., June 15, 1973.

REFERENCES

1. Kinsler, Lawrence E.; and Frey, Austin R.: Fundamentals of Acoustics. Second ed., John Wiley & Sons, Inc., c.1962, pp. 186-216.

2. Streeter, Victor L., ed.: Handbook of Fluid Dynamics. First ed., McGraw-Hill Book Co., Inc., 1961, pp. 20-1 – 20-47.

3. Keller, George R.: Hydraulic System Analysis. Hydraulics & Pneumatics Mag., c.1969.

4. Regetz, John D., Jr.: An Experimental Determination of the Dynamic Response of a Long Hydraulic Line. NASA TN D-576, 1960.

5. D'Souza, A. F.; and Oldenburger, R.: Dynamic Response of Fluid Lines. Trans. ASME, Ser. D: J. Basic Eng., vol. 86, no. 3, Sept. 1964, pp. 589-598.

6. Jarski, E. J.: Dynamics of Viscous Fluid Oscillations in Hydraulic Lines. NSRDC-3201, U.S. Navy, Jan. 1970. (Available from DDC as AD-864595.)

7. Strunk, Richard Dean: Longitudinal Wave Propagation in Liquid Lines of Finite Length Including the Effect of Nonlinear Boundary Conditions. Ph. D. Thesis, Univ. of Illinois, 1969.

8. Ray, Gautam: Finite Element Analysis Methods in Dynamics of Pulsatile Flow. Ph. D. Thesis, Pennsylvania State Univ., 1969.

9. Holland, Carl M.; Blade, Robert J.; and Dorsch, Robert G.: Attenuation of Sinusoidal Perturbations Superimposed on Laminar Flow of a Liquid in a Long Line. NASA TN D-3099, 1965.

10. Zielke, W.: Frequency-Dependent Friction in Transient Pipe Flow. Trans. ASME, Ser. D: J. Basic Eng., vol. 90, no. 1, Mar. 1968, pp. 109-115.

11. Chang, S. S. L.: Transient Effects of Supply and Connecting Conduits in Hydraulic Control Systems. J. Franklin Inst., vol. 262, no. 6, Dec. 1956, pp. 437-452.

12. Gerlach, C. R.; and Parker, J. D.: Wave Propagation in Viscous Fluid Lines Including Higher Mode Effects. Trans. ASME, Ser. D: J. Basic Eng., vol. 89, Dec. 1967, pp. 782-788.

13. Lewis, William; Blade, Robert J.; and Dorsch, Robert G.: Study of the Effect of a Closed-End Side Branch on Sinusoidally Perturbed Flow of Liquid in a Line. NASA TN D-1876, 1963.

14. Blade, Robert J.; and Holland, Carl M.: Attenuation of Sinusoidal Disturbances in Nonviscous Liquid Flowing in a Long Line With Distributed Leakage. NASA TN D-3563, 1966.

15. Davis, Don D., Jr.; Stokes, George M.; Moore, Dewey; and Stevens, George L., Jr.: Theoretical and Experimental Investigation of Mufflers With Comments on Engine-Exhaust Muffler Design. NACA Rep. 1192, 1954. (Supersedes NACA TN 2893 by Davis, Stevens, Moore, and Stokes and TN 2943 by Stokes and Davis.)

16. Gebhardt, George T.: Acoustic Impedance Measurements of Liquid Filled Pipes Containing Lossy, High-Compliance Inserts. D-15871, Boeing Airplane Co., Oct. 15, 1954.

17. Howlett, James T.: Applications of NASTRAN to Coupled Structural and Hydrodynamic Responses in Aircraft Hydraulic Systems. NASTRAN: Users' Experiences, NASA TM X-2378, 1971, pp. 407-419.

TABLE 1.- INDEX TO PLOTS

Test system	Configuration	Figure	
		Analytical	Experimental
I	No branches; l = 152.4 cm (60.0 in.)	30	3
II	No branches; l = 351.8 cm (138.5 in.)	31	8
I	Single branch; l_1 = 15.2 cm (6.0 in.)	37	5
I	Single branch; l_1 = 76.2 cm (30.0 in.)	38	4
II	Single branch; l_1 = 30.5 cm (12.0 in.)	39	[a]18
II	Single branch; l_1 = 99.4 cm (39.1 in.)	40	[a]19
II	Single branch; l_1 = 175.3 cm (69.0 in.)	41	9, [a]16
II	Single branch; l_1 = 251.1 cm (98.9 in.)	42	10, [a]20
I	Two branches; l_1 = 15.2 cm (6.0 in.); l_2 = 61.0 cm (24.0 in.)	43	6
I	Three branches; $l_1 = l_2$ = 15.2 cm (6.0 in.); l_3 = 45.7 cm (18.0 in.)	44	7
II	Two common branches; l_1 = 175.3 cm (69.0 in.) with $\frac{d_1}{d} = \frac{d_2}{d} = 0.65$	45	13, [a]17

[a]Accumulator open at downstream end; accumulator closed (i.e., downstream end closed) for all other experimental figures in table.

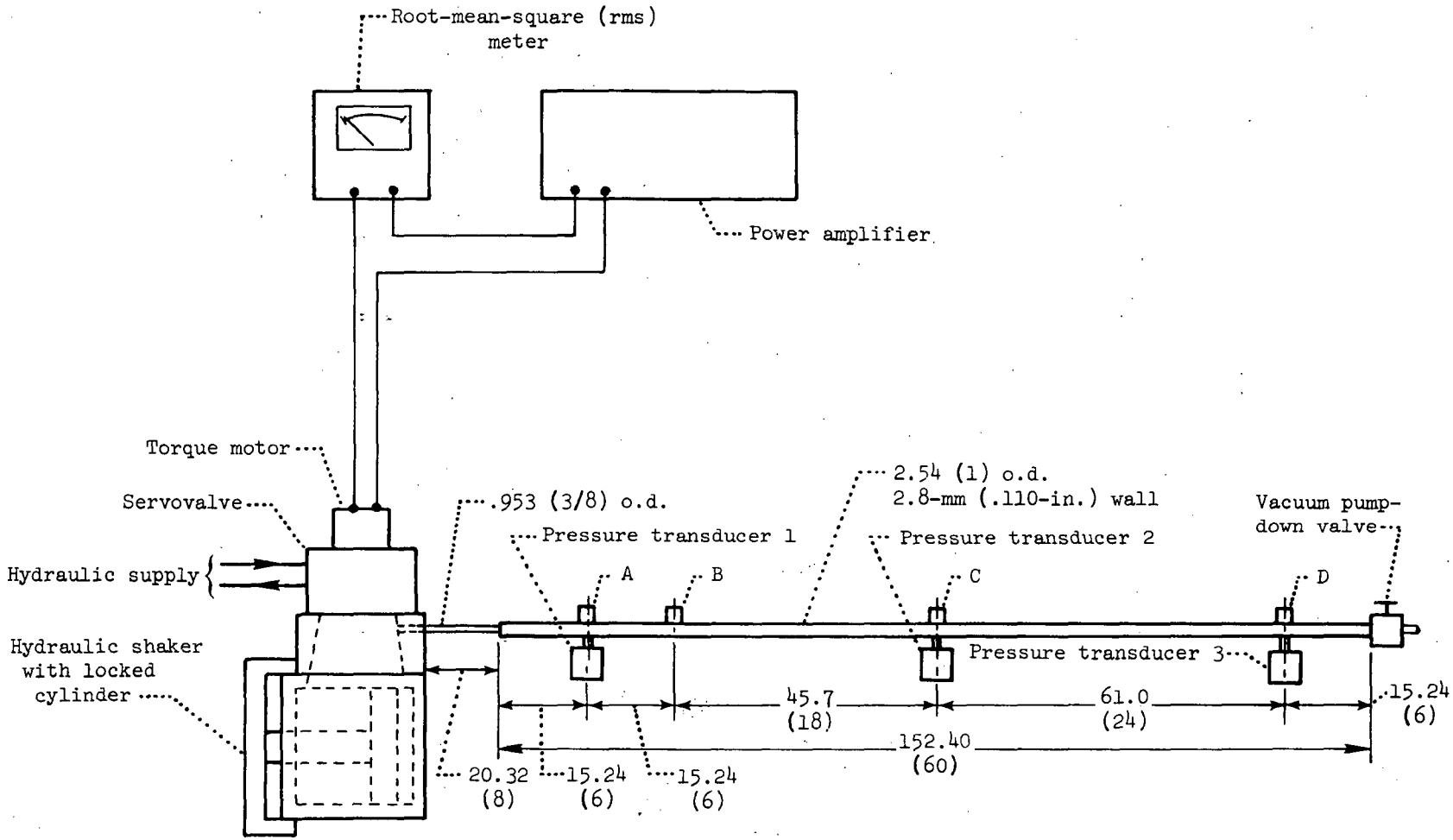

Figure 1.- Schematic diagram of hydraulic-shaker system (test system I). All dimensions in centimeters (inches) except as noted. Branch resonator connections at stations A, B, C, and D.

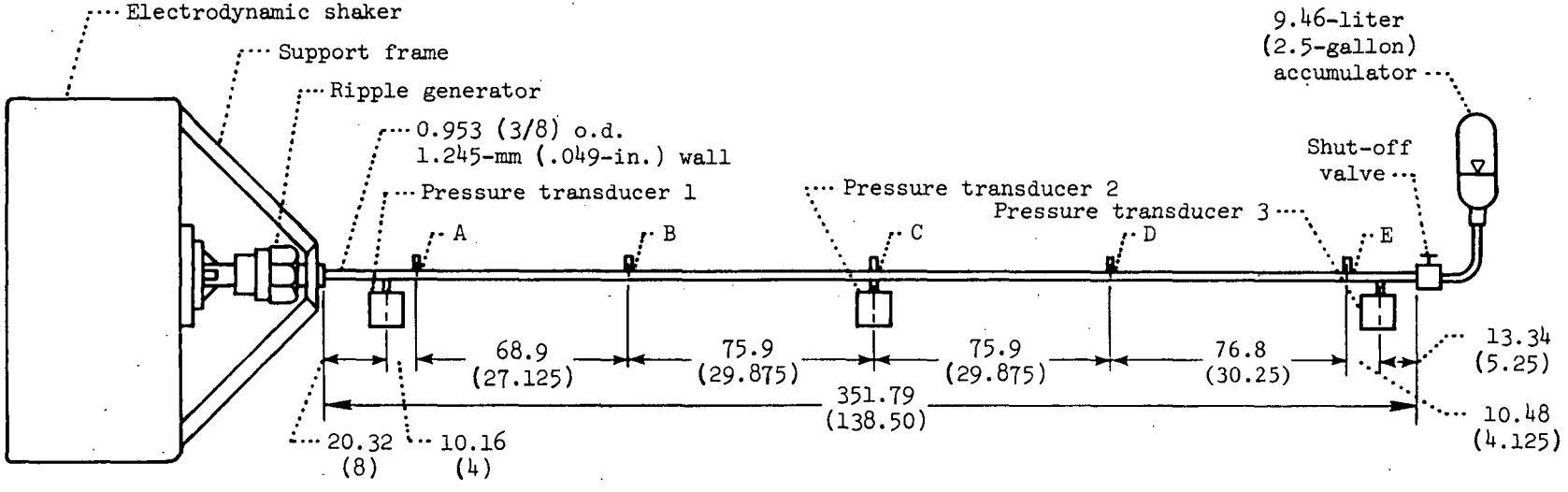

Figure 2.- Schematic diagram of electrodynamic-shaker and ripple-generator system (test system II). All dimensions in centimeters (inches) except as noted. Resonant damper connections at stations A, B, C, D, and E.

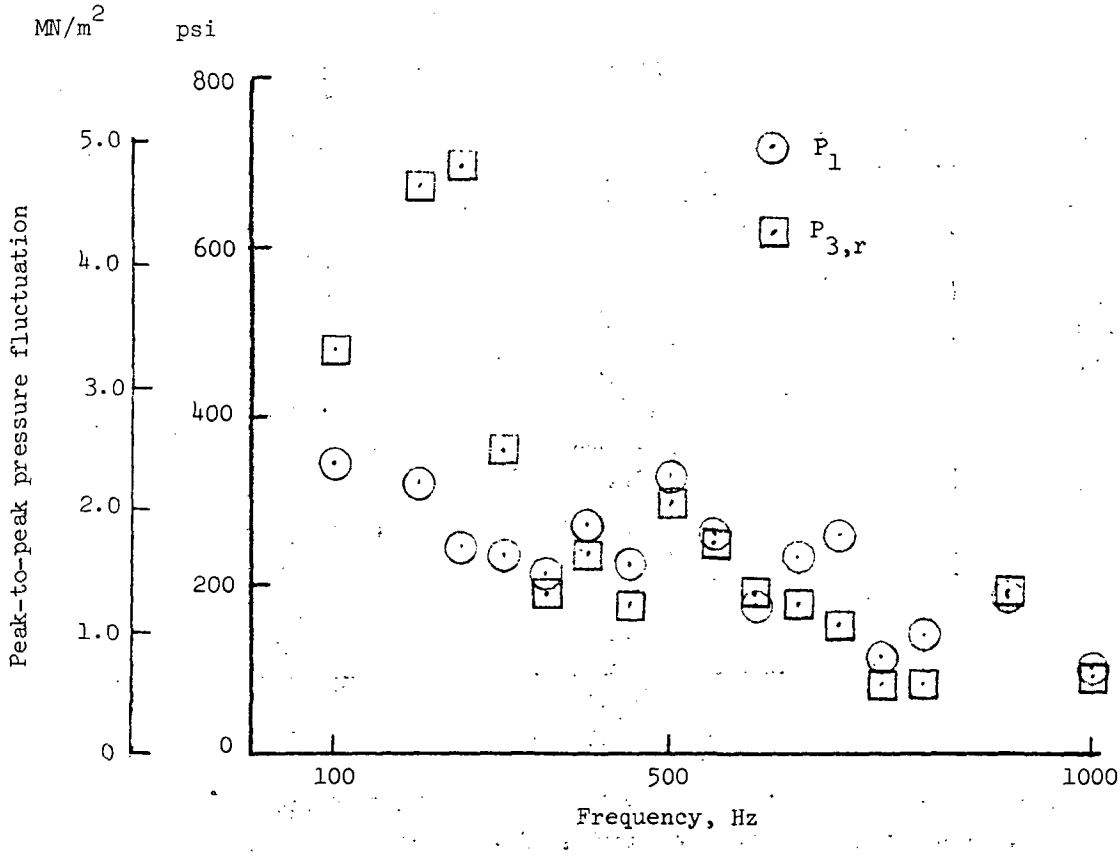

Figure 3.- Peak-to-peak pressure fluctuation versus frequency for test system I (fig. 1) with no branches.

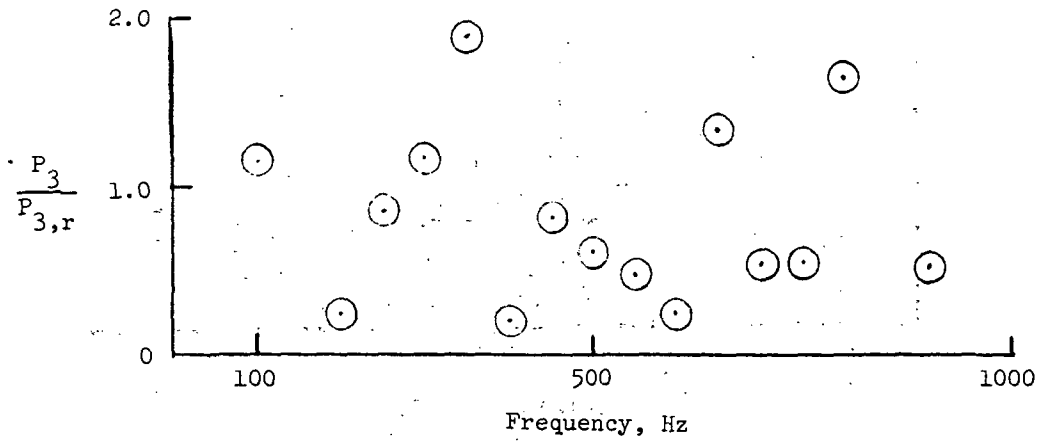

Figure 4.- Pressure ratio versus frequency for test system I (fig. 1); single-branch configuration with 76.2-cm (30.0-in.) branch at station C.

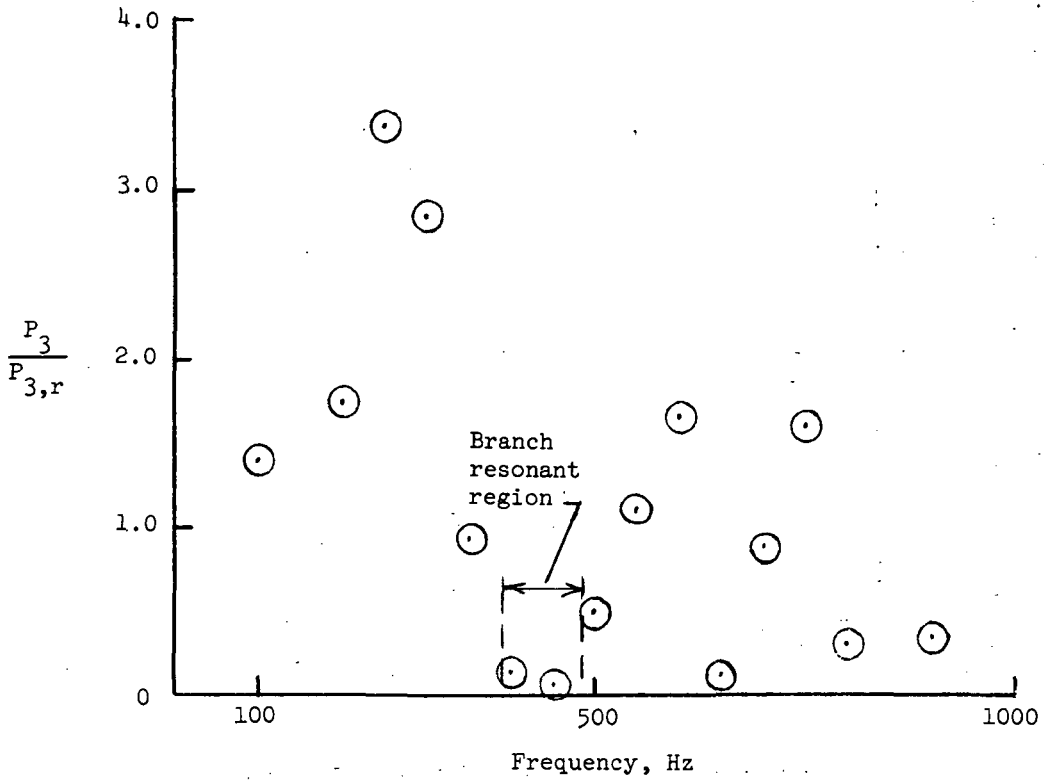

Figure 5.- Pressure ratio versus frequency for test system I (fig. 1); single-branch configuration with 76.2-cm (30.0-in.) branch at station A.

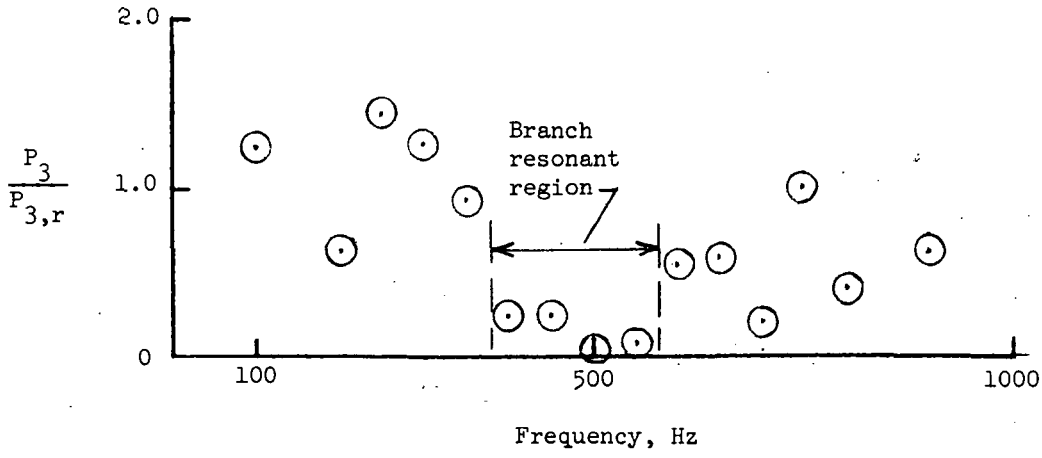

Figure 6.- Pressure ratio versus frequency for test system I (fig. 1); two-branch configuration with 76.2-cm (30.0-in.) branch at station A and 50.8-cm (20.0-in.) branch at station C.

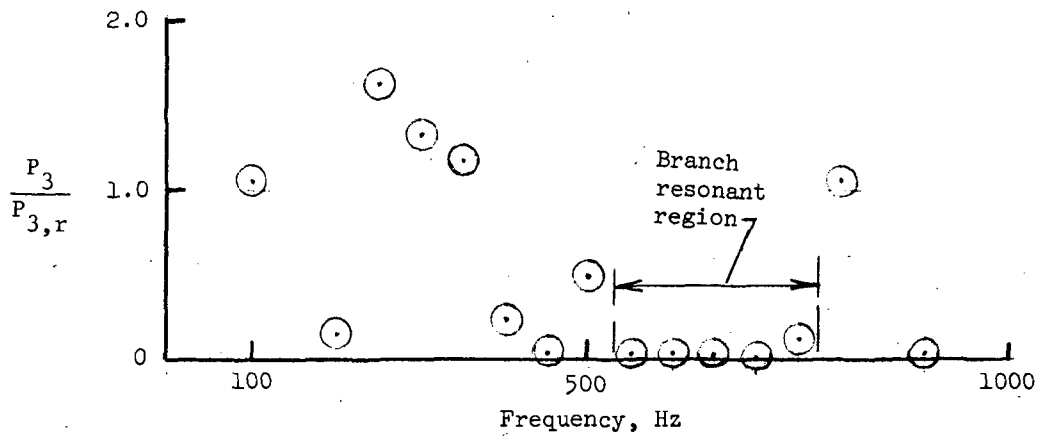

Figure 7.- Pressure ratio versus frequency for test system I (fig. 1); three-branch configuration with 50.8-cm (20.0-in.) branch at station A, 76.2-cm (30.0-in.) branch at station B, and 42.6-cm (16.8-in.) branch at station C.

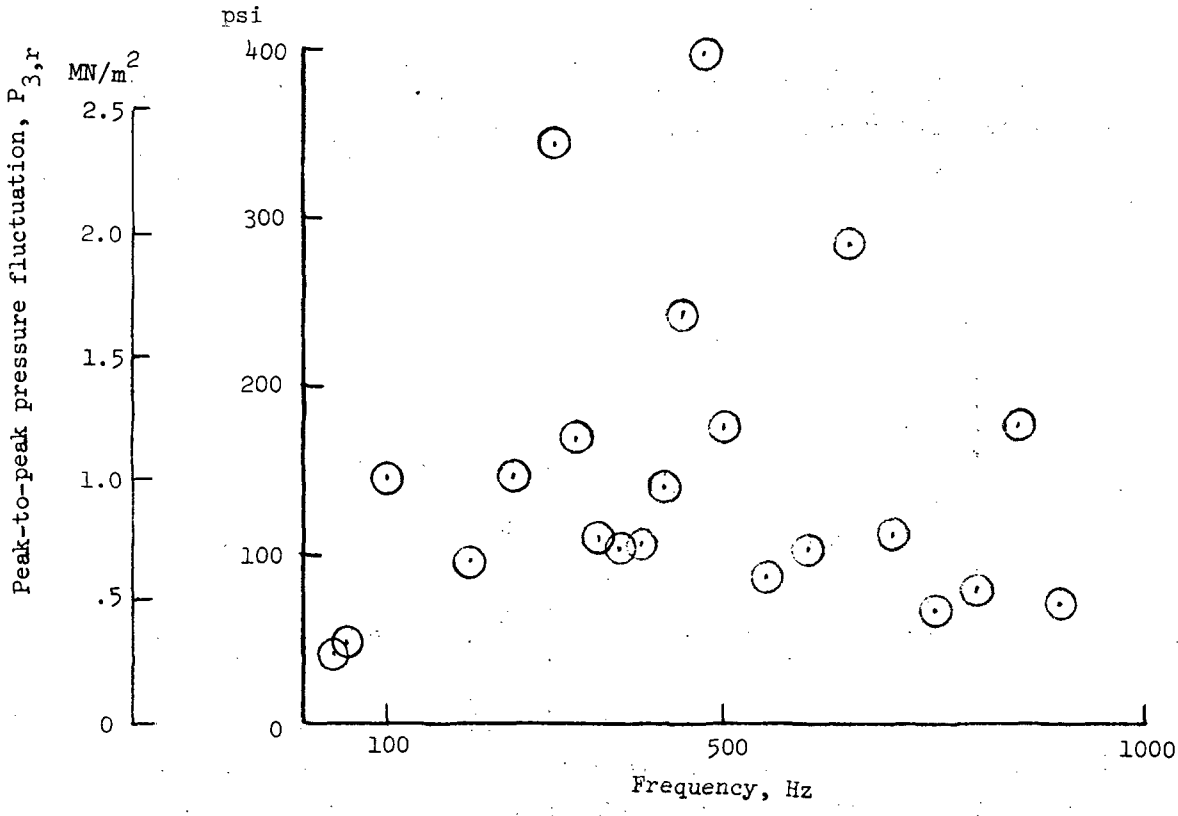

Figure 8.- Peak-to-peak pressure fluctuation versus frequency for test system II (fig. 2) with no branches; accumulator closed.

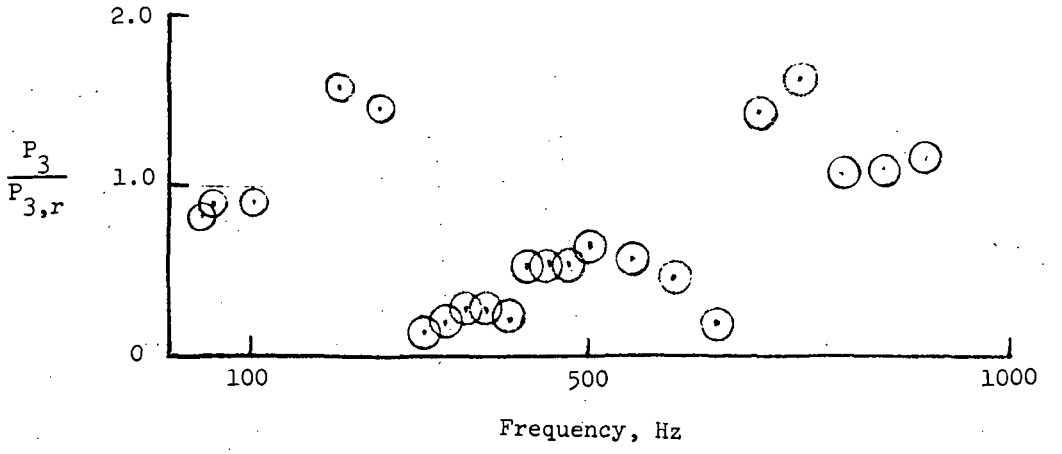

Figure 9.- Pressure ratio versus frequency for test system II (fig. 2); single-branch configuration with 76.2-cm (30.0-in.) branch at station C; accumulator closed.

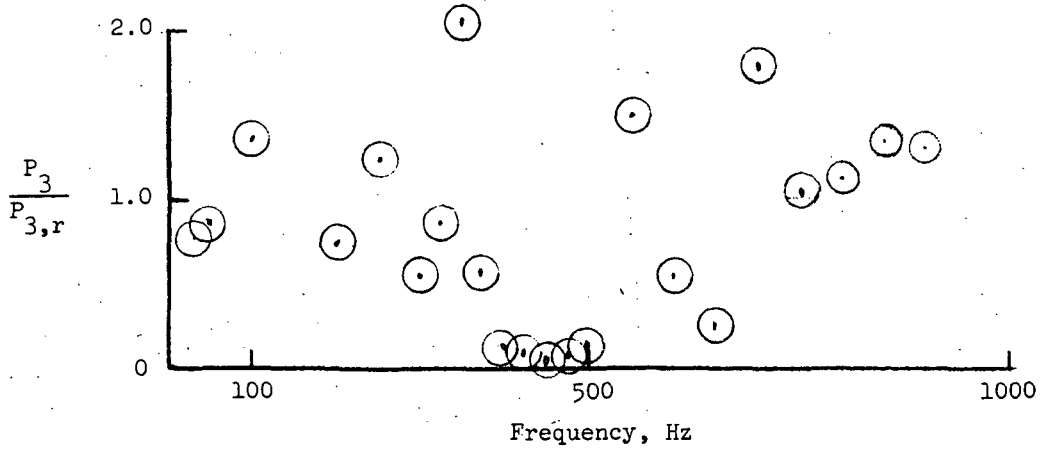

Figure 10.- Pressure ratio versus frequency for test system II (fig. 2); single-branch configuration with 76.2-cm (30.0-in.) branch at station D; accumulator closed.

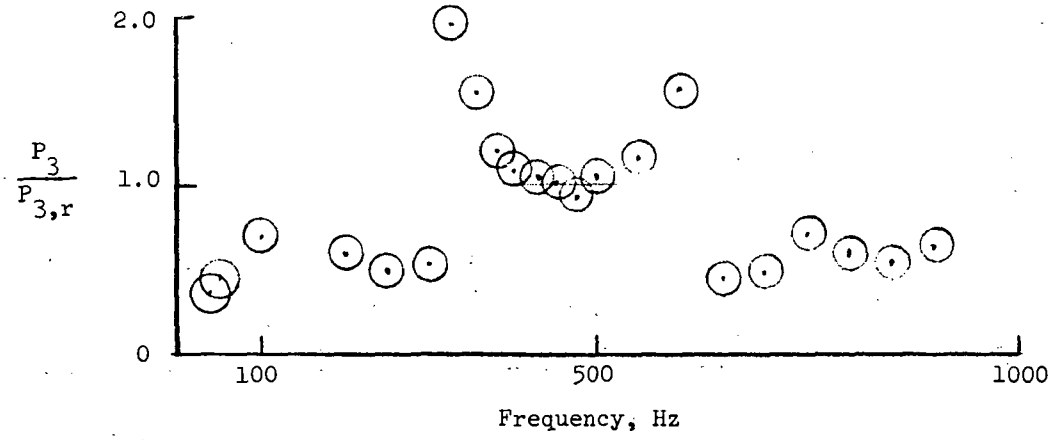

Figure 11.- Pressure ratio versus frequency for test system II (fig. 2); single-branch configuration with 76.2-cm (30.0-in.) branch inlet at station C; 90° bend in the branch near its inlet; accumulator closed.

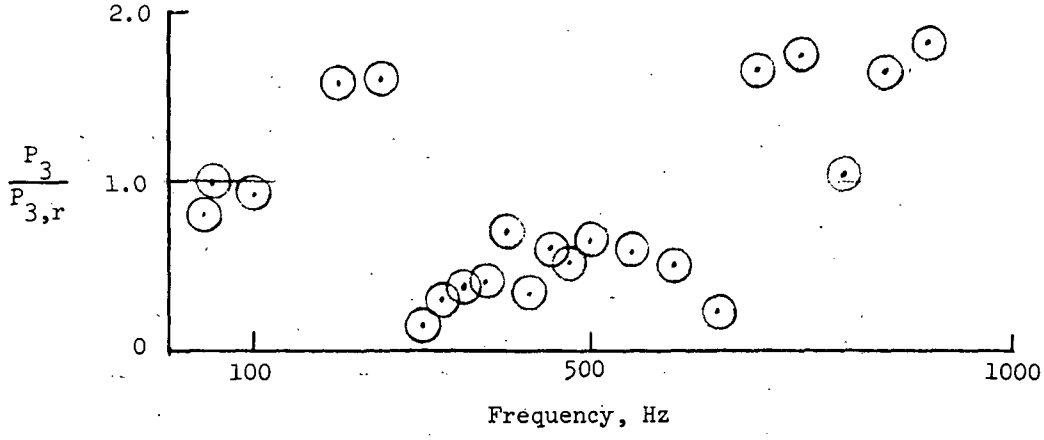

Figure 12.- Pressure ratio versus frequency for test system II (fig. 2); single-branch configuration with 76.2-cm (30.0-in.) branch at station C; rounded branch inlet; accumulator closed.

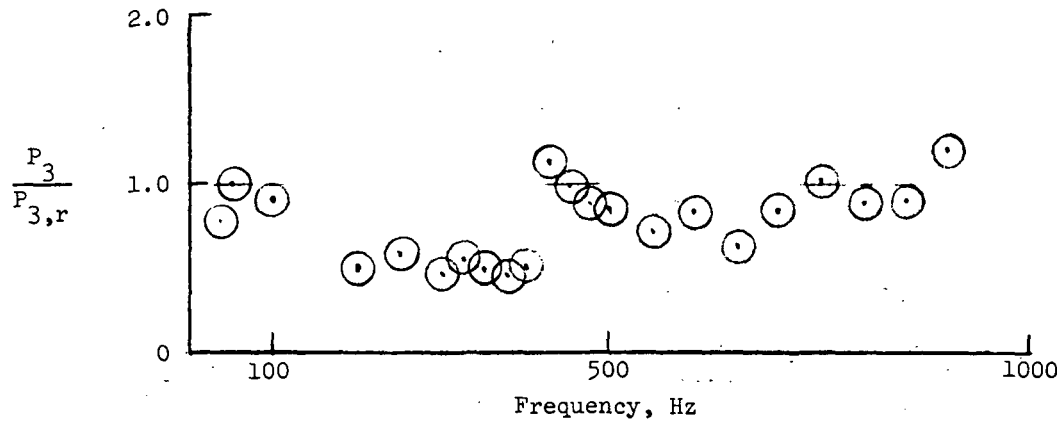

Figure 13.- Pressure ratio versus frequency for test system II (fig. 2); two-common-branch configuration with 0.635-cm (1/4-in.) outside diameter, 76.2-cm (30.0-in.) branches at station C; accumulator closed.

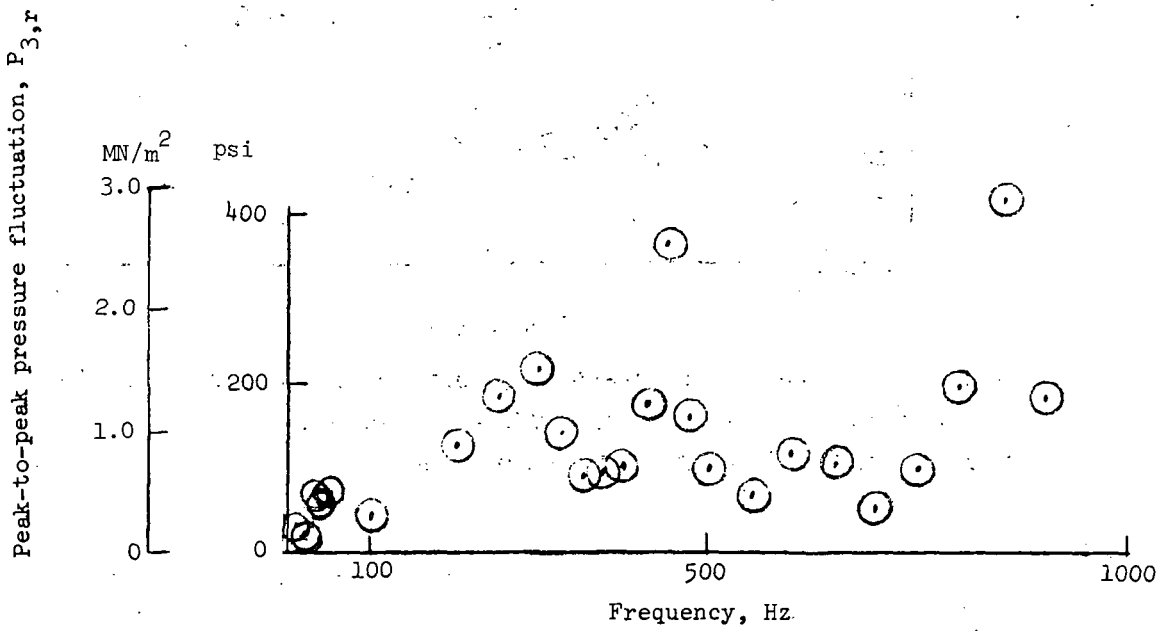

Figure 14.- Peak-to-peak pressure fluctuation versus frequency for test system II (fig. 2) with no branches; accumulator open.

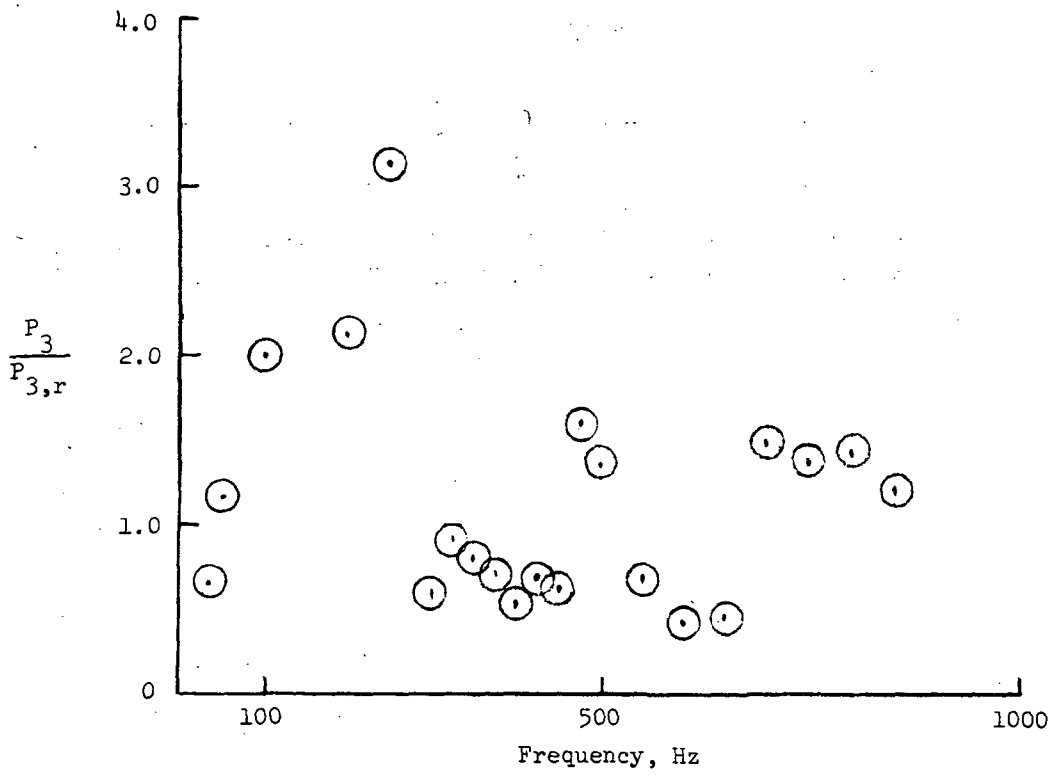

Figure 15.- Pressure ratio versus frequency for test system II (fig. 2); single-branch configuration with 76.2-cm (30.0-in.) branch at station C; standard T-joint; accumulator open.

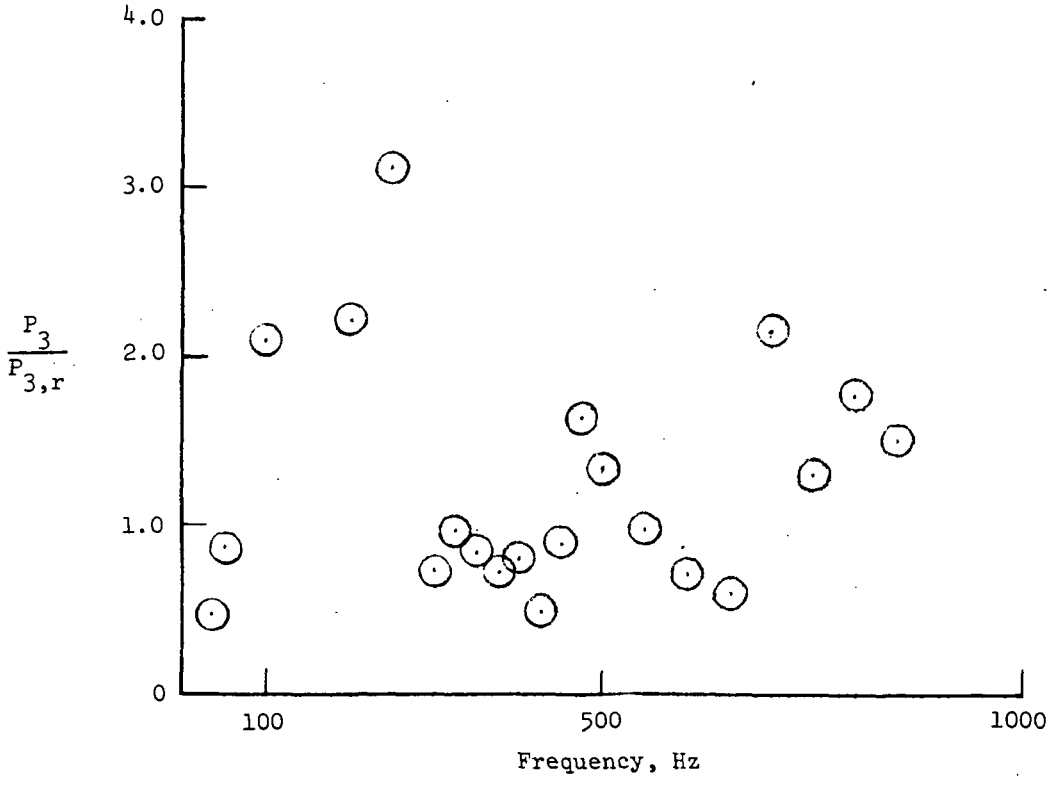

Figure 16.- Pressure ratio versus frequency for test system II (fig. 2); single-branch configuration with 76.2-cm (30.0-in.) branch at station C; standard T-joint; 90° bend at branch inlet; accumulator open.

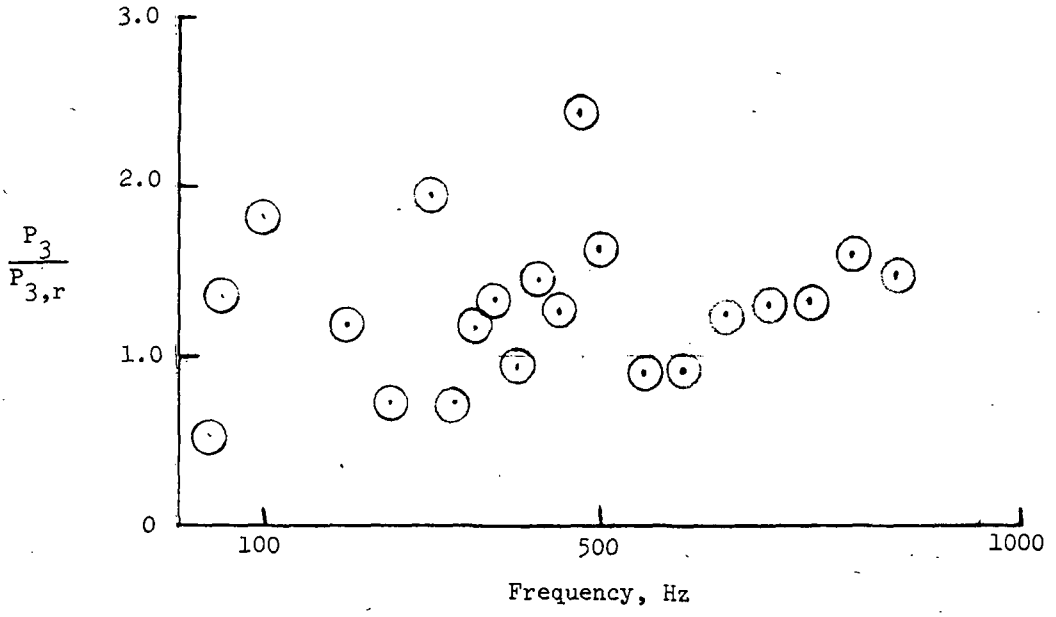

Figure 17.- Pressure ratio versus frequency for test system II (fig. 2); two-common-branch configuration with 0.635-cm (1/4-in.) outside diameter, 76.2-cm (30.0-in.) branches at station C; accumulator open.

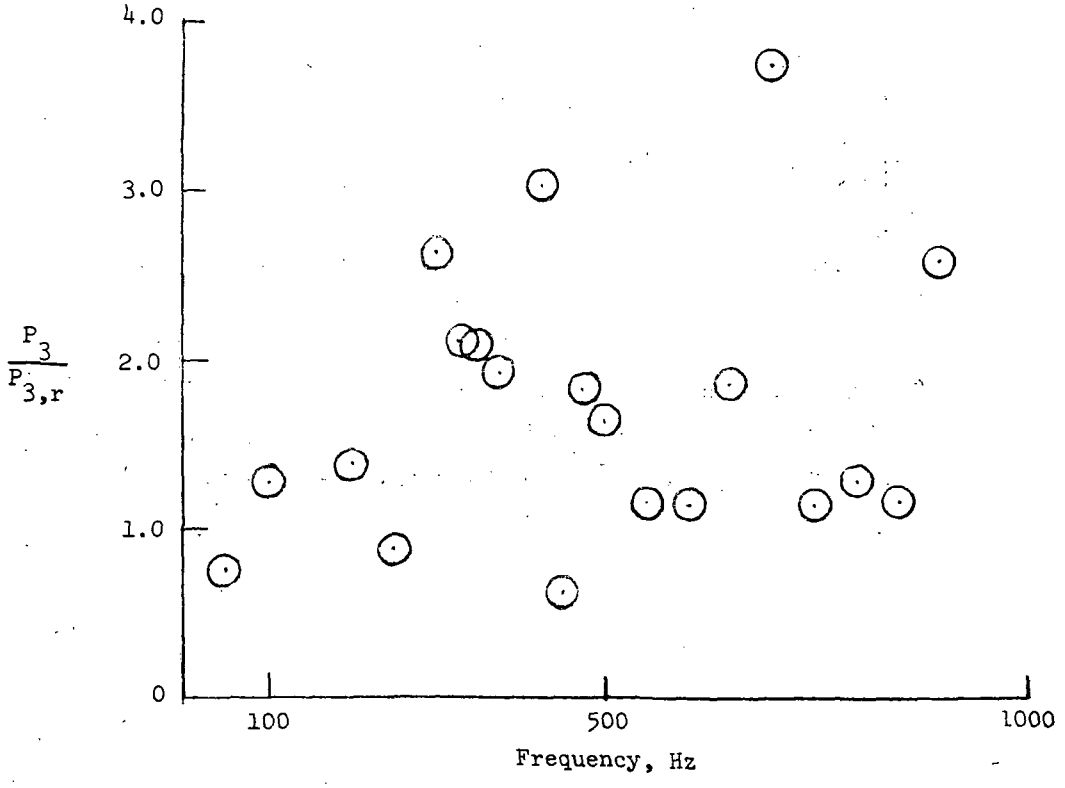

Figure 18.- Pressure ratio versus frequency for test system II (fig. 2); single-branch configuration with 76.2-cm (30.0-in.) branch at station A; accumulator open.

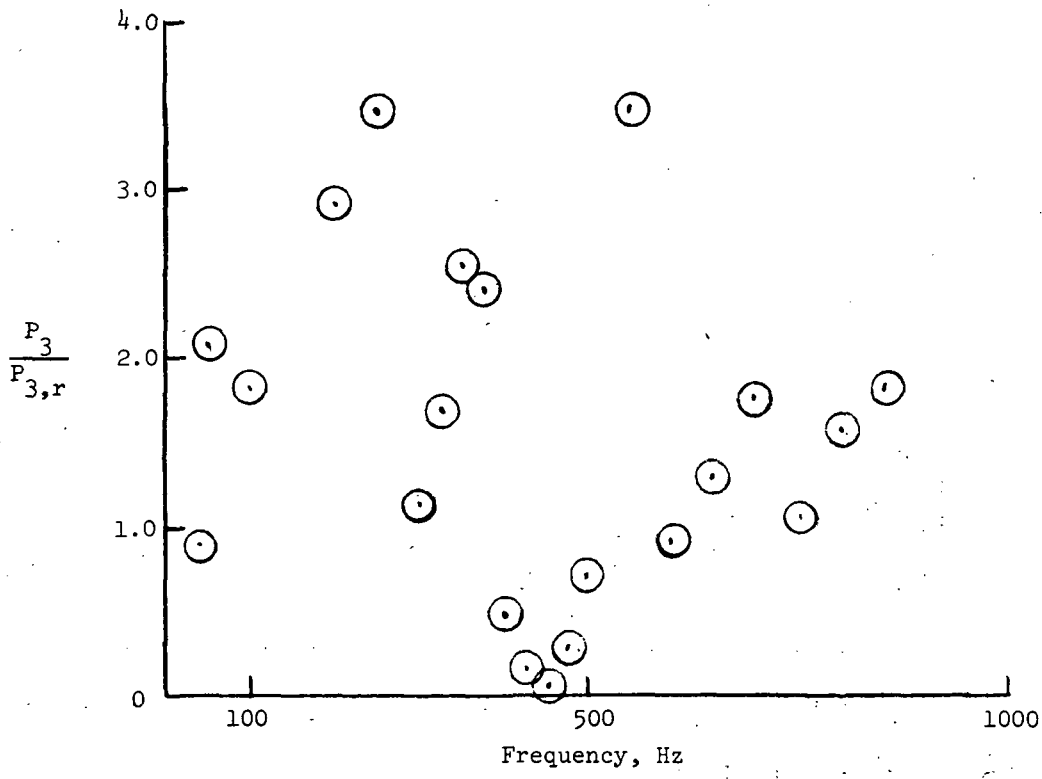

Figure 19.- Pressure ratio versus frequency for test system II (fig. 2); single-branch configuration with 76.2-cm (30.0-in.) branch at station B; accumulator open.

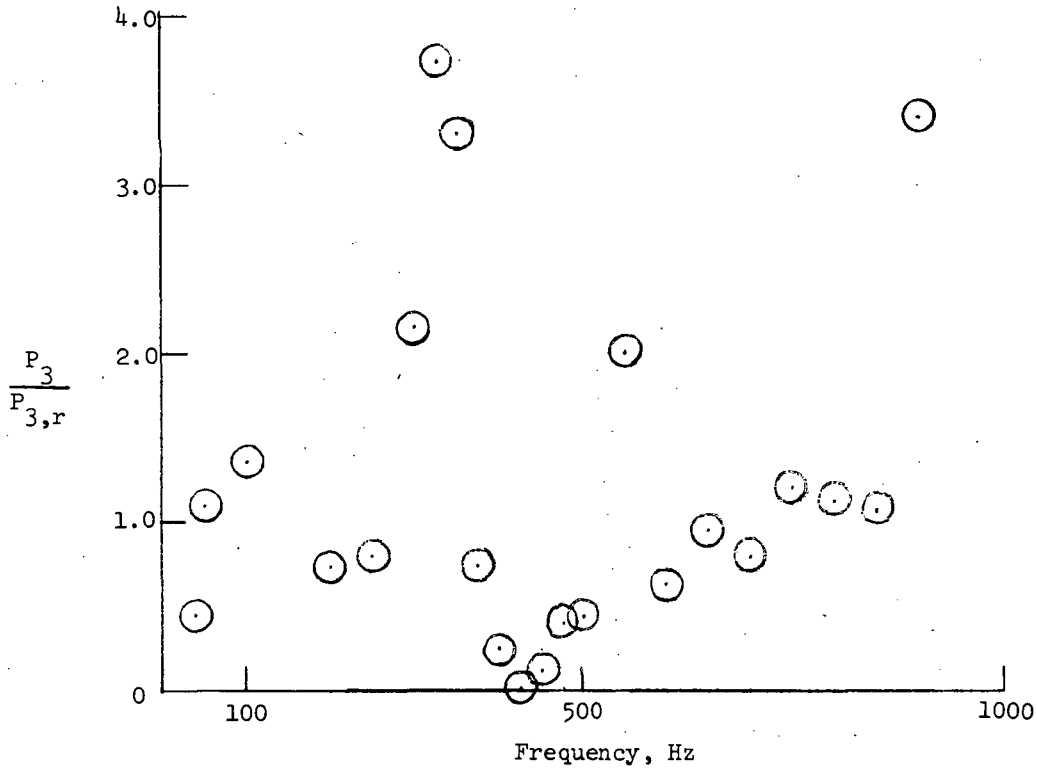

Figure 20.- Pressure ratio versus frequency for test system II (fig. 2); single-branch configuration with 76.2-cm (30.0-in.) branch at station D; accumulator open.

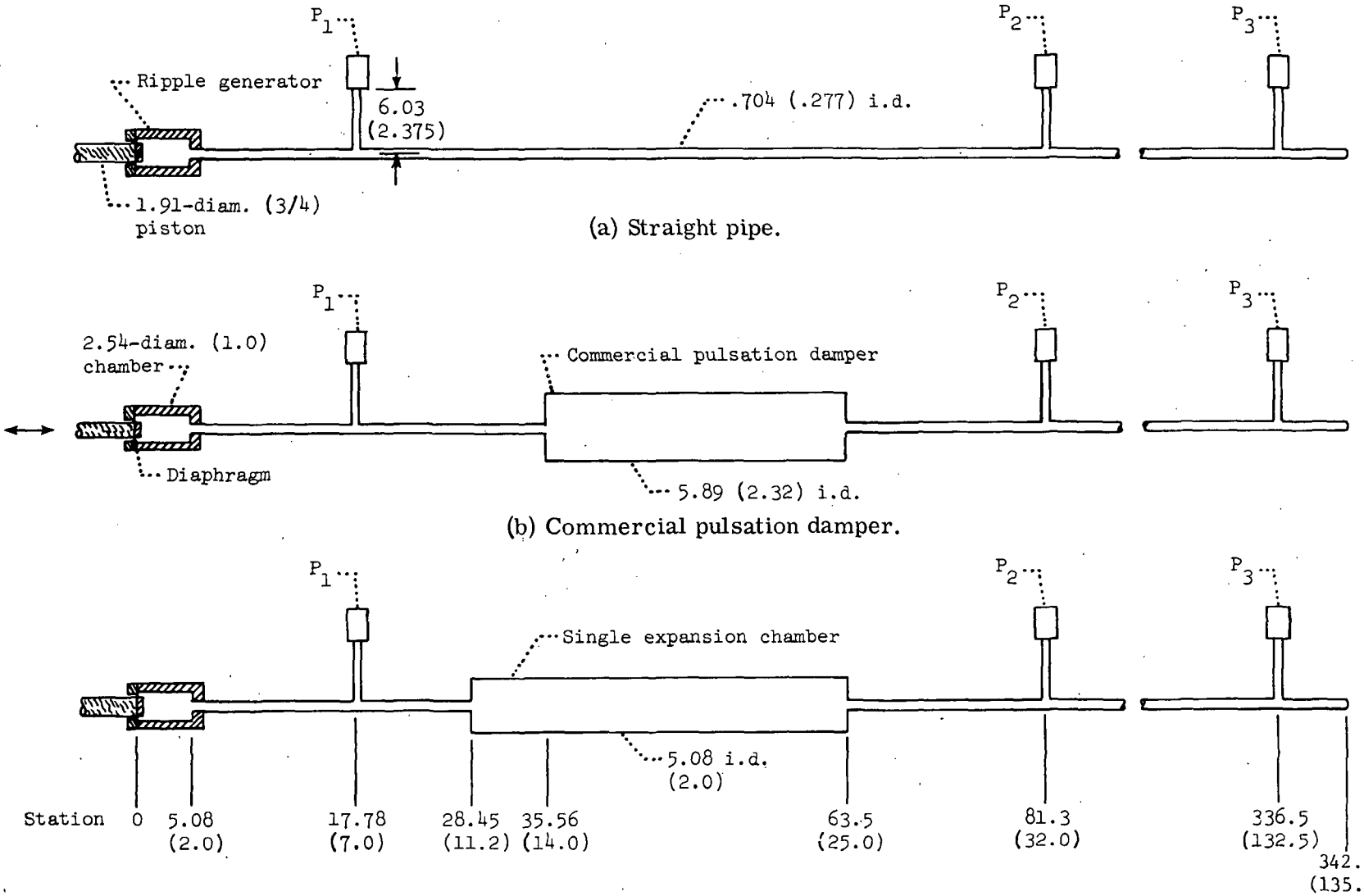

Figure 21.- Test systems for pulsation dampers. Dimensions are in centimeters (inches).

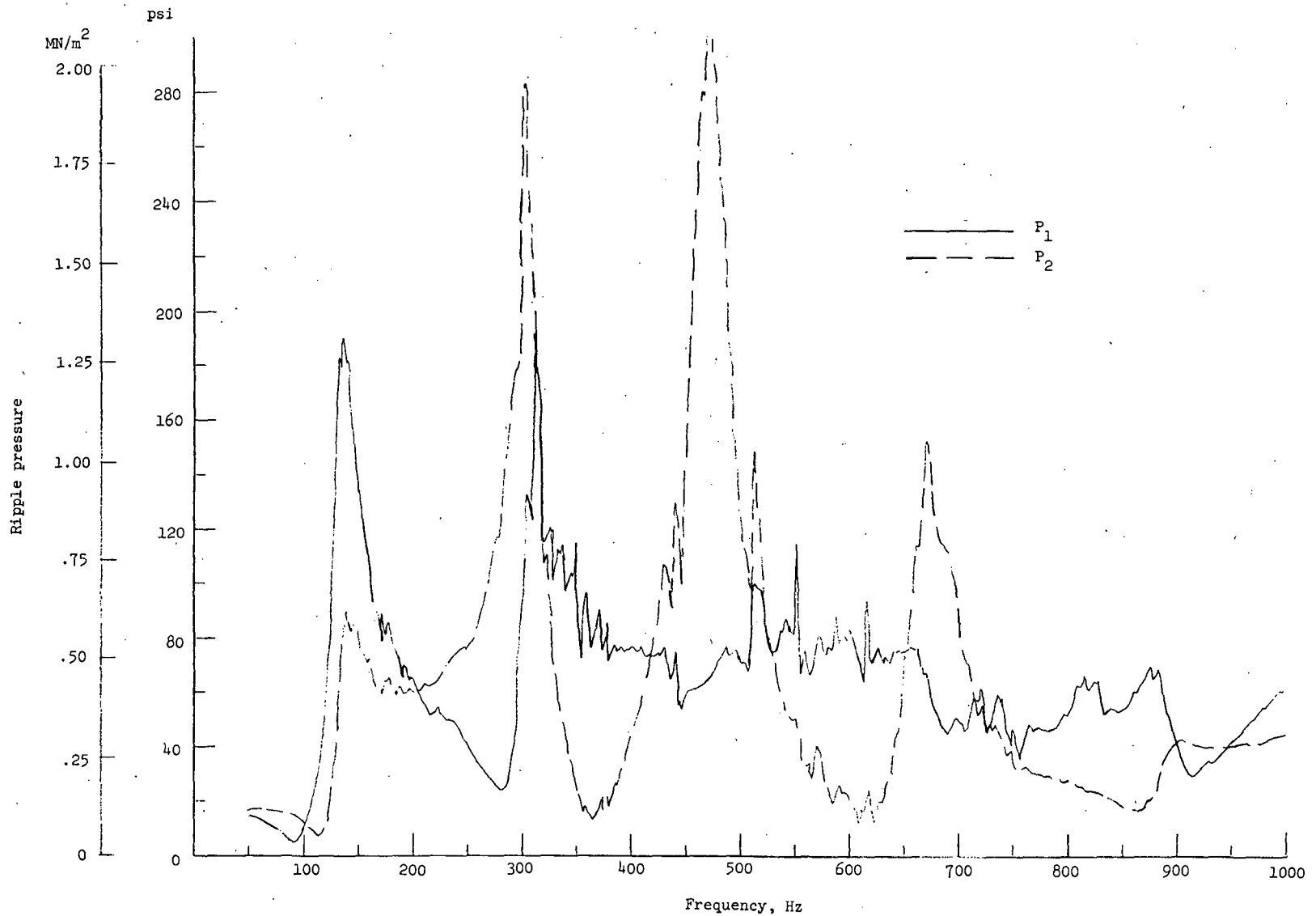

(a) P_1 and P_2.

Figure 22.- Ripple pressure as function of frequency for straight pipe (see fig. 21(a)).

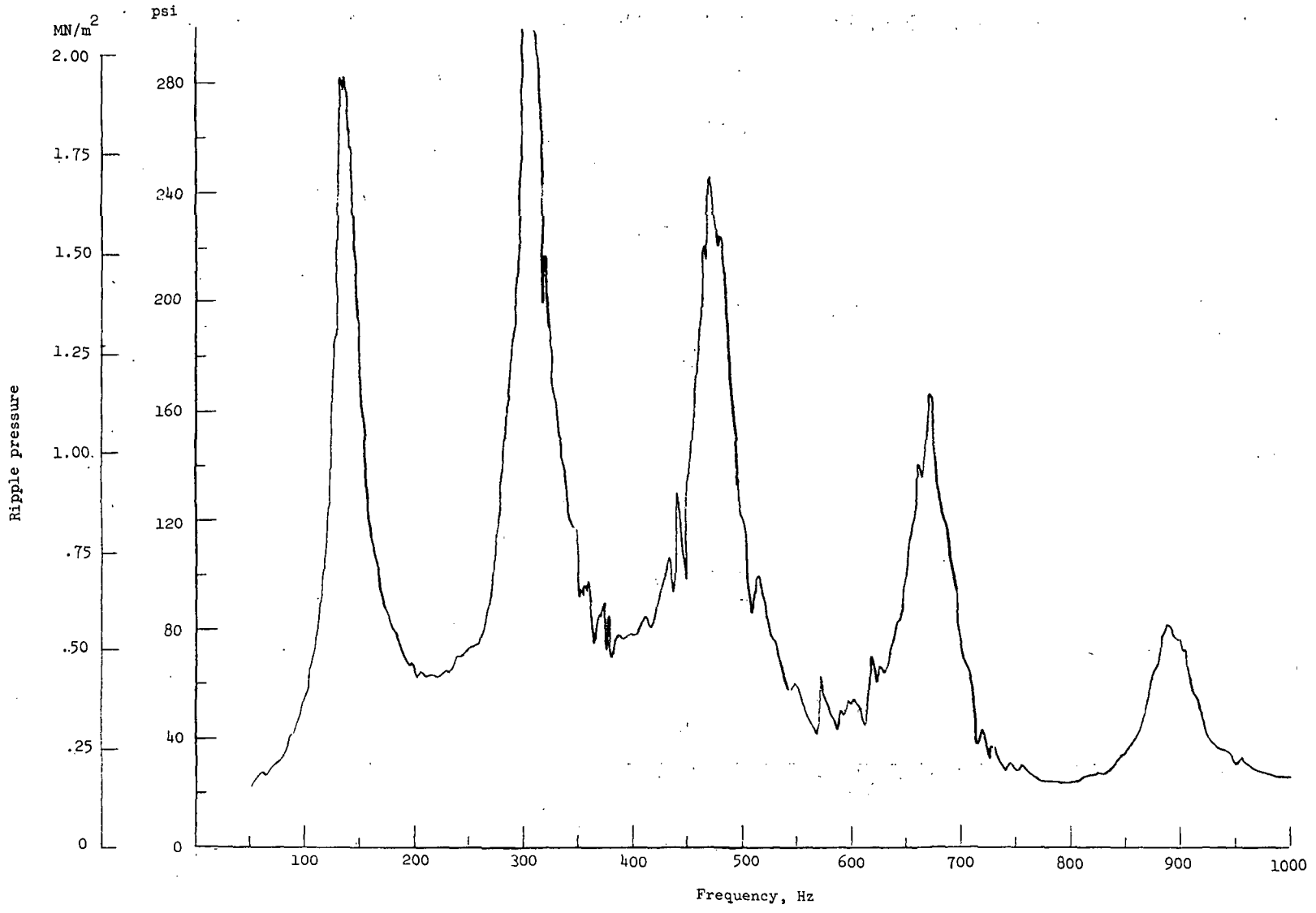

(b) P_3.

Figure 22.- Concluded.

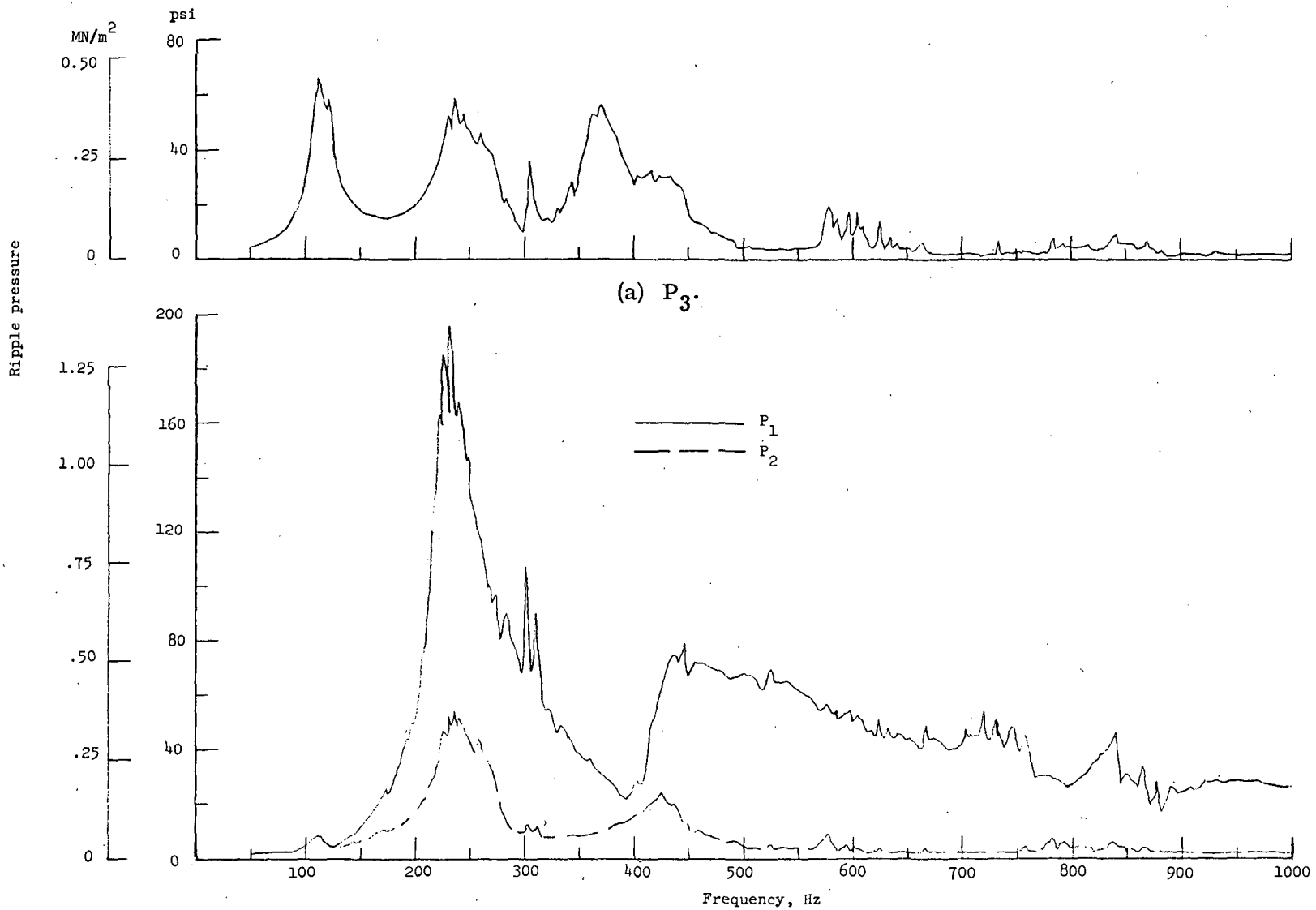

Figure 23.- Ripple pressure as function of frequency for commercial pulsation damper (see fig. 21(b)).

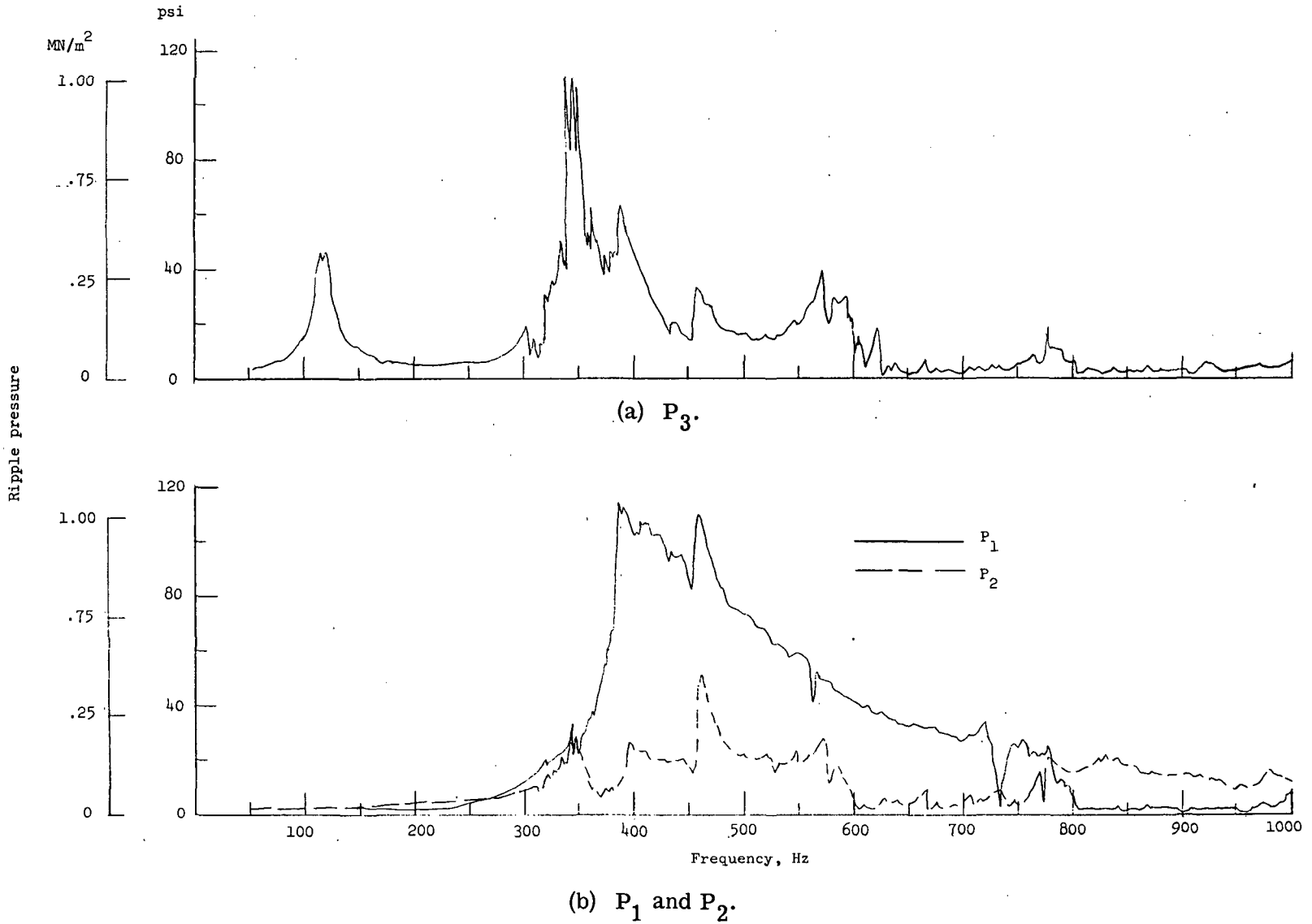

Figure 24.- Ripple pressure as function of frequency for single expansion chamber (see fig. 21(c)).

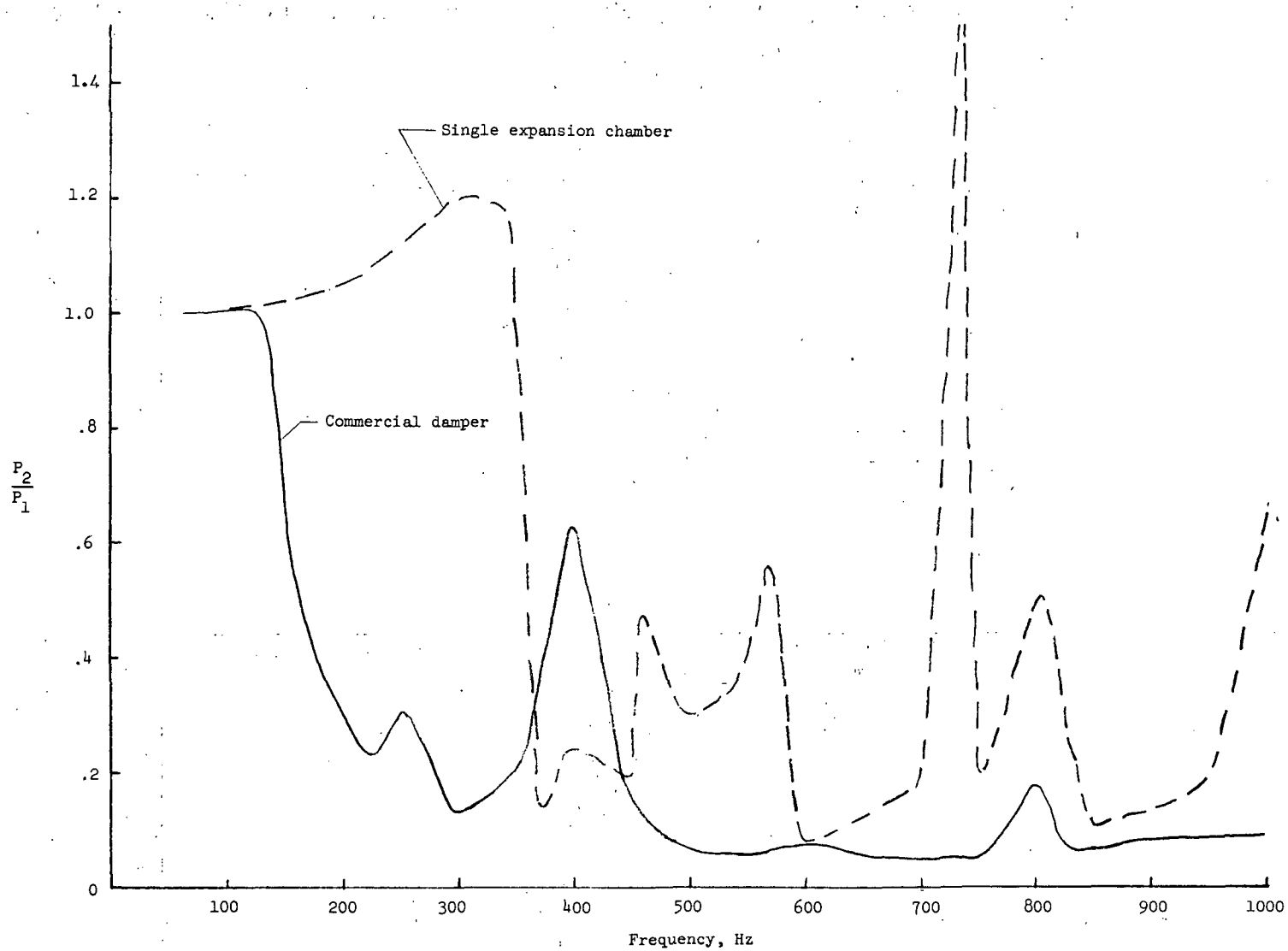

Figure 25.- Ratios of damper outlet-to-inlet pressure.

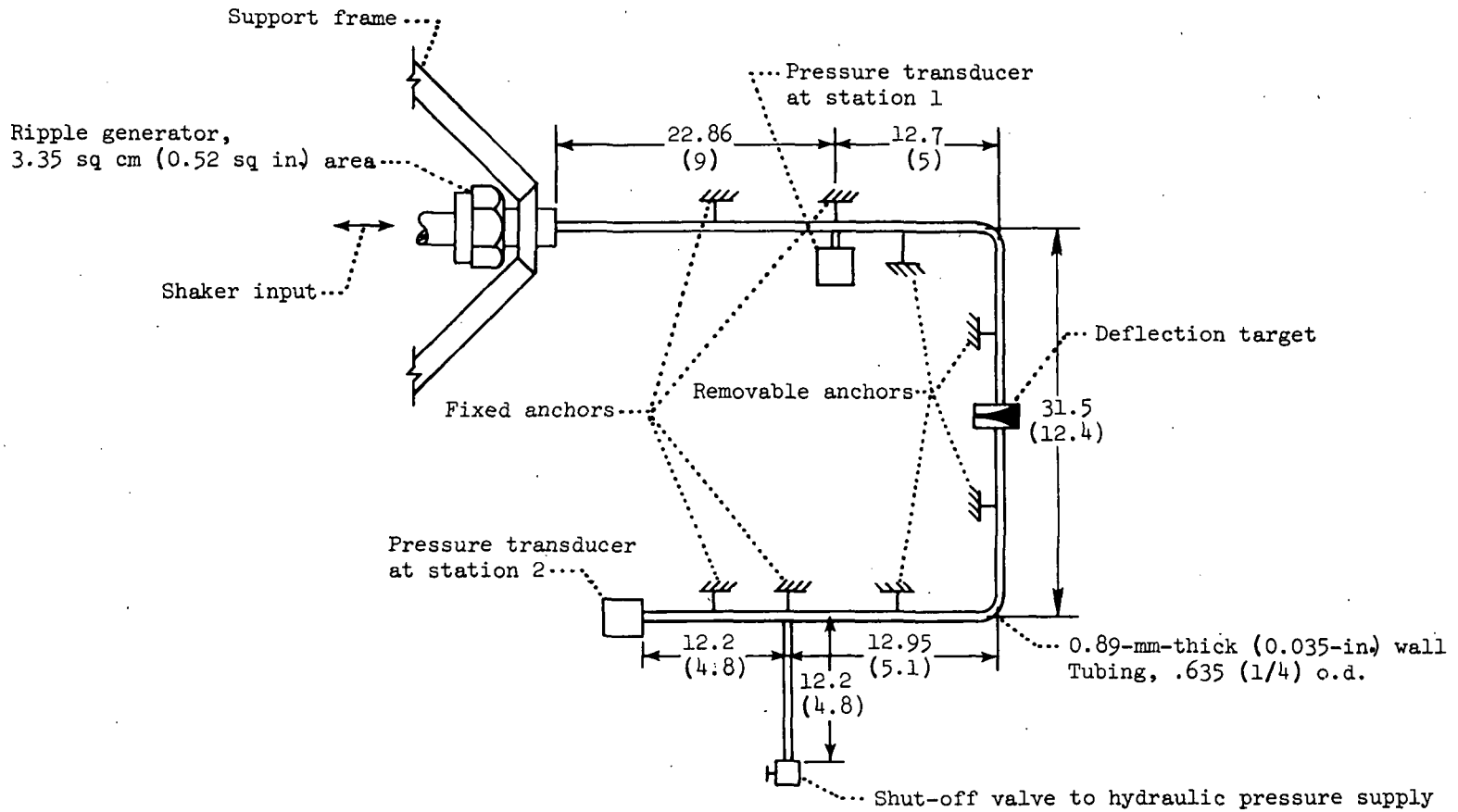

Figure 26.- Schematic diagram of U-tube test configuration. All dimensions in centimeters (inches) except as noted.

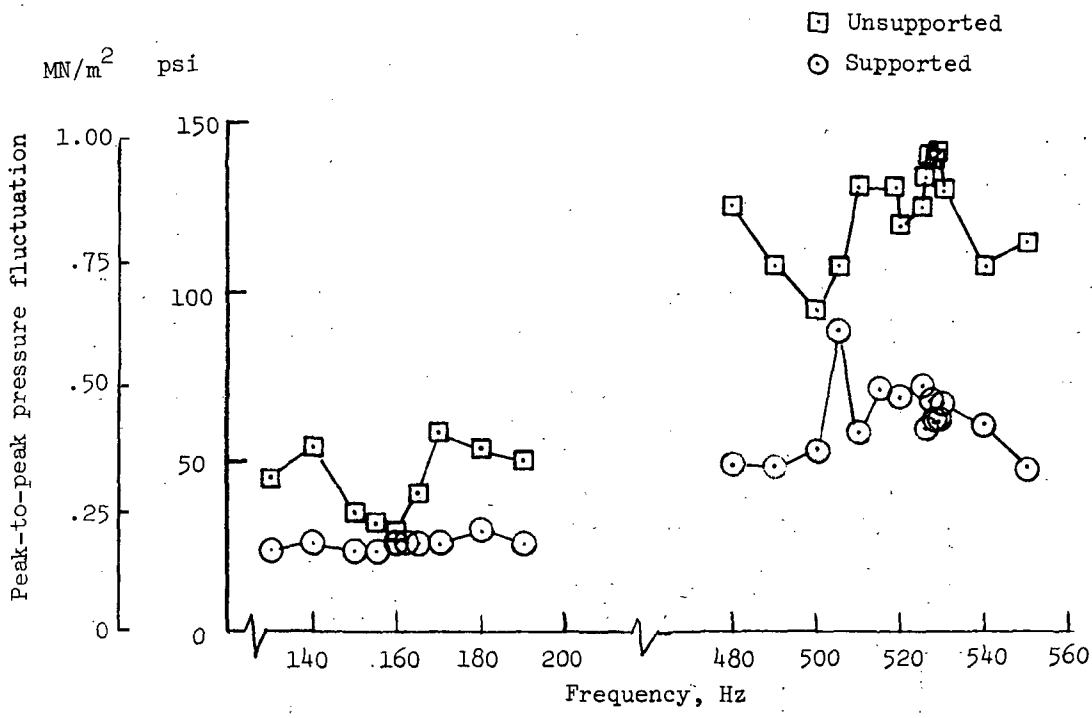

Figure 27.- Upstream pressure (station 1) versus frequency for U-tube configuration (see fig. 26).

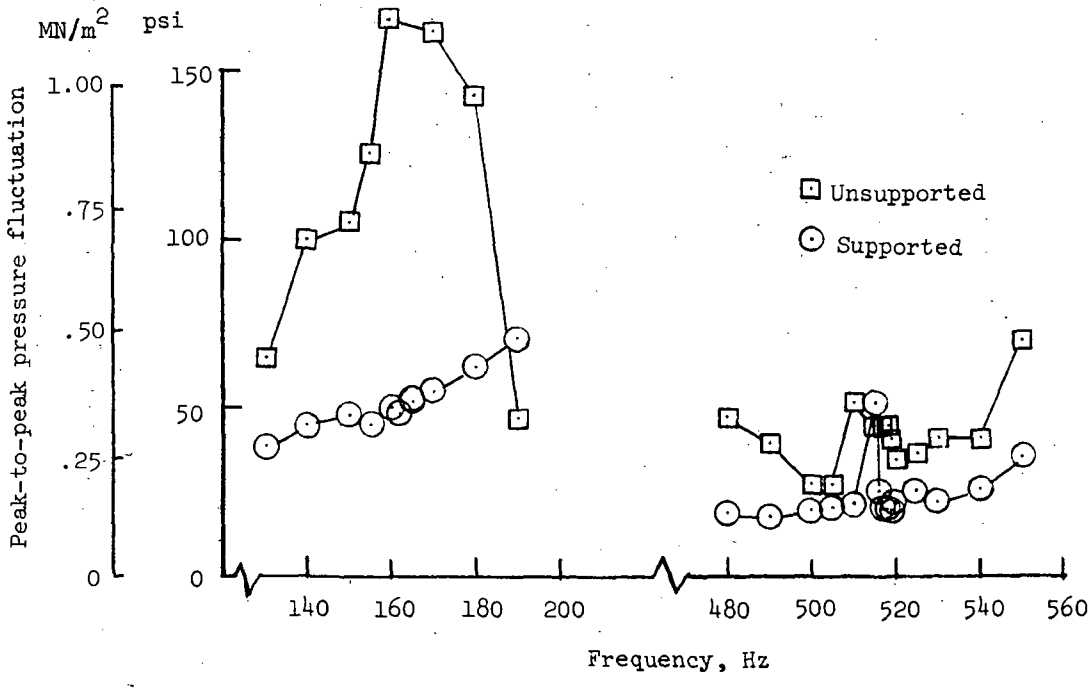

Figure 28.- Downstream pressure (station 2) versus frequency for U-tube configuration (see fig. 26).

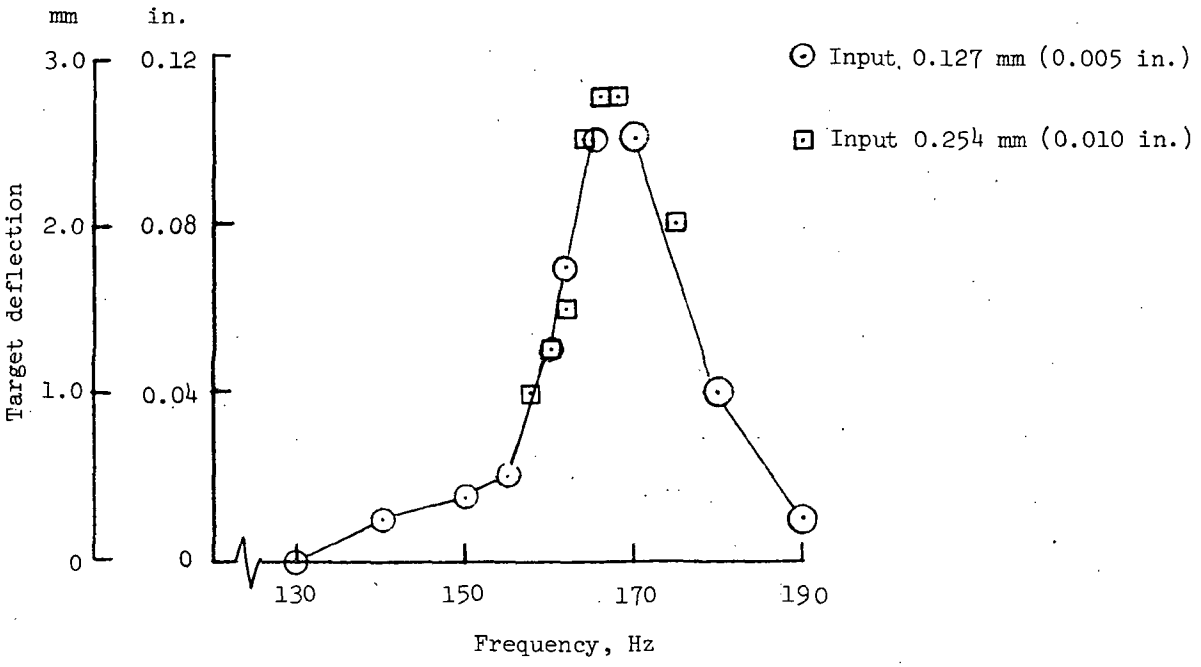

Figure 29.- Target deflection versus frequency of two inputs for U-tube configuration (see fig. 26).

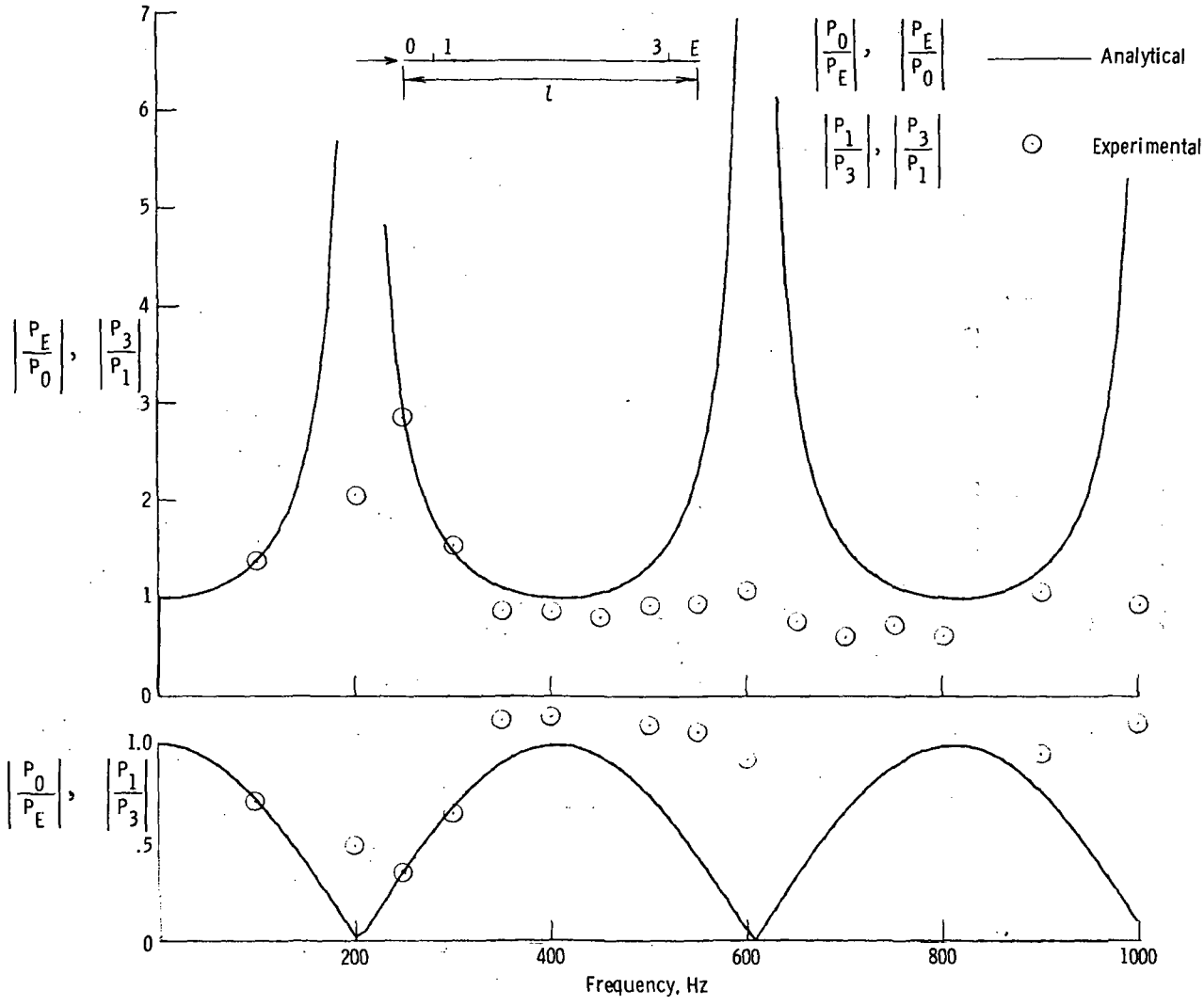

Figure 30.- Perturbation pressure ratios for test system I (fig. 1) without branches; ℓ = 152.4 cm (60.0 in.).

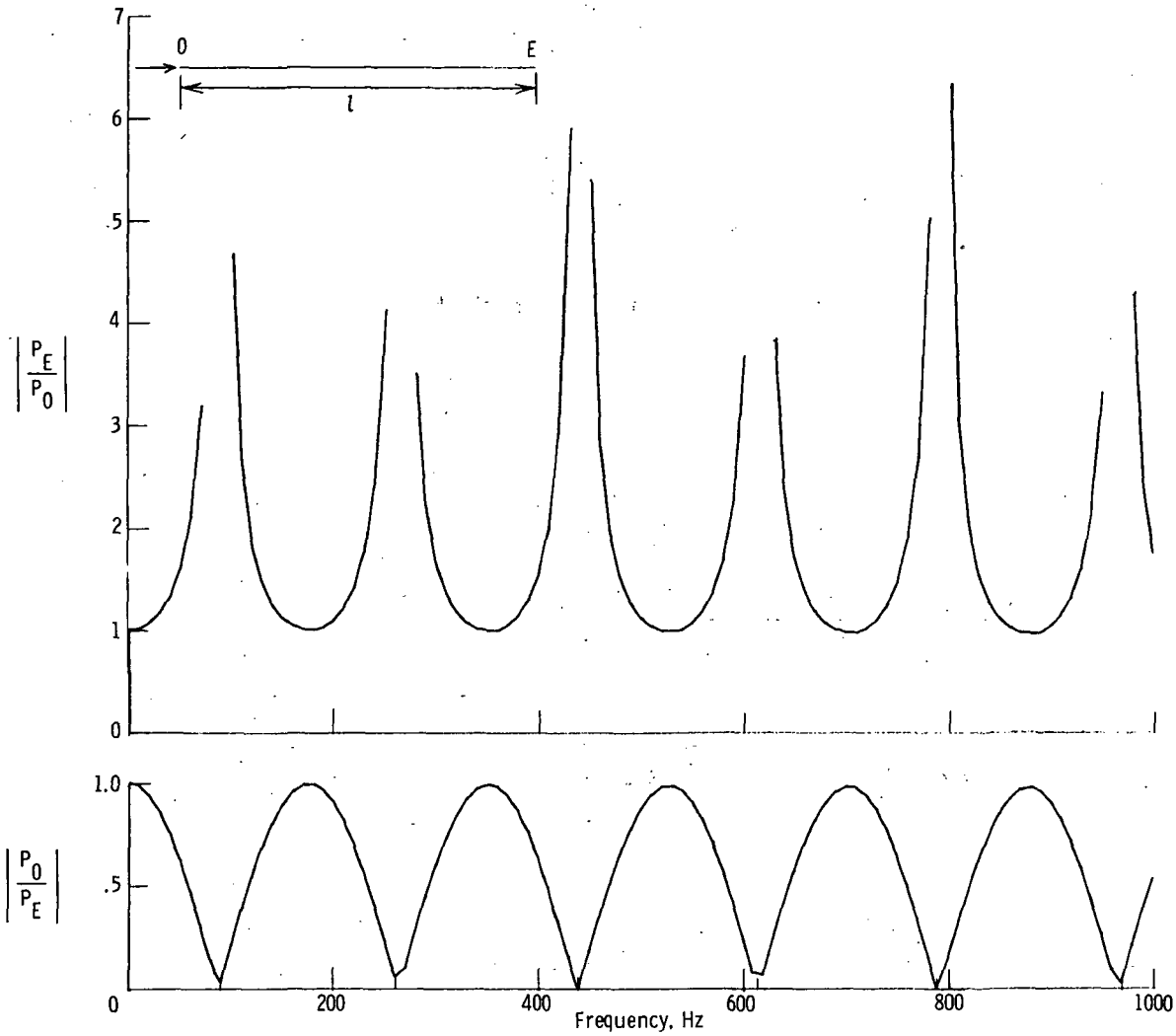

Figure 31. - Terminal perturbation pressure ratios for test system II (fig. 2) without branches; l = 351.8 cm (138.5 in.).

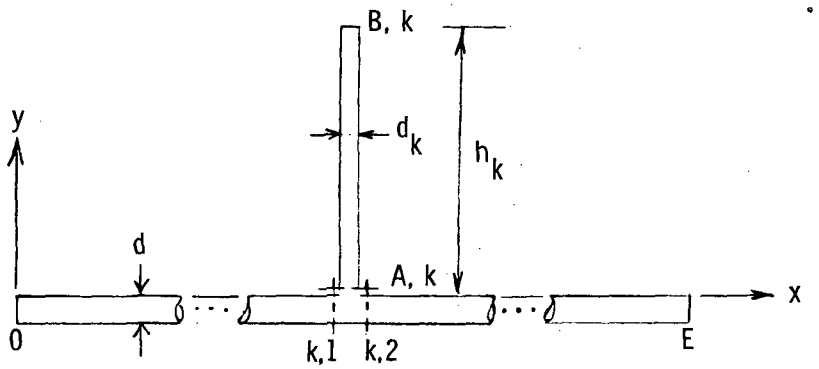

Figure 32.- Geometry of the kth branch.

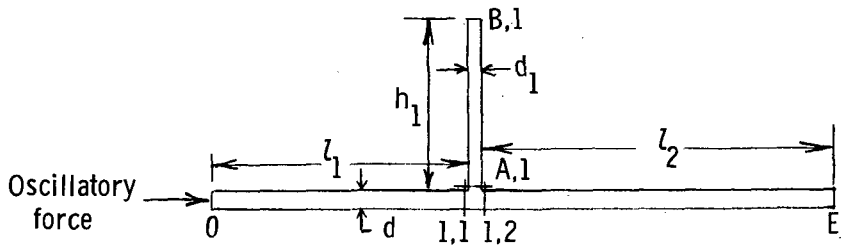

$$\frac{P_0}{P_E} = \cos\frac{\omega}{c}(l_1 + l_2) - \left(\frac{d_1}{d}\right)^2 \tan\frac{\omega h_1}{c} \sin\frac{\omega l_1}{c} \cos\frac{\omega l_2}{c}$$

$$+ j\frac{Z_0}{Z_E}\left[\sin\frac{\omega}{c}(l_1 + l_2) - \left(\frac{d_1}{d}\right)^2 \tan\frac{\omega h_1}{c} \sin\frac{\omega l_1}{c} \sin\frac{\omega l_2}{c}\right]$$

$$\frac{Z_0 U_0}{P_E} = \frac{Z_0}{Z_E}\left[\cos\frac{\omega}{c}(l_1 + l_2) - \left(\frac{d_1}{d}\right)^2 \tan\frac{\omega h_1}{c} \cos\frac{\omega l_1}{c} \sin\frac{\omega l_2}{c}\right]$$

$$+ j\left[\sin\frac{\omega}{c}(l_1 + l_2) + \left(\frac{d_1}{d}\right)^2 \tan\frac{\omega h_1}{c} \cos\frac{\omega l_1}{c} \cos\frac{\omega l_2}{c}\right]$$

Figure 33.- Geometry and terminal perturbation pressure and velocity ratios for single-branch configuration.

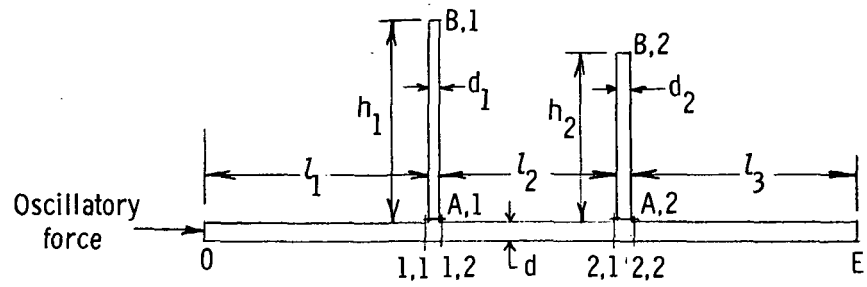

$$\frac{P_0}{P_E} = \cos\frac{\omega}{c}(l_1 + l_2 + l_3) - \left(\frac{d_1}{d}\right)^2 \tan\frac{\omega h_1}{c} \sin\frac{\omega l_1}{c} \cos\frac{\omega}{c}(l_2 + l_3)$$

$$+ \left(\frac{d_2}{d}\right)^2 \tan\frac{\omega h_2}{c} \cos\frac{\omega l_3}{c}\left[\left(\frac{d_1}{d}\right)^2 \tan\frac{\omega h_1}{c} \sin\frac{\omega l_1}{c} \sin\frac{\omega l_2}{c} - \sin\frac{\omega}{c}(l_1 + l_2)\right]$$

$$+ j\frac{Z_0}{Z_E}\left\{\sin\frac{\omega}{c}(l_1 + l_2 + l_3) - \left(\frac{d_1}{d}\right)^2 \tan\frac{\omega h_1}{c} \sin\frac{\omega l_1}{c} \sin\frac{\omega}{c}(l_2 + l_3)\right.$$

$$\left. + \left(\frac{d_2}{d}\right)^2 \tan\frac{\omega h_2}{c} \sin\frac{\omega l_3}{c}\left[\left(\frac{d_1}{d}\right)^2 \tan\frac{\omega h_1}{c} \sin\frac{\omega l_1}{c} \sin\frac{\omega l_2}{c} - \sin\frac{\omega}{c}(l_1 + l_2)\right]\right\}$$

$$\frac{Z_0 U_0}{P_E} = \frac{Z_0}{Z_E}\left\{\cos\frac{\omega}{c}(l_1 + l_2 + l_3) - \left(\frac{d_1}{d}\right)^2 \tan\frac{\omega h_1}{c} \cos\frac{\omega l_1}{c} \sin\frac{\omega}{c}(l_2 + l_3)\right.$$

$$\left. + \left(\frac{d_2}{d}\right)^2 \tan\frac{\omega h_2}{c} \sin\frac{\omega l_3}{c}\left[\left(\frac{d_1}{d}\right)^2 \tan\frac{\omega h_1}{c} \cos\frac{\omega l_1}{c} \sin\frac{\omega l_2}{c} - \cos\frac{\omega}{c}(l_1 + l_2)\right]\right\}$$

$$+ j\left\{\sin\frac{\omega}{c}(l_1 + l_2 + l_3) + \left(\frac{d_1}{d}\right)^2 \tan\frac{\omega h_1}{c} \cos\frac{\omega l_1}{c} \cos\frac{\omega}{c}(l_2 + l_3)\right.$$

$$\left. - \left(\frac{d_2}{d}\right)^2 \tan\frac{\omega h_2}{c} \cos\frac{\omega l_3}{c}\left[\left(\frac{d_1}{d}\right)^2 \tan\frac{\omega h_1}{c} \cos\frac{\omega l_1}{c} \sin\frac{\omega l_2}{c} - \cos\frac{\omega}{c}(l_1 + l_2)\right]\right\}$$

Figure 34.- Geometry and terminal perturbation pressure and velocity ratios for two-branch configuration.

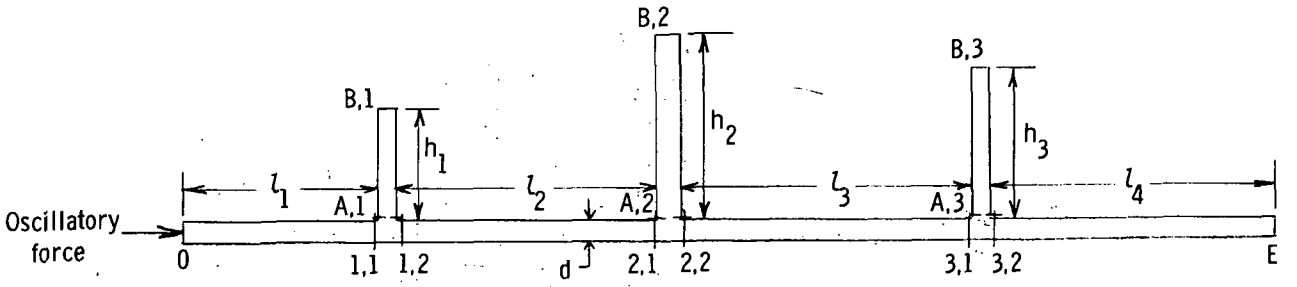

$$\frac{P_0}{P_E} = \cos\frac{\omega}{c}(l_1 + l_2 + l_3 + l_4) - \left(\frac{d_1}{d}\right)^2 \tan\frac{\omega h_1}{c} \sin\frac{\omega l_1}{c} \cos\frac{\omega}{c}(l_2 + l_3 + l_4)$$

$$+ \left(\frac{d_2}{d}\right)^2 \tan\frac{\omega h_2}{c}\left[\left(\frac{d_1}{d}\right)^2 \tan\frac{\omega h_1}{c} \sin\frac{\omega l_1}{c} \sin\frac{\omega l_2}{c} - \sin\frac{\omega}{c}(l_1 + l_2)\right]\left[\cos\frac{\omega}{c}(l_3 + l_4) - \left(\frac{d_3}{d}\right)^2 \tan\frac{\omega h_3}{c} \sin\frac{\omega l_3}{c} \cos\frac{\omega l_4}{c}\right]$$

$$+ \left(\frac{d_3}{d}\right)^2 \tan\frac{\omega h_3}{c} \cos\frac{\omega l_4}{c}\left[\left(\frac{d_1}{d}\right)^2 \tan\frac{\omega h_1}{c} \sin\frac{\omega l_1}{c} \sin\frac{\omega}{c}(l_2 + l_3) - \sin\frac{\omega}{c}(l_1 + l_2 + l_3)\right]$$

$$+ j\frac{Z_0}{Z_E}\left\{\sin\frac{\omega}{c}(l_1 + l_2 + l_3 + l_4) - \left(\frac{d_1}{d}\right)^2 \tan\frac{\omega h_1}{c} \sin\frac{\omega l_1}{c} \sin\frac{\omega}{c}(l_2 + l_3 + l_4)\right.$$

$$+ \left(\frac{d_2}{d}\right)^2 \tan\frac{\omega h_2}{c}\left[\left(\frac{d_1}{d}\right)^2 \tan\frac{\omega h_1}{c} \sin\frac{\omega l_1}{c} \sin\frac{\omega l_2}{c} - \sin\frac{\omega}{c}(l_1 + l_2)\right]\left[\sin\frac{\omega}{c}(l_3 + l_4) - \left(\frac{d_3}{d}\right)^2 \tan\frac{\omega h_3}{c} \sin\frac{\omega l_3}{c} \sin\frac{\omega l_4}{c}\right]$$

$$\left. + \left(\frac{d_3}{d}\right)^2 \tan\frac{\omega h_3}{c} \sin\frac{\omega l_4}{c}\left[\left(\frac{d_1}{d}\right)^2 \tan\frac{\omega h_1}{c} \sin\frac{\omega l_1}{c} \sin\frac{\omega}{c}(l_2 + l_3) - \sin\frac{\omega}{c}(l_1 + l_2 + l_3)\right]\right\}$$

$$\frac{Z_0 U_0}{P_E} = \frac{Z_0}{Z_E}\left\{\cos\frac{\omega}{c}(l_1 + l_2 + l_3 + l_4) - \left(\frac{d_1}{d}\right)^2 \tan\frac{\omega h_1}{c} \cos\frac{\omega l_1}{c} \sin\frac{\omega}{c}(l_2 + l_3 + l_4)\right.$$

$$+ \left(\frac{d_2}{d}\right)^2 \tan\frac{\omega h_2}{c}\left[\left(\frac{d_1}{d}\right)^2 \tan\frac{\omega h_1}{c} \cos\frac{\omega l_1}{c} \sin\frac{\omega l_2}{c} - \cos\frac{\omega}{c}(l_1 + l_2)\right]\left[\sin\frac{\omega}{c}(l_3 + l_4) - \left(\frac{d_3}{d}\right)^2 \tan\frac{\omega h_3}{c} \sin\frac{\omega l_3}{c} \sin\frac{\omega l_4}{c}\right]$$

$$\left. + \left(\frac{d_3}{d}\right)^2 \tan\frac{\omega h_3}{c} \sin\frac{\omega l_4}{c}\left[\left(\frac{d_1}{d}\right)^2 \tan\frac{\omega h_1}{c} \cos\frac{\omega l_1}{c} \sin\frac{\omega}{c}(l_2 + l_3) - \cos\frac{\omega}{c}(l_1 + l_2 + l_3)\right]\right\}$$

$$+ j\left\{\sin\frac{\omega}{c}(l_1 + l_2 + l_3 + l_4) + \left(\frac{d_1}{d}\right)^2 \tan\frac{\omega h_1}{c} \cos\frac{\omega l_1}{c} \cos\frac{\omega}{c}(l_2 + l_3 + l_4)\right.$$

$$- \left(\frac{d_2}{d}\right)^2 \tan\frac{\omega h_2}{c}\left[\left(\frac{d_1}{d}\right)^2 \tan\frac{\omega h_1}{c} \cos\frac{\omega l_1}{c} \sin\frac{\omega l_2}{c} - \cos\frac{\omega}{c}(l_1 + l_2)\right]\left[\cos\frac{\omega}{c}(l_3 + l_4) - \left(\frac{d_3}{d}\right)^2 \tan\frac{\omega h_3}{c} \sin\frac{\omega l_3}{c} \cos\frac{\omega l_4}{c}\right]$$

$$\left. - \left(\frac{d_3}{d}\right)^2 \tan\frac{\omega h_3}{c} \cos\frac{\omega l_4}{c}\left[\left(\frac{d_1}{d}\right)^2 \tan\frac{\omega h_1}{c} \cos\frac{\omega l_1}{c} \sin\frac{\omega}{c}(l_2 + l_3) - \cos\frac{\omega}{c}(l_1 + l_2 + l_3)\right]\right\}$$

Figure 35.- Geometry and terminal perturbation pressure and velocity ratios for three-branch configuration.

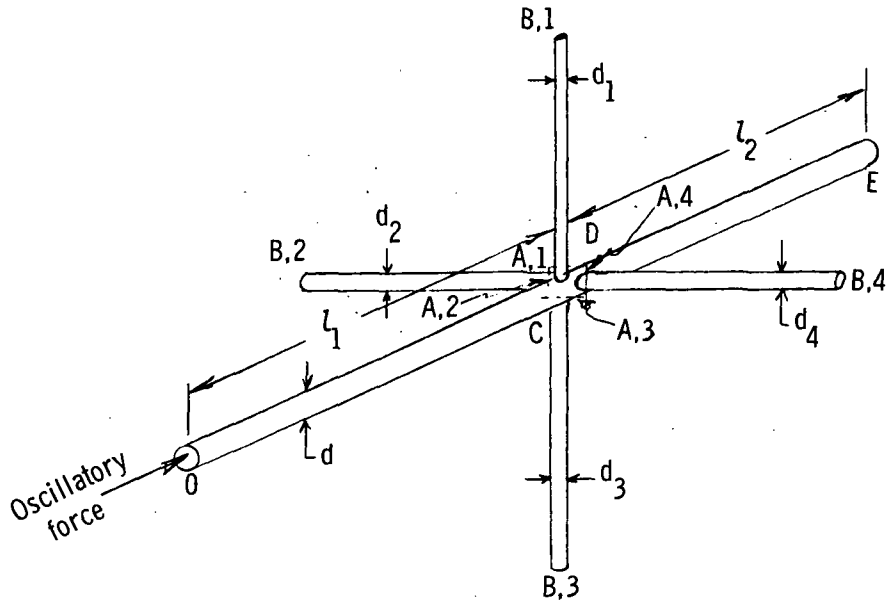

$$\frac{P_0}{P_E} = \cos\frac{\omega}{c}(l_1 + l_2) - \sin\frac{\omega l_1}{c}\cos\frac{\omega l_2}{c}\sum_{m=1}^{M}\left(\frac{d_m}{d}\right)^2\tan\frac{\omega h_m}{c}$$

$$+ j\frac{Z_o}{Z_E}\left[\sin\frac{\omega}{c}(l_1 + l_2) - \sin\frac{\omega l_1}{c}\sin\frac{\omega l_2}{c}\sum_{m=1}^{M}\left(\frac{d_m}{d}\right)^2\tan\frac{\omega h_m}{c}\right]$$

$$\frac{Z_o U_0}{P_E} = \frac{Z_o}{Z_E}\left[\cos\frac{\omega}{c}(l_1 + l_2) - \cos\frac{\omega l_1}{c}\sin\frac{\omega l_2}{c}\sum_{m=1}^{M}\left(\frac{d_m}{d}\right)^2\tan\frac{\omega h_m}{c}\right]$$

$$+ j\left[\sin\frac{\omega}{c}(l_1 + l_2) + \cos\frac{\omega l_1}{c}\cos\frac{\omega l_2}{c}\sum_{m=1}^{M}\left(\frac{d_m}{d}\right)^2\tan\frac{\omega h_m}{c}\right]$$

Figure 36.- Geometry and terminal perturbation pressure and velocity ratios for configuration with several branches at a common location (e.g., in above sketch, M = 4).

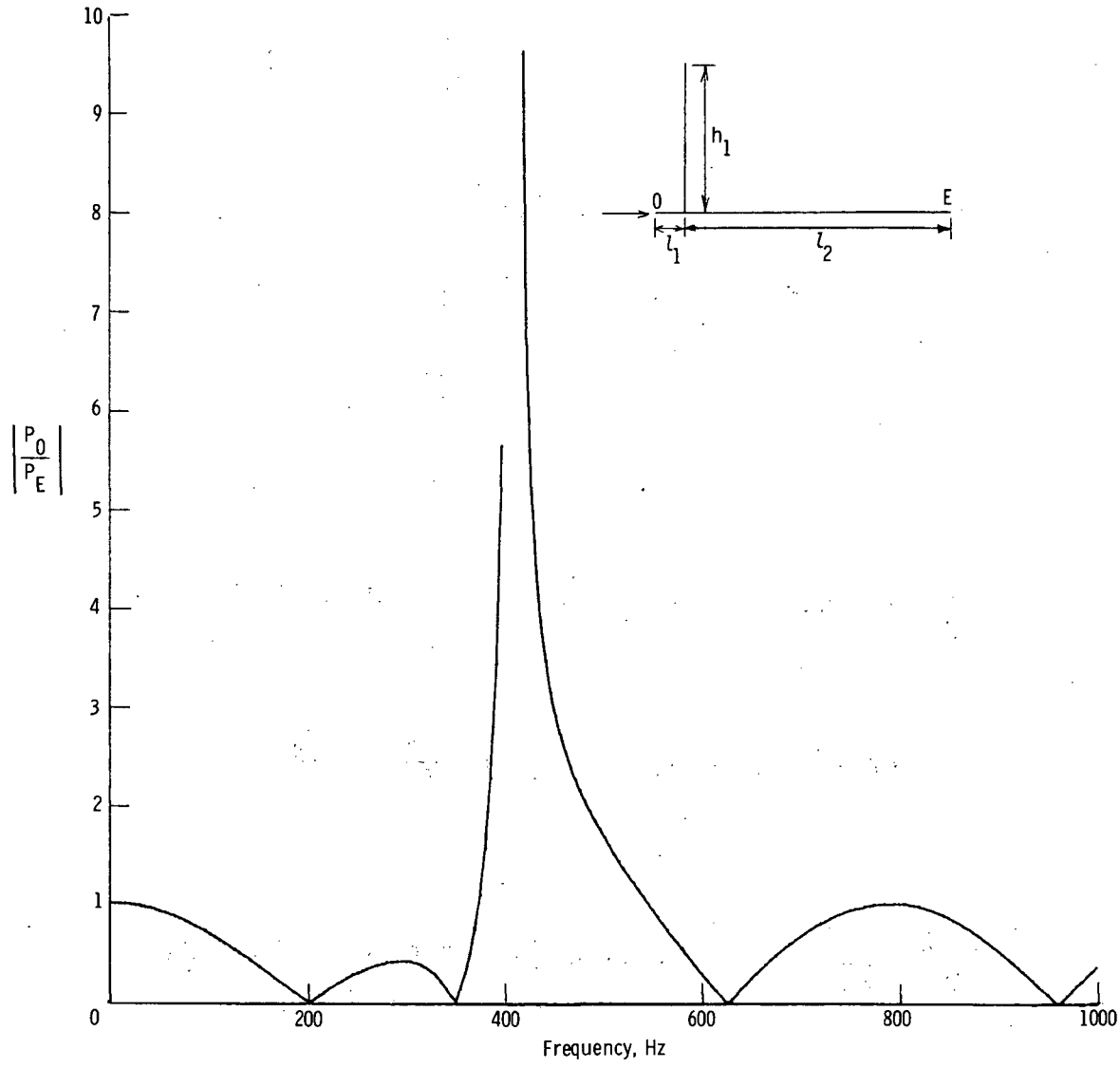

(a) Inlet-to-exit pressure ratio.

Figure 37.- Terminal perturbation pressure ratios for test system I with single branch close to the inlet; l_1 = 15.2 cm (6.0 in.); l_2 = 137.2 cm (54.0 in.); h_1 = 76.2 cm (30.0 in.).

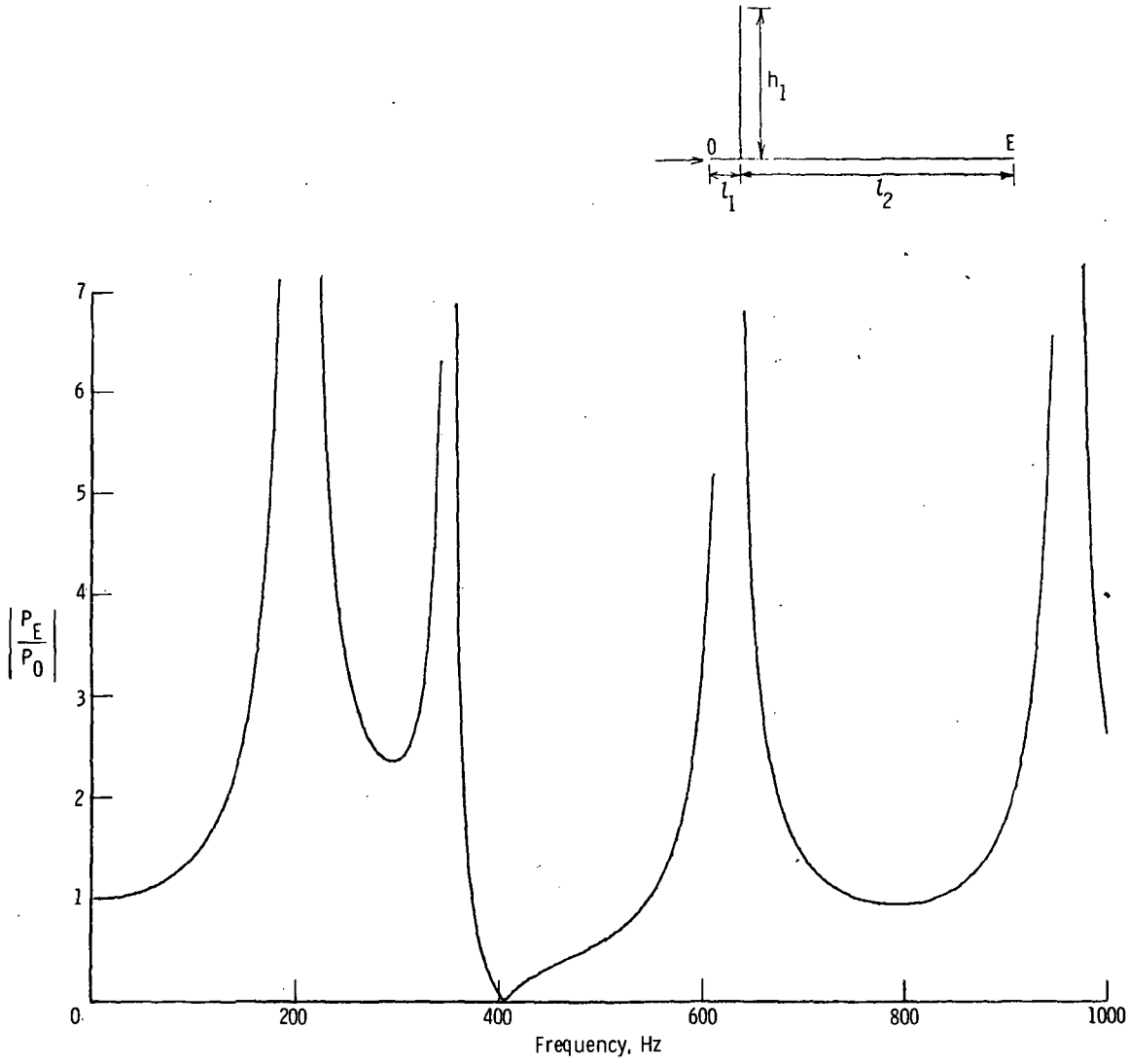

(b) Exit-to-inlet pressure ratio.

Figure 37.- Concluded.

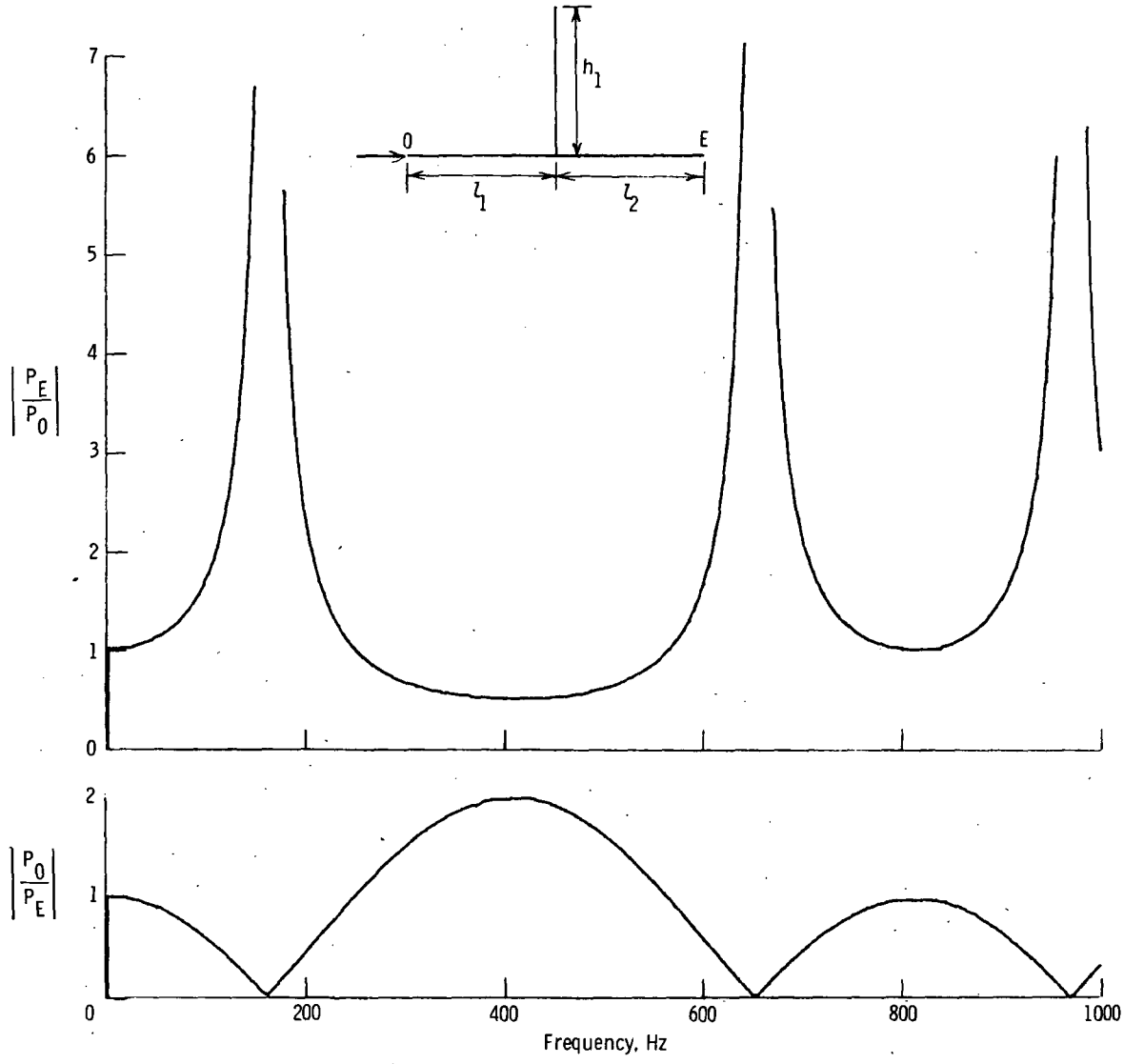

Figure 38.- Terminal perturbation pressure ratios for test system I with single-branch equilateral configuration; $l_1 = l_2 = h_1 = 76.2$ cm (30.0 in.).

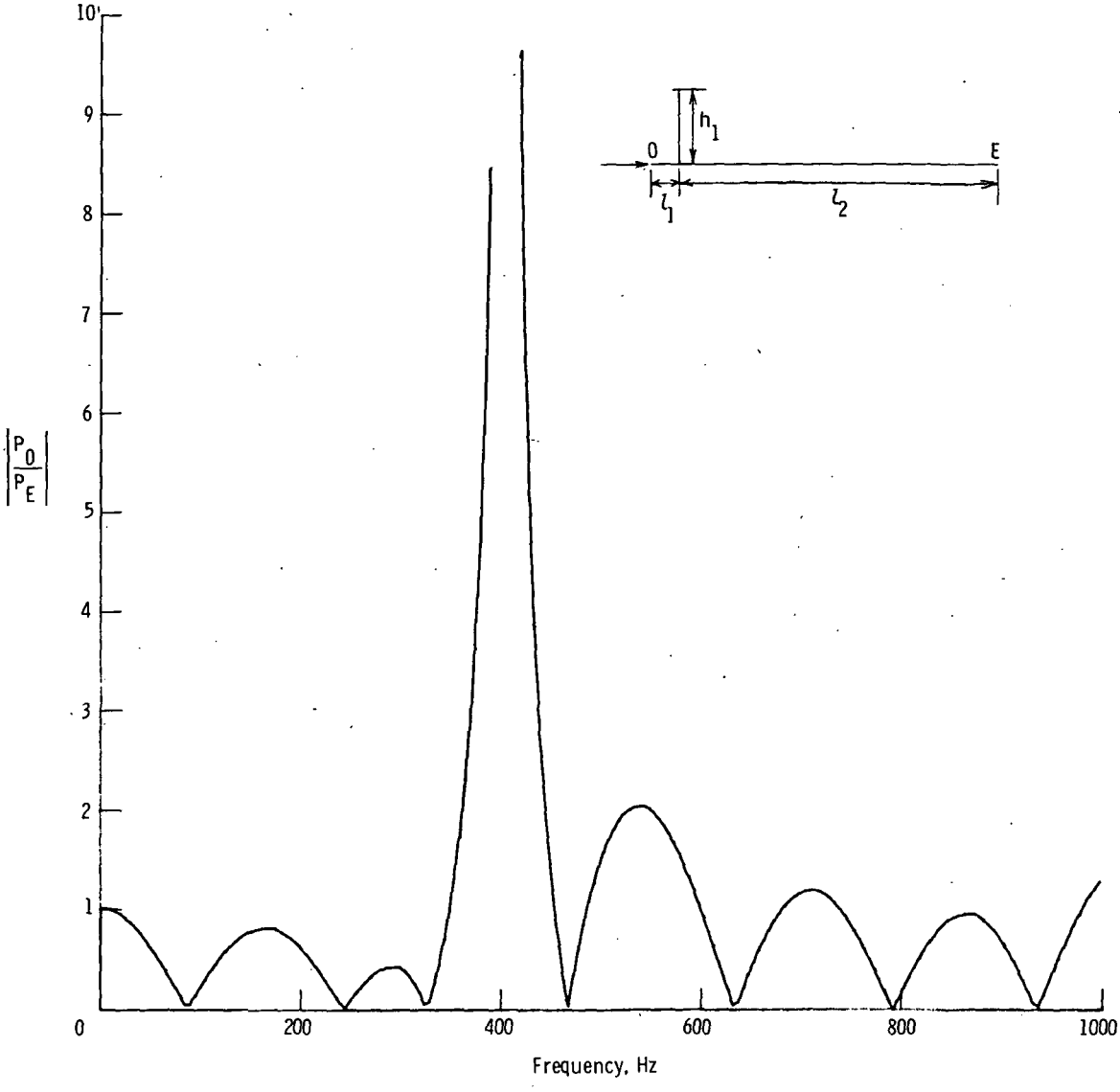

(a) Inlet-to-exit pressure ratio.

Figure 39.- Terminal perturbation pressure ratios for test system II with single branch close to the inlet; l_1 = 30.5 cm (12.0 in.); l_2 = 321.3 cm (126.5 in.); h_1 = 76.2 cm (30.0 in.).

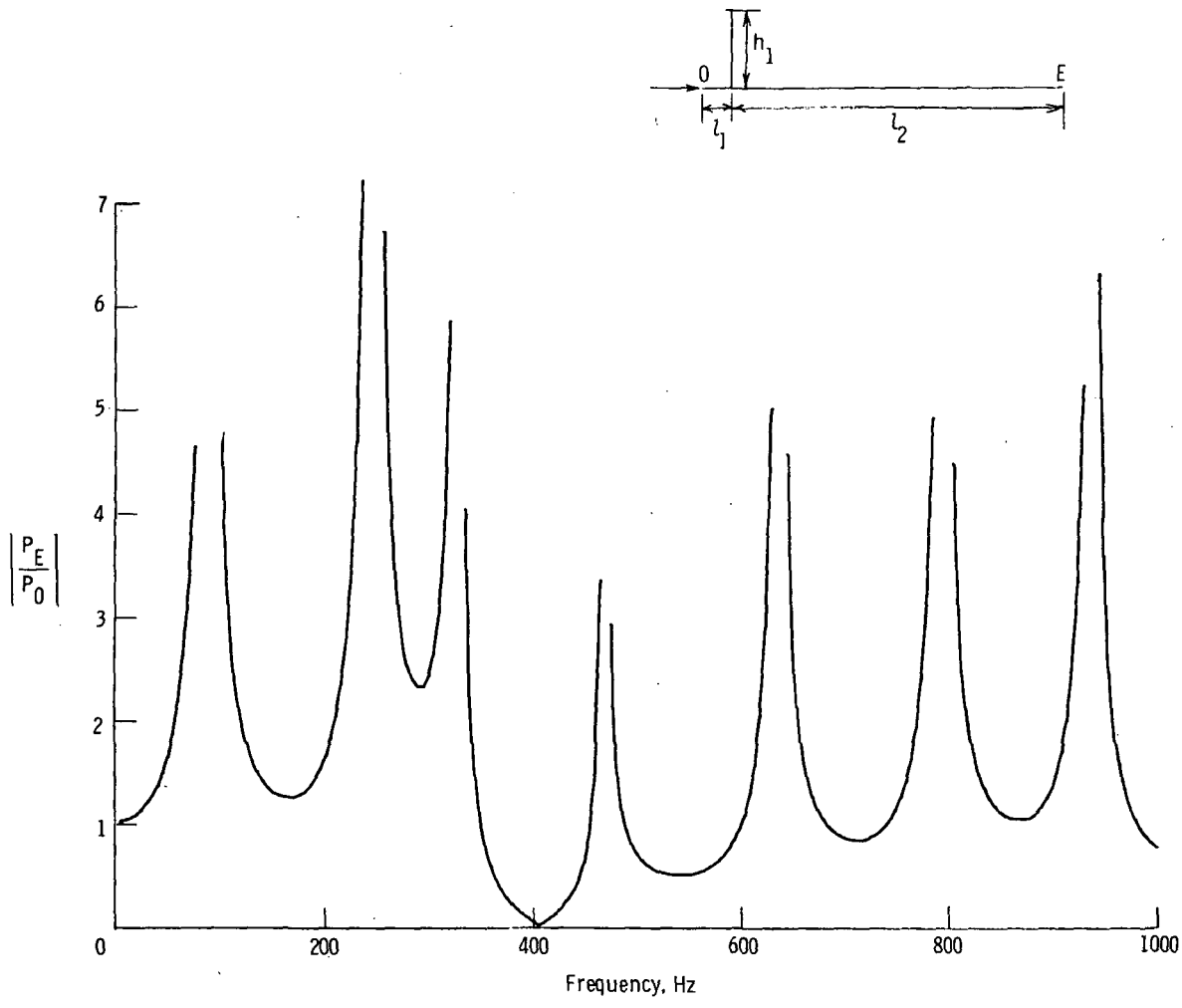

(b) Exit-to-inlet pressure ratio.

Figure 39.- Concluded.

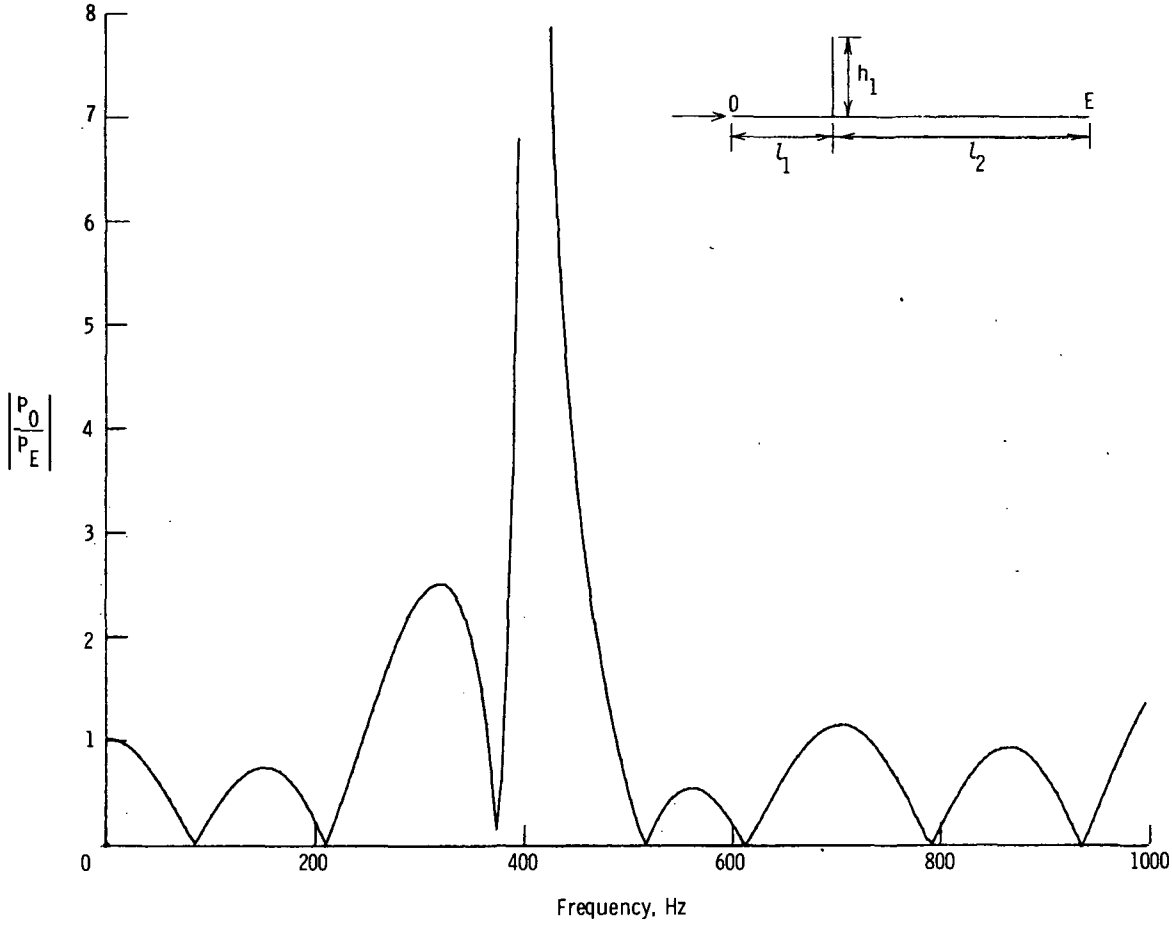

(a) Inlet-to-exit pressure ratio.

Figure 40.- Terminal perturbation pressure ratios for test system II with single branch; l_1 = 99.4 cm (39.1 in.); l_2 = 252.4 cm (99.4 in.); h_1 = 76.2 cm (30.0 in.).

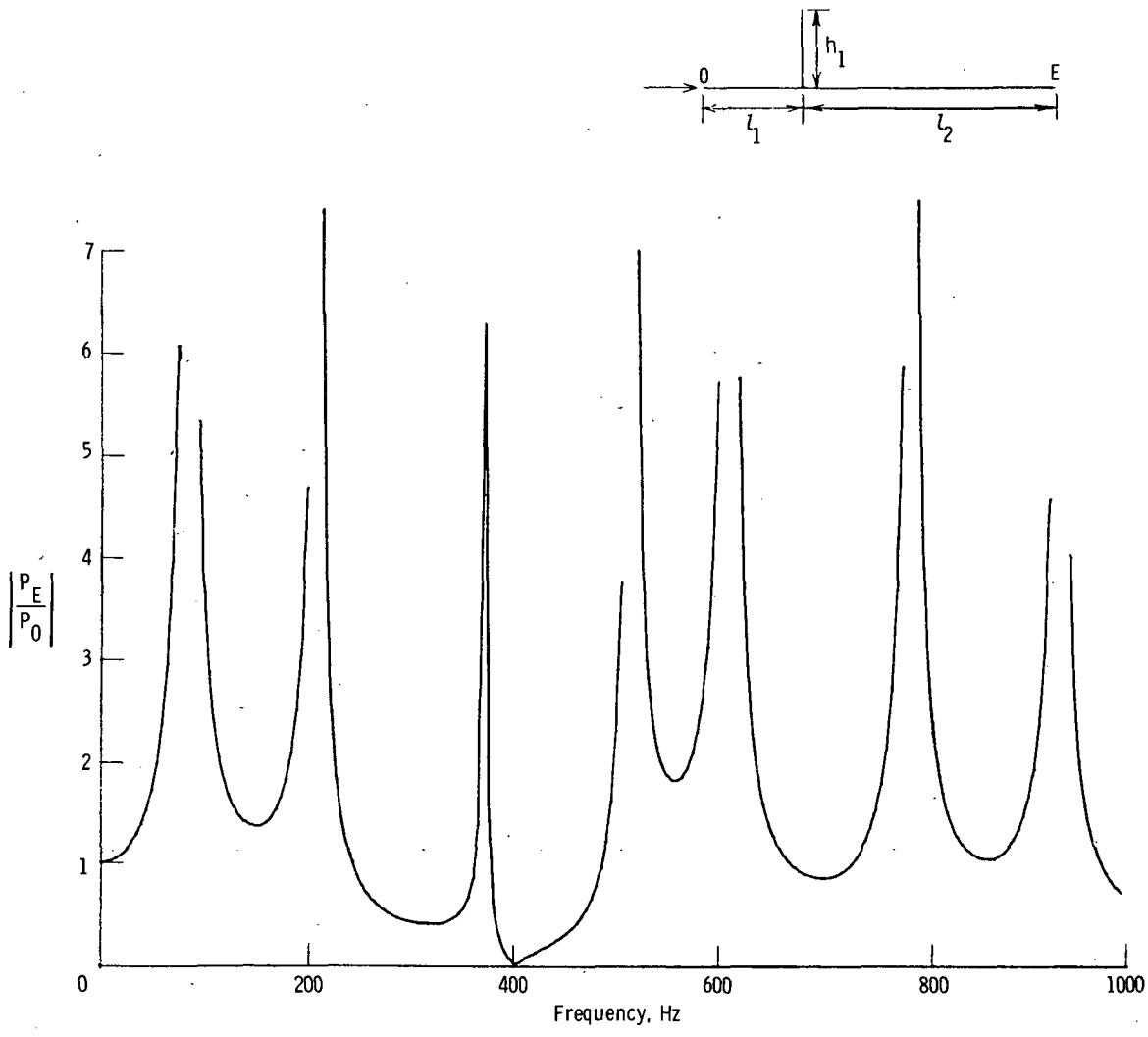

(b) Exit-to-inlet pressure ratio.

Figure 40.- Concluded.

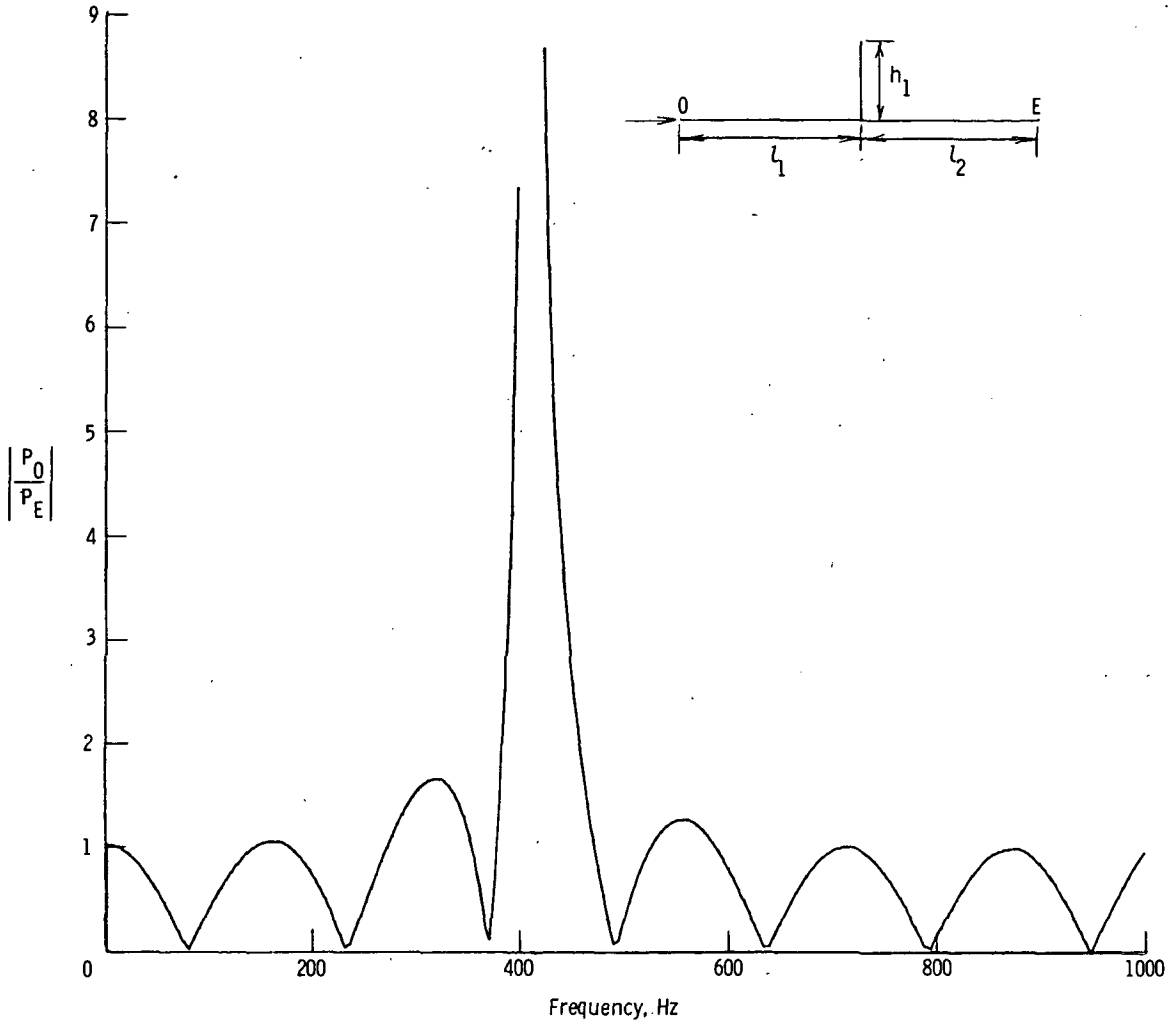

(a) Inlet-to-outlet pressure ratio.

Figure 41.- Terminal perturbation pressure ratios for test system II with single branch about halfway from inlet to exit; l_1 = 175.3 cm (69.0 in.); l_2 = 176.5 cm (69.5 in.); h_1 = 76.2 cm (30.0 in.).

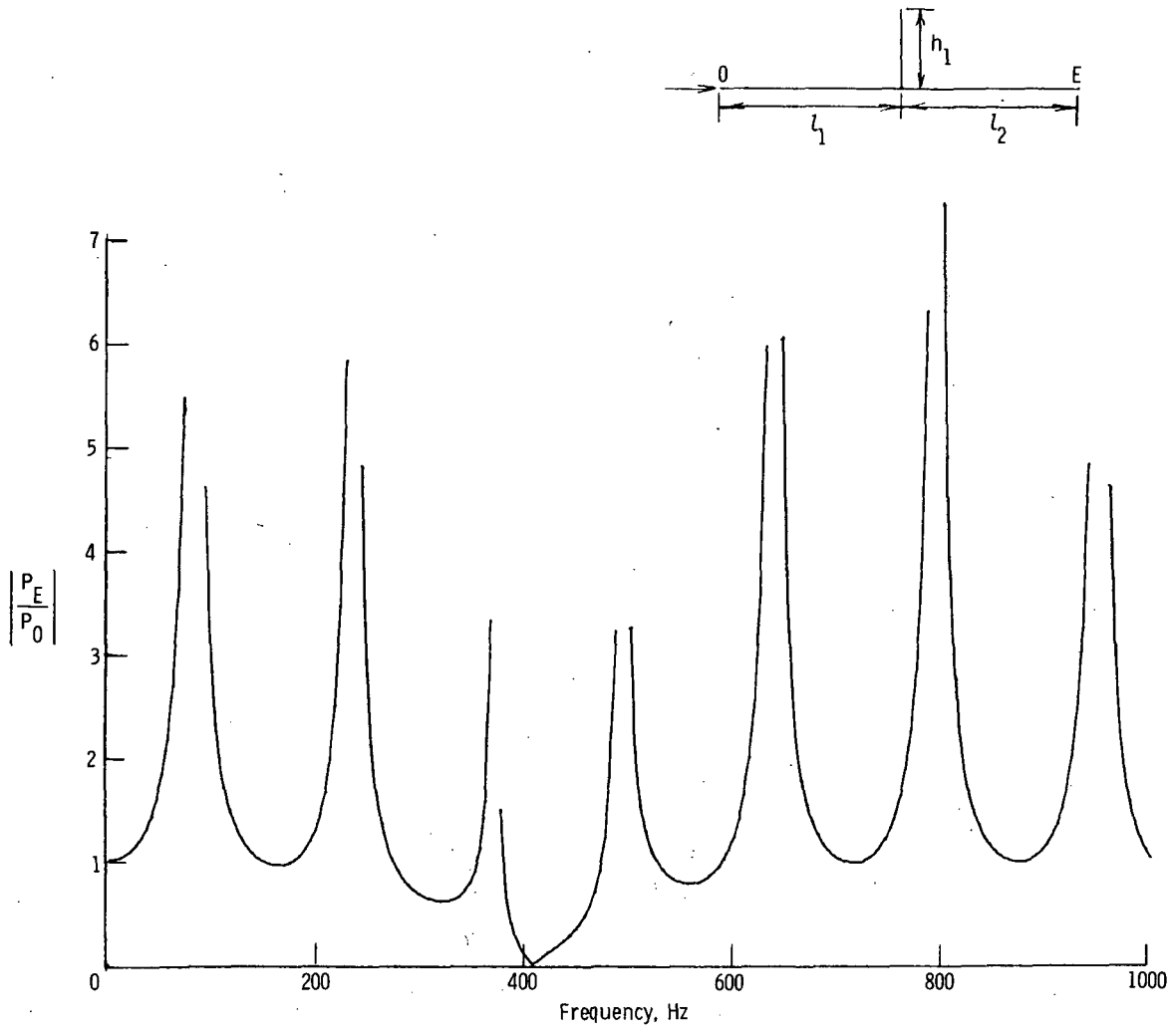

(b) Exit-to-inlet pressure ratio.

Figure 41.- Concluded.

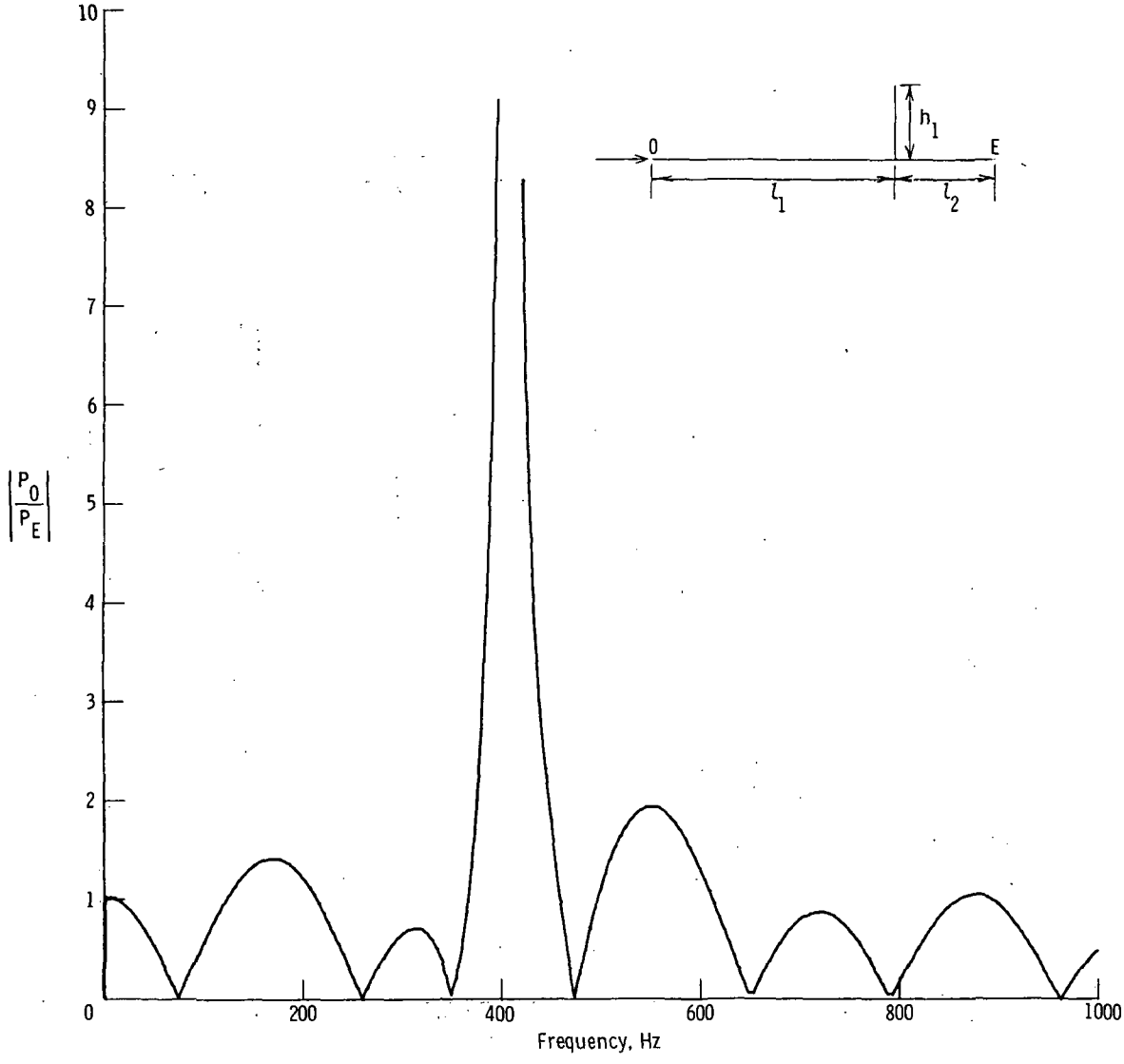

(a) Inlet-to-exit pressure ratio.

Figure 42.- Terminal perturbation pressure ratios for test system II with single branch; l_1 = 251.1 cm (98.9 in.); l_2 = 100.6 cm (39.6 in.); h_1 = 76.2 cm (30.0 in.).

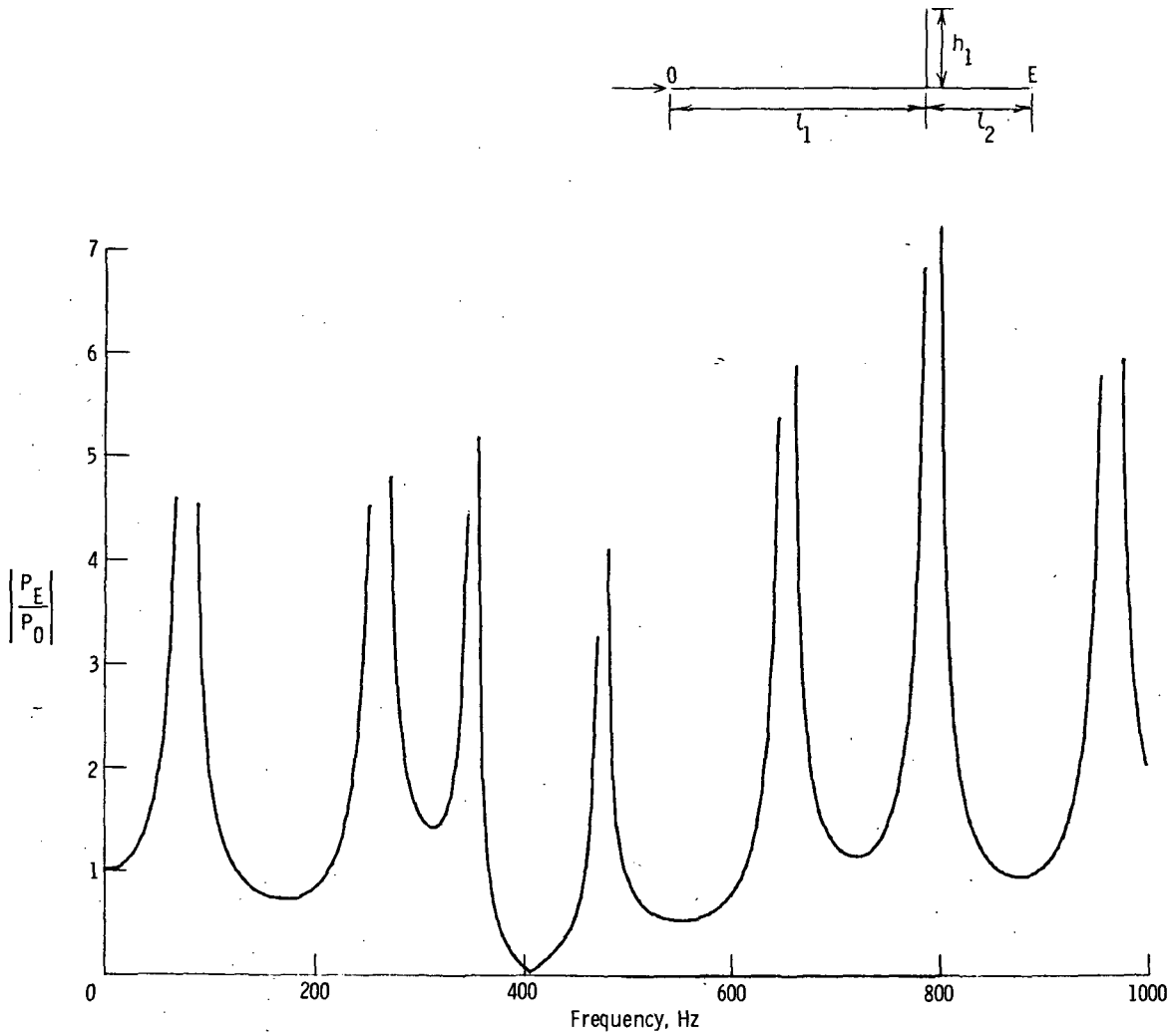

(b) Exit-to-inlet pressure ratio.

Figure 42.- Concluded.

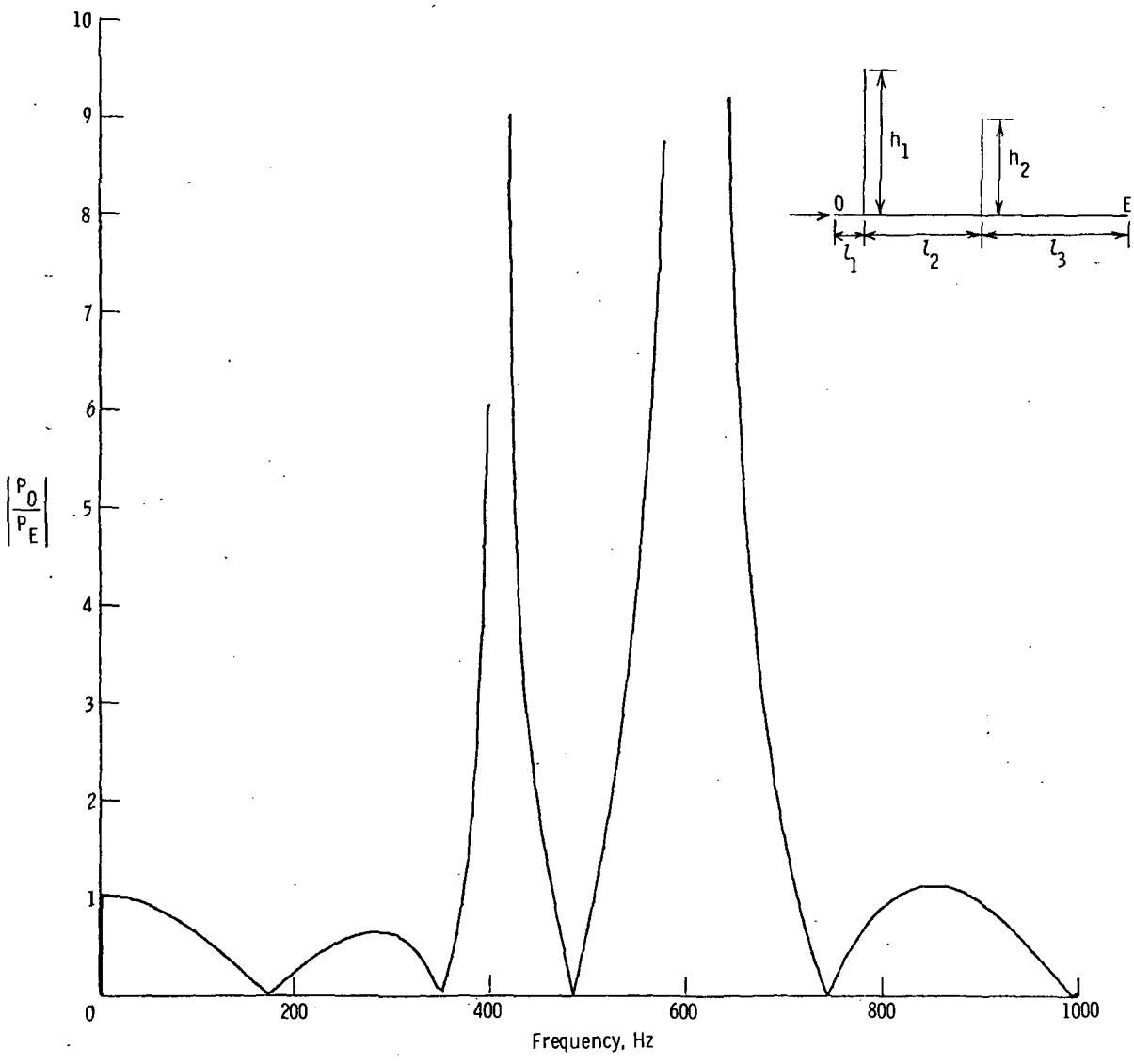

(a) Inlet-to-outlet pressure ratio.

Figure 43.- Terminal perturbation pressure ratios for test system I with two branches; l_1 = 15.2 cm (6.0 in.); l_2 = 61.0 cm (24.0 in.); l_3 = 76.2 cm (30.0 in.); h_1 = 76.2 cm (30.0 in.); h_2 = 50.8 cm (20.0 in.).

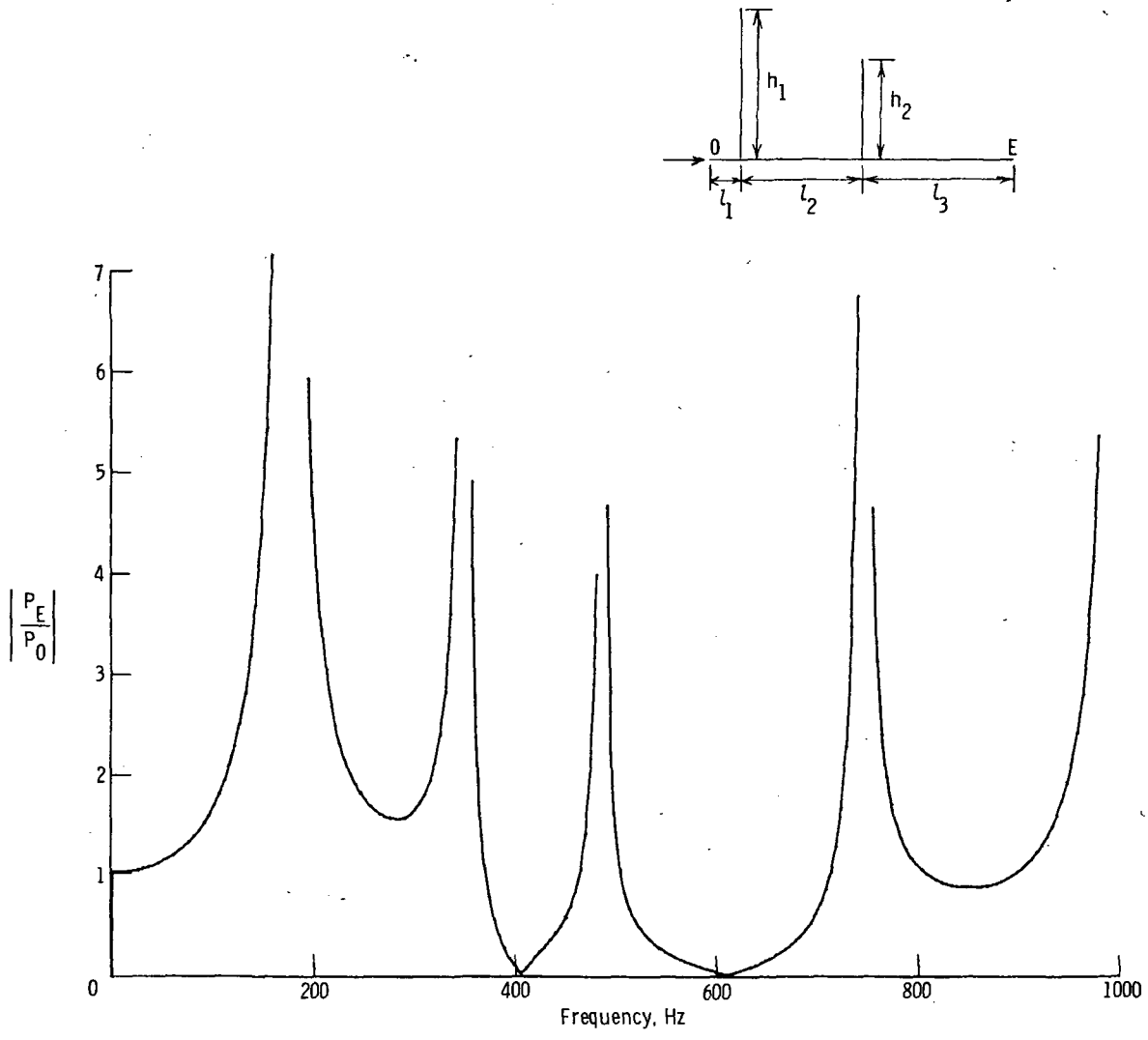

(b) Exit-to-inlet pressure ratio.

Figure 43. - Concluded.

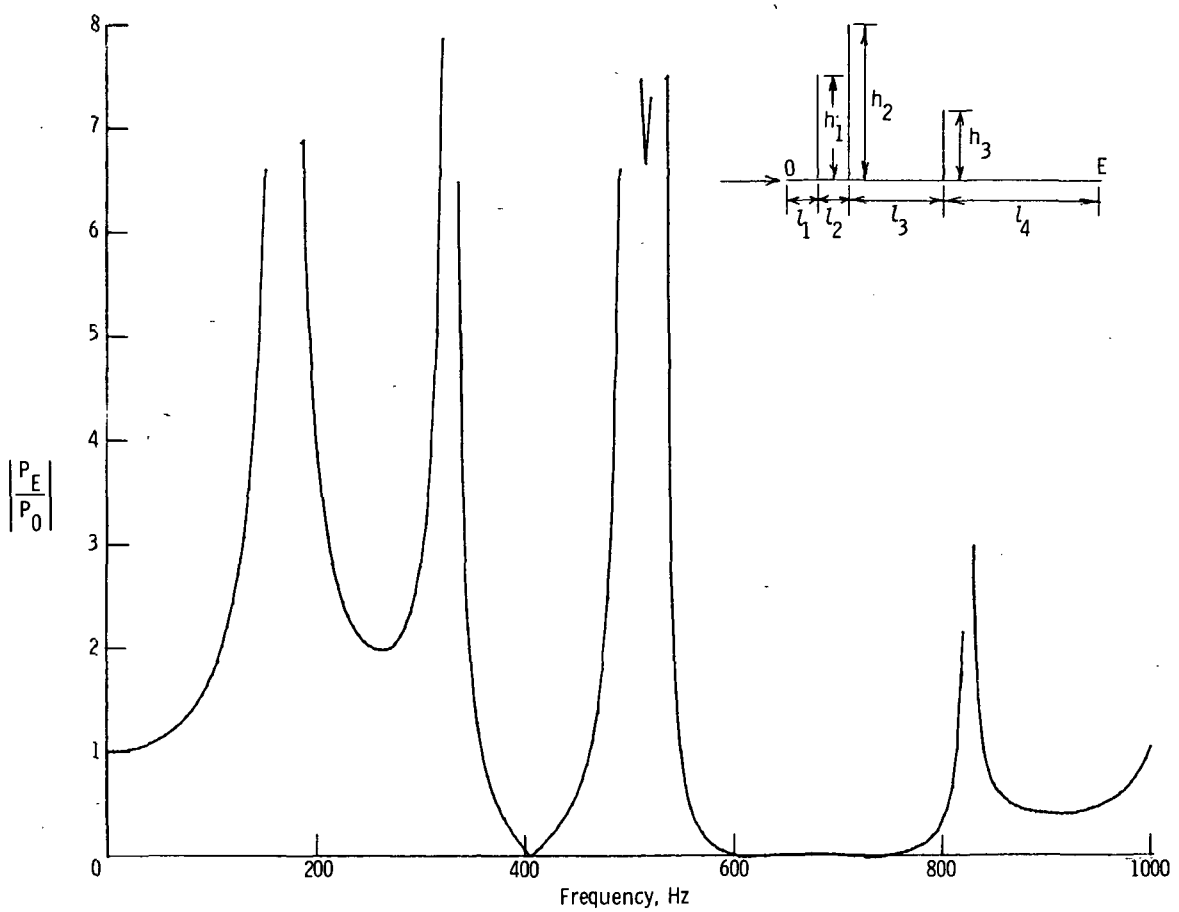

Figure 44.- Terminal perturbation pressure ratios for test system I with three branches; $l_1 = l_2 = 15.2$ cm (6.0 in.); $l_3 = 45.7$ cm (18.0 in.); $l_4 = 76.2$ cm (30.0 in.); $h_1 = 50.8$ cm (20.0 in.); $h_2 = 76.2$ cm (30.0 in.); $h_3 = 42.6$ cm (16.8 in.).

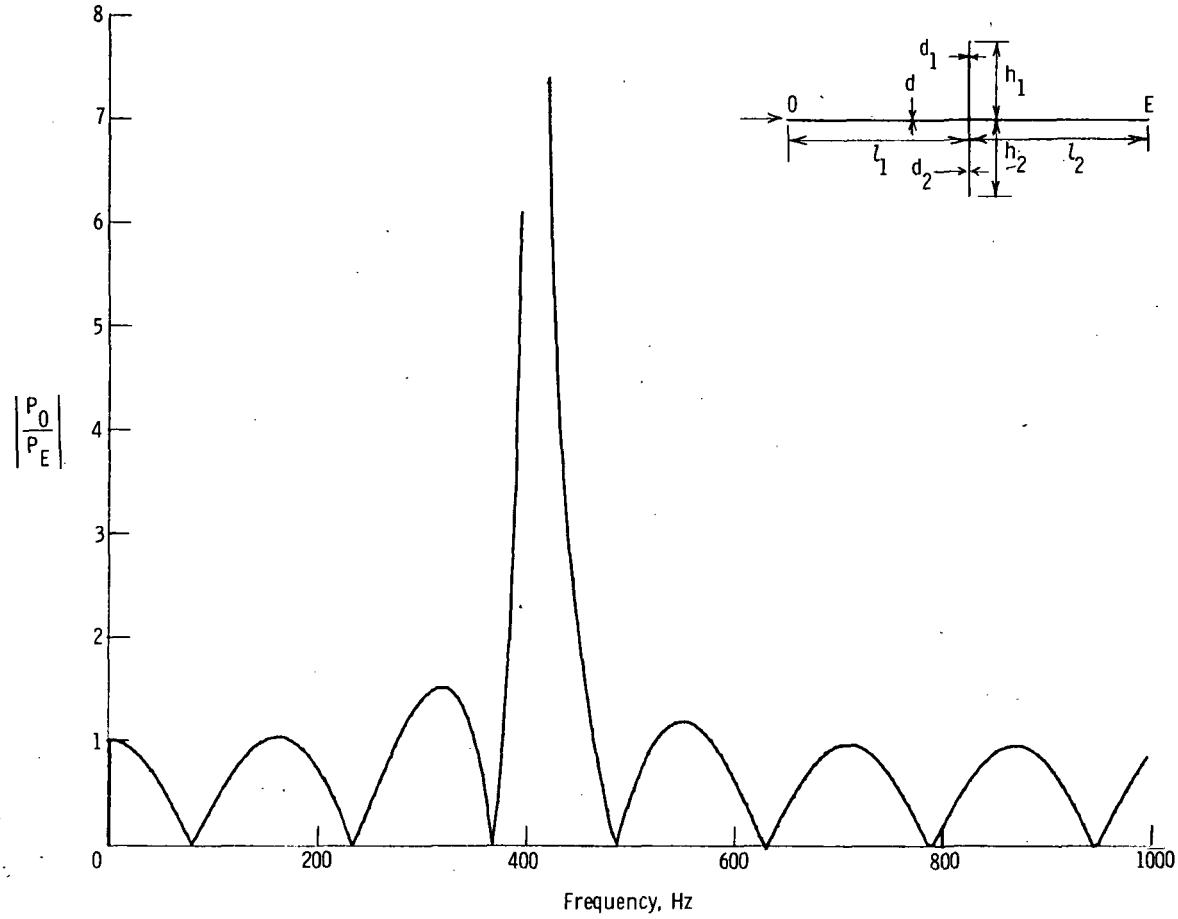

(a) Inlet-to-outlet pressure ratio.

Figure 45.- Terminal perturbation pressure ratios for test system II with two branches; l_1 = 175.3 cm (69.0 in.); l_2 = 176.5 cm (69.5 in.); $h_1 = h_2$ = 76.2 cm (30.0 in.); $\frac{d_1}{d} = \frac{d_2}{d} = 0.65$.

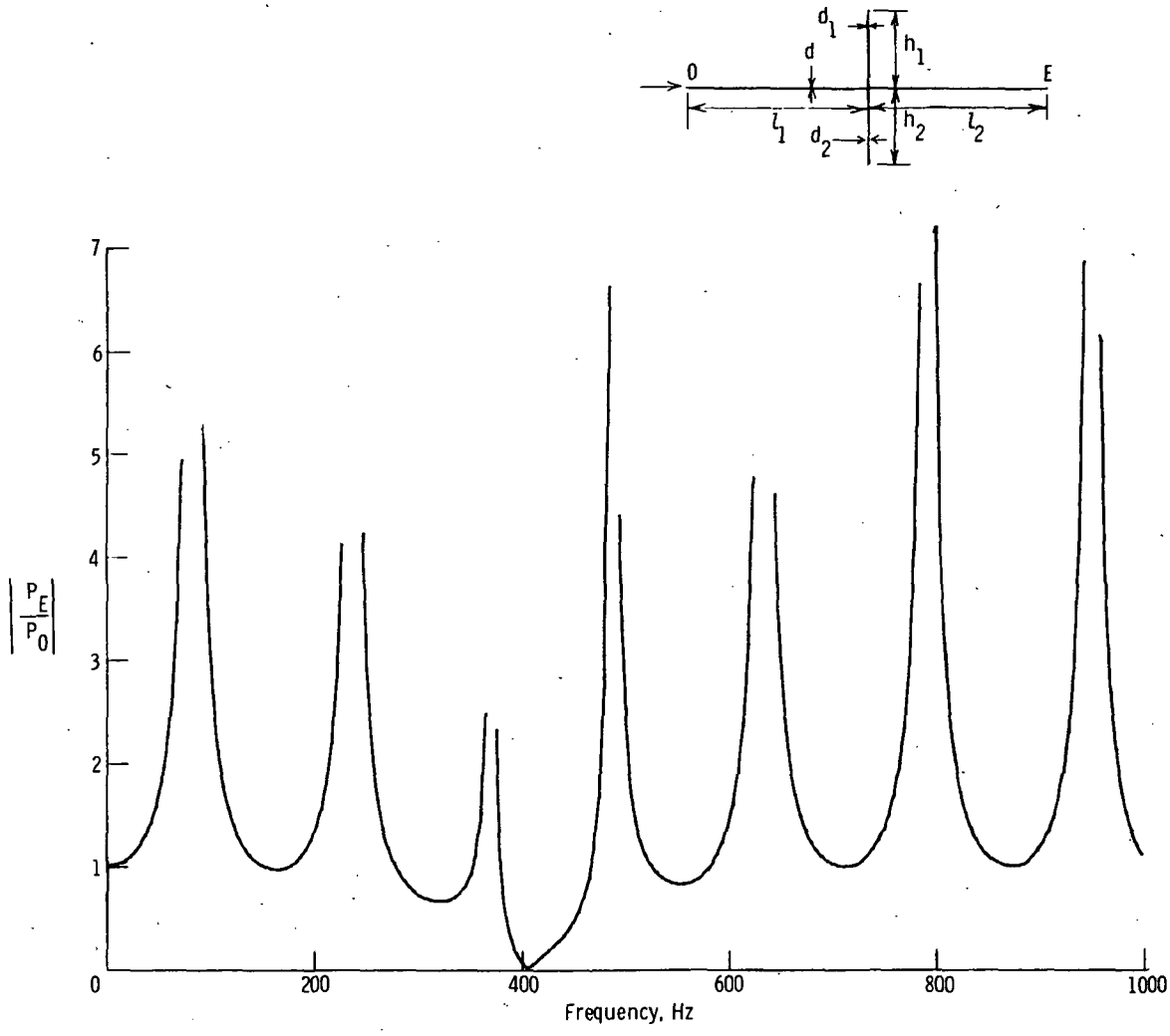

(b) Exit-to-inlet pressure ratio.

Figure 45.- Concluded.

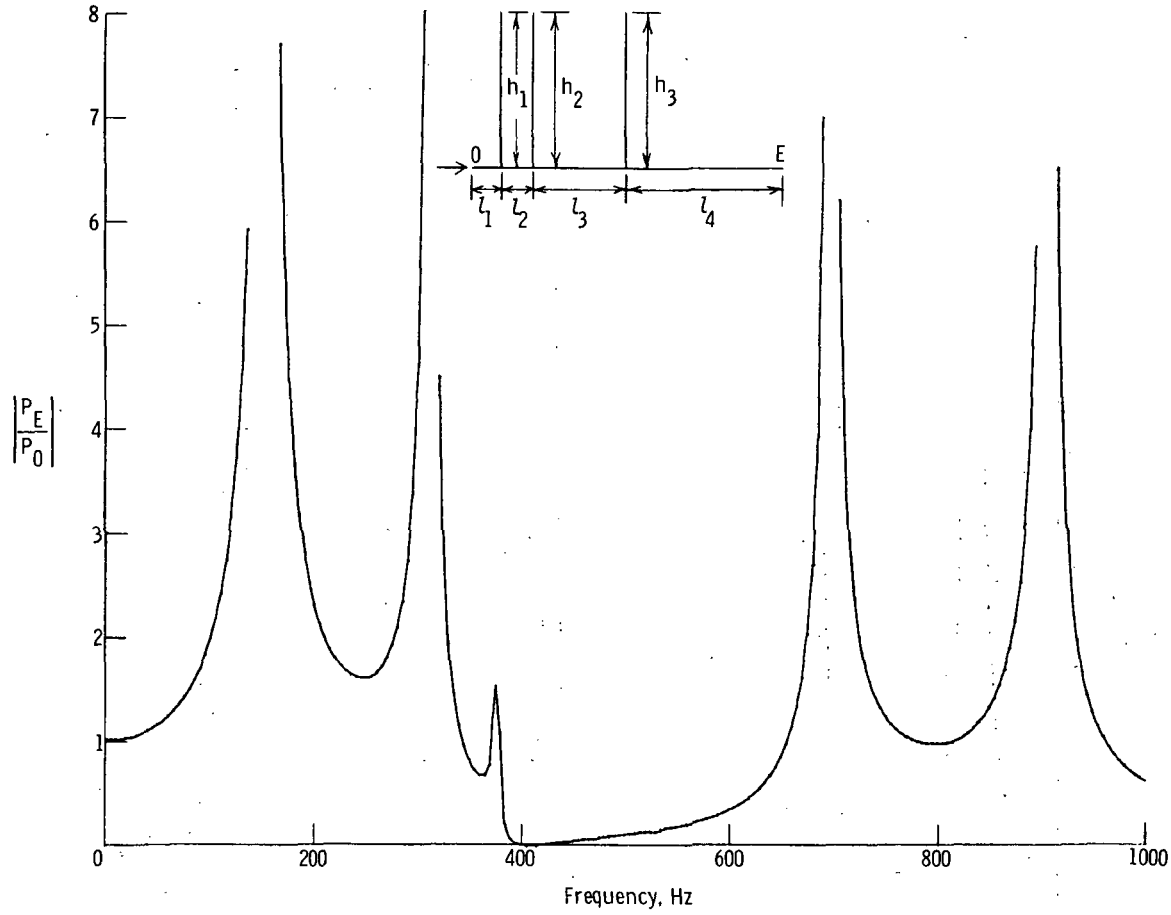

Figure 46.- Terminal perturbation pressure ratios for test system I with three branches of equal length; $l_1 = l_2 = 15.2$ cm (6.0 in.); $l_3 = 45.7$ cm (18.0 in.); $l_4 = 76.2$ cm (30.0 in.); $h_1 = h_2 = h_3 = 76.2$ cm (30.0 in.).

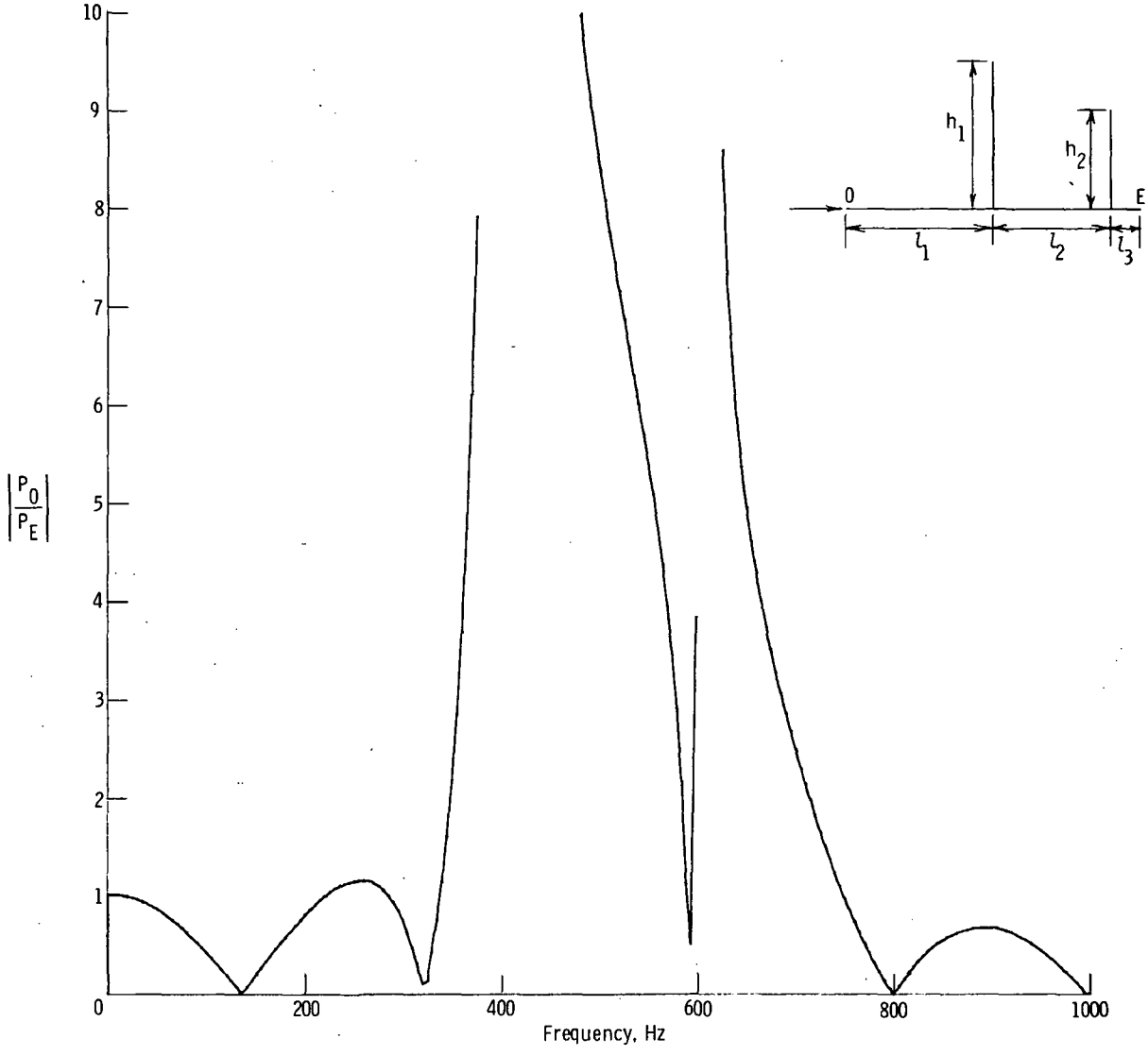

(a) Inlet-to-exit pressure ratio.

Figure 47.- Terminal perturbation pressure ratios for test system I with two branches; l_1 = 76.2 cm (30.0 in.); l_2 = 61.0 cm (24.0 in.); l_3 = 15.2 cm (6.0 in.); h_1 = 76.2 cm (30.0 in.); h_2 = 50.8 cm (20.0 in.).

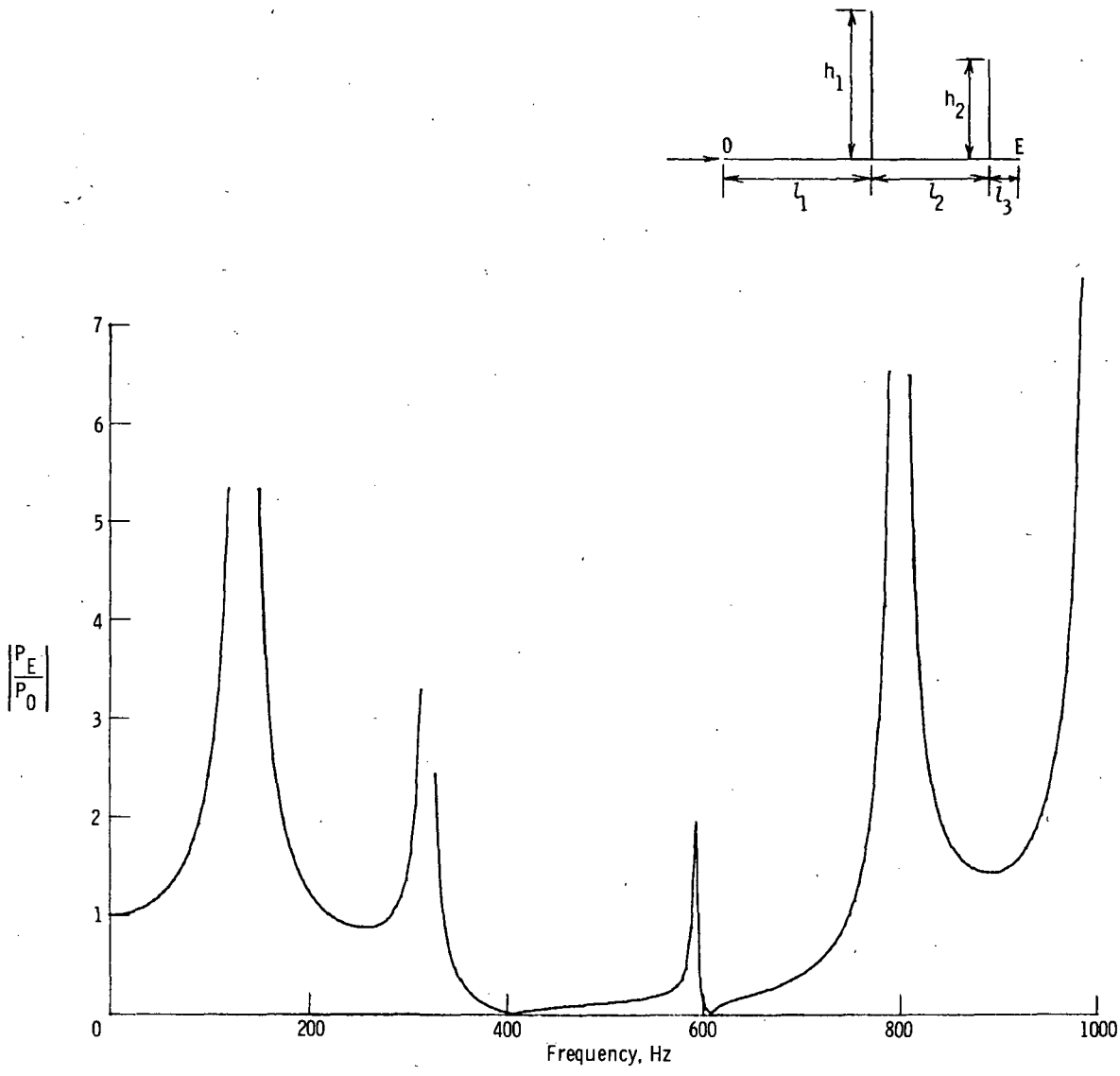

(b) Exit-to-inlet pressure ratio.

Figure 47.- Concluded.

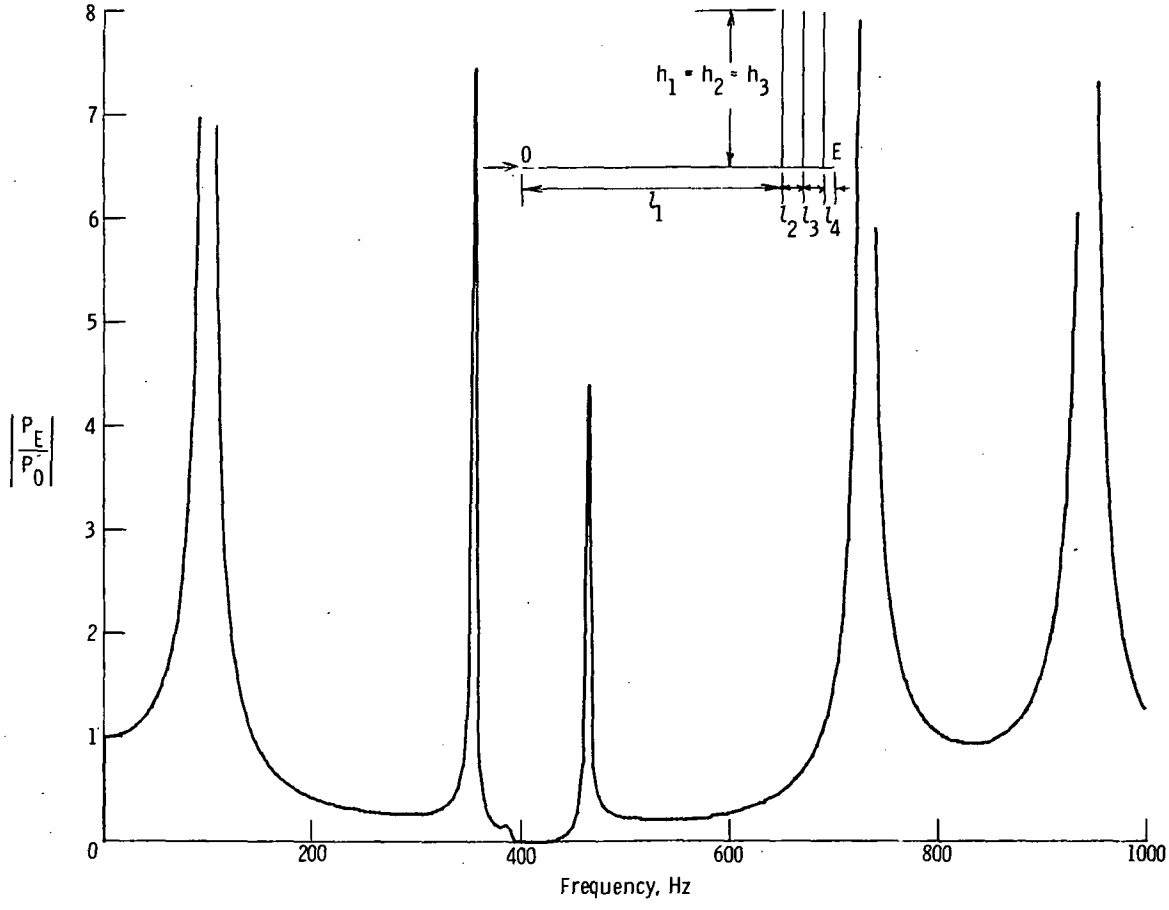

Figure 48.- Terminal perturbation pressure ratios for test system I with three equal-length branches near the exit; l_1 = 127.0 cm (50.0 in.); $l_2 = l_3$ = 10.2 cm (4.0 in.); l_4 = 5.1 cm (2.0 in.); $h_1 = h_2 = h_3$ = 76.2 cm (30.0 in.).

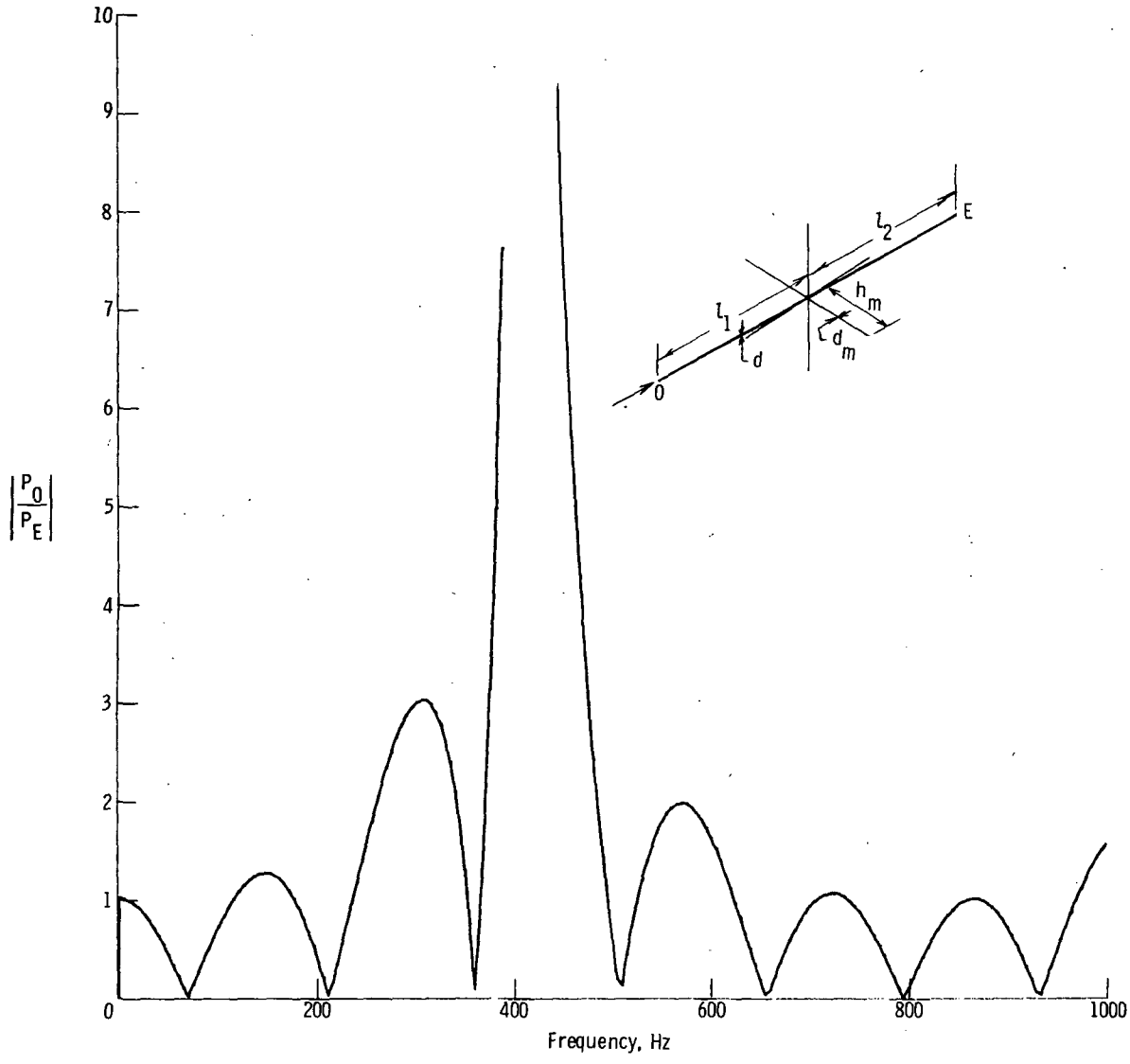

(a) Inlet-to-exit pressure ratio.

Figure 49.- Terminal perturbation pressure ratios for test system II with six branches; l_1 = 175.3 cm (69.0 in.); l_2 = 176.5 cm (69.5 in.); $h_1 = h_2 = \ldots = h_6$ = 76.2 cm (30.0 in.); $\frac{d_1}{d} = \frac{d_2}{d} = \ldots = \frac{d_6}{d} = 0.65$.

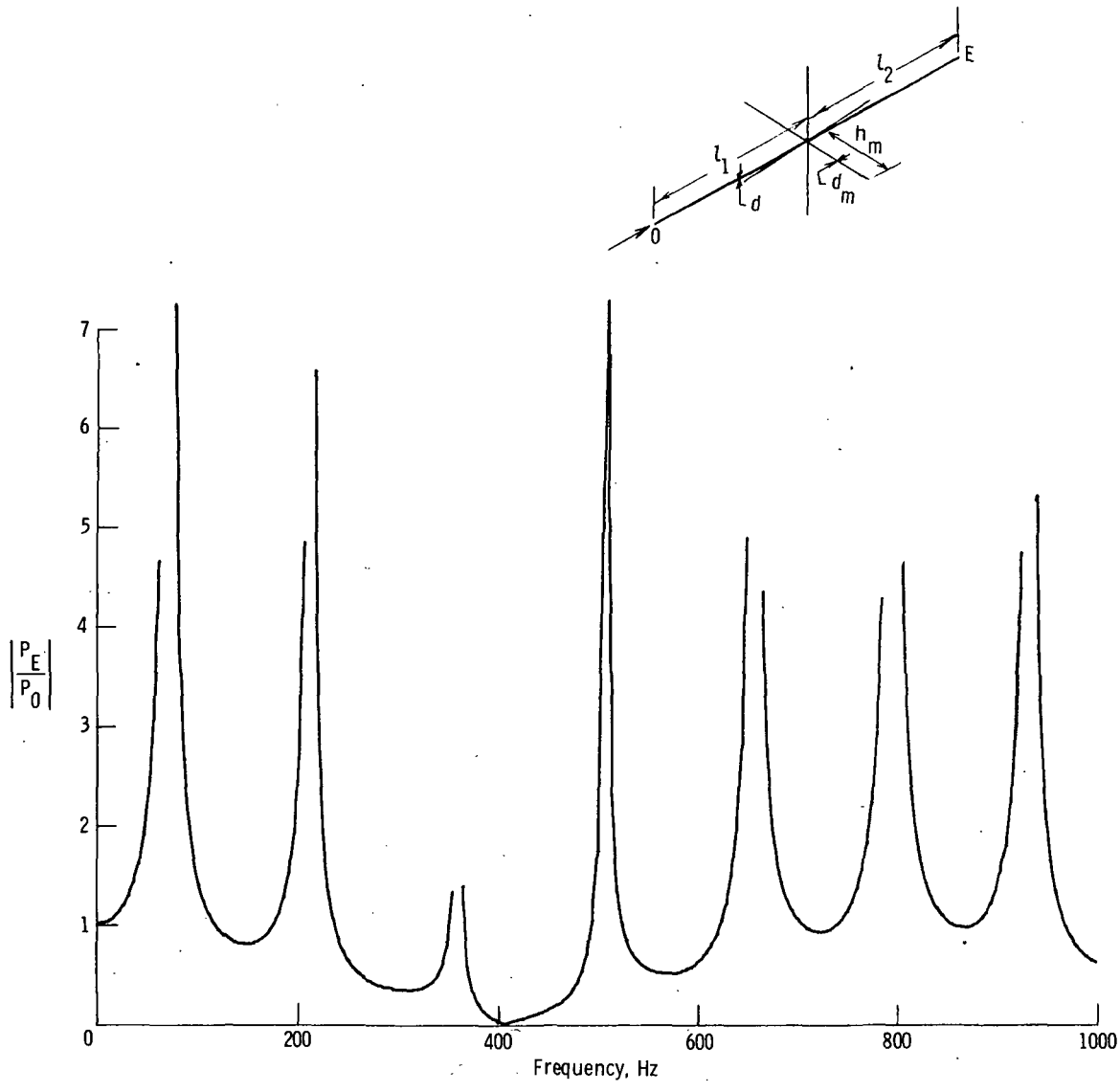

(b) Exit-to-inlet pressure ratio.

Figure 49.- Concluded.

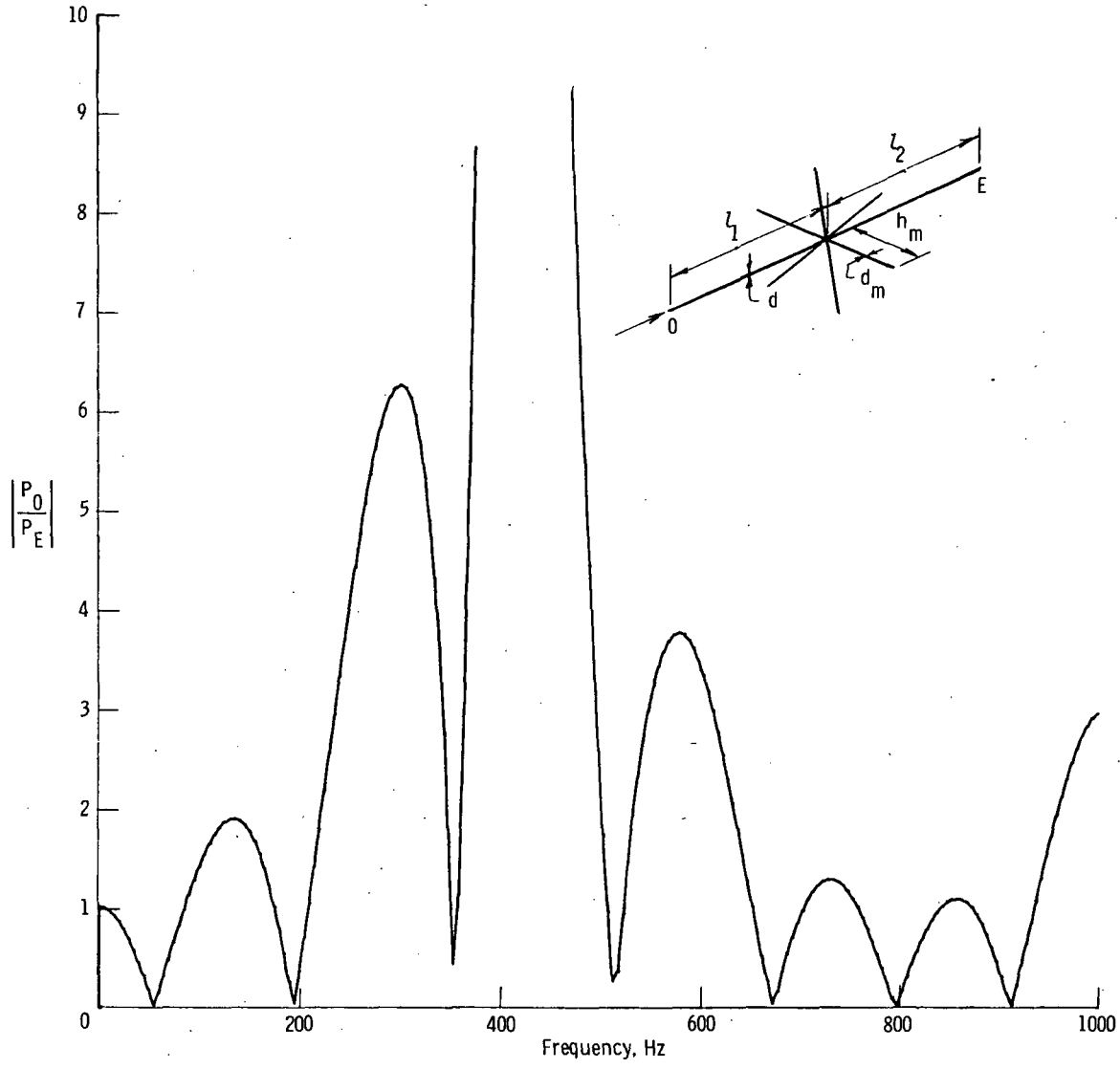

(a) Inlet-to-exit pressure ratio.

Figure 50.- Terminal perturbation pressure ratios for test system II with six branches; l_1 = 175.3 cm (69.0 in.); l_2 = 176.5 cm (69.5 in.); $h_1 = h_2 = \ldots = h_6$ = 76.2 cm (30.0 in.); $\frac{d_1}{d} = \frac{d_2}{d} = \ldots = \frac{d_6}{d} = 1.0$.

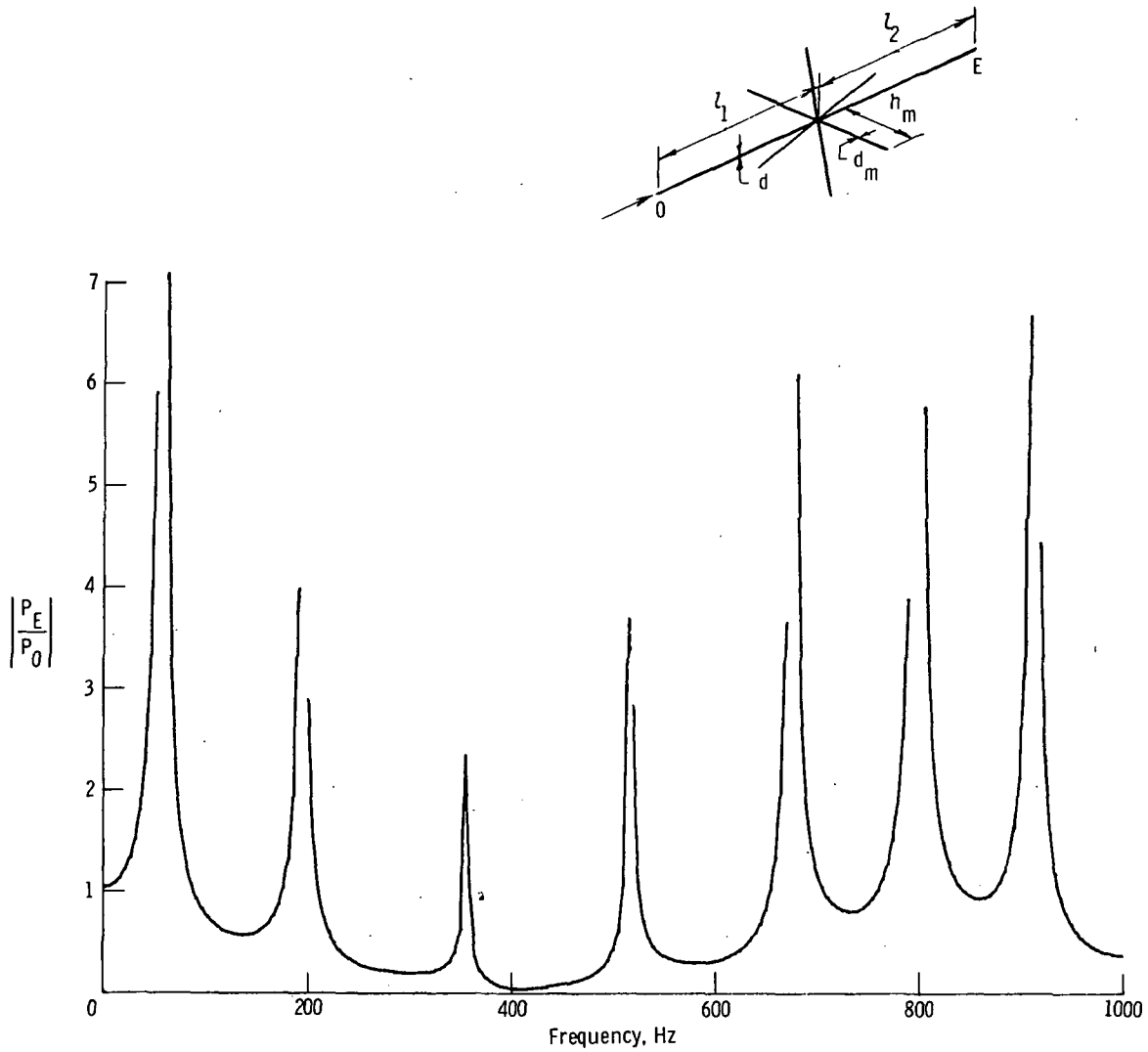

(b) Exit-to-inlet pressure ratio.

Figure 50.- Concluded.

NATIONAL AERONAUTICS AND SPACE ADMINISTRATION
WASHINGTON, D.C. 20546

OFFICIAL BUSINESS
PENALTY FOR PRIVATE USE $300

SPECIAL FOURTH-CLASS RATE BOOK

POSTAGE AND FEES PAID
NATIONAL AERONAUTICS AND SPACE ADMINISTRATION
451

U.S.MAIL

POSTMASTER : If Undeliverable (Section 158 Postal Manual) Do Not Return

"The aeronautical and space activities of the United States shall be conducted so as to contribute . . . to the expansion of human knowledge of phenomena in the atmosphere and space. The Administration shall provide for the widest practicable and appropriate dissemination of information concerning its activities and the results thereof."

—NATIONAL AERONAUTICS AND SPACE ACT OF 1958

NASA SCIENTIFIC AND TECHNICAL PUBLICATIONS

TECHNICAL REPORTS: Scientific and technical information considered important, complete, and a lasting contribution to existing knowledge.

TECHNICAL NOTES: Information less broad in scope but nevertheless of importance as a contribution to existing knowledge.

TECHNICAL MEMORANDUMS: Information receiving limited distribution because of preliminary data, security classification, or other reasons. Also includes conference proceedings with either limited or unlimited distribution.

CONTRACTOR REPORTS: Scientific and technical information generated under a NASA contract or grant and considered an important contribution to existing knowledge.

TECHNICAL TRANSLATIONS: Information published in a foreign language considered to merit NASA distribution in English.

SPECIAL PUBLICATIONS: Information derived from or of value to NASA activities. Publications include final reports of major projects, monographs, data compilations, handbooks, sourcebooks, and special bibliographies.

TECHNOLOGY UTILIZATION PUBLICATIONS: Information on technology used by NASA that may be of particular interest in commercial and other non-aerospace applications. Publications include Tech Briefs, Technology Utilization Reports and Technology Surveys.

Details on the availability of these publications may be obtained from:

SCIENTIFIC AND TECHNICAL INFORMATION OFFICE

NATIONAL AERONAUTICS AND SPACE ADMINISTRATION

Washington, D.C. 20546